ELASTIC CONSTANTS OF ORTHORHOMBIC POTASSIUM NIOBATE BY X-RAY DIFFUSE SCATTERING

BY

SADANAND DATTATREYA PHATAK

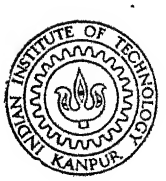

DEPARTMENT OF PHYSICS

INDIAN INSTITUTE OF TECHNOLOGY KANPUR

JULY 1970

ELASTIC CONSTANTS OF ORTHORHOMBIC POTASSIUM NIOBATE BY X-RAY DIFFUSE SCATTERING

A Thesis Submitted
In Partial Fulfilment of the Requirements
for the Degree of
DOCTOR OF PHILOSOPHY

BY

SADANAND DATTATREYA PHATAK

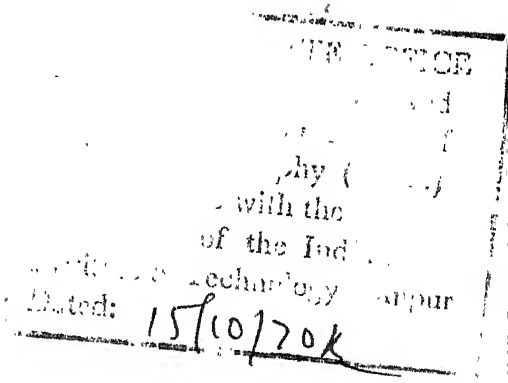

to the

DEPARTMENT OF PHYSICS

INDIAN INSTITUTE OF TECHNOLOGY KANPUR

JULY 1970

PHY-1970-D-PAT.-ELA

TO

MY PARENTS AND BROTHER

CERTIFICATE

Certified that the work presented in this thesis has been carried out by Mr. S. D. Phatak, Physics Department, under my supervision and has not been submitted elsewhere for a degree.

(E.C. Subbarao)
Professor
Department of Metallurgical Engg.,
Indian Institute of Technology,
Kanpur, India

ACKNOWLEDGEMENTS

The author is highly indebted to Professor E. C. Subbarao for his keen interest, guidance and encouragement throughout the progress of the work.

The author expresses his deep gratitude to Professor R. C. Srivastava for his invaluable help, inspiration and active involvement in all phases of the problem.

The author wishes to express his sincere thanks to his friends Dr. S. D. Pandey and Mr. U. N. Sinha for their help in computer programming, proof reading and for some useful discussions.

The author is grateful to Professor S. K. Joshi (Roorkee Univ.) for his invaluable suggestions and useful discussions and to Professors A. K. Rajgopal (TIFR) and V. D. Gupta for useful discussions. Encouragement and financial assistance from Prof. V. D. Gupta and Prof. S. C. Sen is gratefully acknowledged.

The author is also grateful to Professor Putcha Venkateswarlu for bringing the author to Kanpur and giving him an opportunity for research.

The author is thankful to Professors J. Mahanty and A. S. Parasnis for their interest in the present work.

The author is thankful to Shri J. S. Sharma for his help in the fabrication of the Camera and to Shri B. L. Arora for drawings of the same.

Further, the author is thankful to Sarva sri Dayal Saran, Dr. R.N. Patil, Dr. M. Yussouff, Dr. Tulsi Dass, K.N.S. Rao, Dr. Miss Indira Kakkar, Dr. L.P. Verma (Alld.) N.R. Yadav, Dr. G.C. Upreti, G.L. Dwivedi, V.K. Sharma, V.K.Agrawal, V.N.Sarin, A.N. Bishnoi, Dr. B.K. Agrawal (Alld.), Mrs. K. Kakkar (Alld.) M.B. Borwankar, Vishwanath Singh, V.L. Rajani and Dasgupta for their help in many ways.

Finally, author is thankful to Shri J. K. Misra for careful typing, Sri H.K. Panda and Sri Lallu Singh for cyclo-styling the same.

S. D. PHATAK

CONTENTS

LIST OF FIGURES AND PLATES

LIST OF TABLES

SYNOPSIS

In the present work the elastic properties of single crystals of Potassium Niobate ($KNbO_3$) have been studied by X-ray (thermal) diffuse scattering at room temperature. In this phase, $KNbO_3$ is an orthorhombic perovskite type ferroelectric crystal with space group Bmm2. The work is presented in five sections and four appendices.

Section one gives a brief account of the theories of elasticity, namely the old (Voigt's) theory based on the central force assumptions and the new (Laval's) theory which takes into account the non-central forces in the crystalline medium besides the usual central force. The various experimental methods available for the determination of the elastic constants are discussed, with emphasis on the X-ray diffuse scattering method. Then, a summary of the properties of $KNbO_3$ is presented, followed by the lattice dynamical (Cochran's) theory of ferroelectricity of the perovskite type crystals.

Section two contains a statement of the problem tackled, namely, the determination of the elastic properties of $KNbO_3$ at room temperature, i.e. in the orthorhombic phase, by X-ray diffuse scattering method and to relate the same to other properties of $KNbO_3$.

Section three gives a simplified formula to obtain elastic constants from the diffuse intensity obtained by the diffractometer and photographic methods. The elastic matrices for the old theory, having 9 elastic constants, and for the new theory, having 15 elastic constants are also given in this section. The details of the values of wave normals for various directions from a given reciprocal lattice point (relp) in the orthorhombic system and their relation to the corresponding elastic constants are tabulated.

Section four describes the experimental procedures. Specimen preparation is described, followed by a comparison of the photographic and diffractometer methods for the diffuse scattering studies. A simple rotation, oscillation and Laue camera (Radius = 5.70 cm), designed and fabricated as a part of this work, has been used for the photographic measurements. G.E. XRD-6 diffractometer with single crystal orienter was used for the counter method. Monochromatic radiation from Mo target was employed. The various corrections involved in the methods (photographic and diffractometer), viz., general scattering, divergence, skew, polarization, absorption, second order, mosaic and white radiation and the application of the same to the observed diffuse intensity have been described. For the estimation of absorption correction, the linear absorption coefficient, μ, of the crystal was determined by the diffractometer method

using a scintillation counter to be 55.9 cm^{-1} (Appendix III), in excellent agreement with the calculated value (58.2 cm^{-1}). The value of the direct beam intensity I_o was also obtained using the Compton scattering from diamond as intermediate standard (Appendix II), in order to determine the absolute values of the elastic constants. The trigonometrical evaluation of the thermal wave vectors, the procedure for studying some properties like equiscattering contours and K-surfaces around a given relp, and the choice of the reflecting planes for the determination of elastic constants, are also discussed in this section.

The last part i.e. section five describes results obtained and a discussion of the same. The values of the (nine) elastic constants of $KNbO_3$, based on the old (Voigt's) theory are C_{11} = 0.3 (54), C_{22} = 0.5 (16), C_{33} = 0.6 (32), C_{44} = 3.5 (58), C_{55} = 3.6 (51), C_{66} = 2.0 (69), C_{12} = -1.0(58), C_{13} = -2.0(27), C_{23} = -1.9(14) in units of 10^{12} dynes/cm^2. Details of these calculations are described in Appendix I. An attempt to obtain elastic constants on the basis of the new theory shows that the differences in the elastic constants along certain directions obtained from both the theories are not appreciably larger than the errors involved in the method.

The C_{55} values obtained by the photographic and diffractometer techniques employing a very small crystal (volume $\sim$ 1-2 x 10^{-4} cm^3) were found to be nearly identical. Hence the time-consuming photographic method has been abandoned for

the major portion of the work in favour of the convenient, more accurate diffractometer method employing a proportional counter. Equiscattering contours around the (4,0,0) and (6,0,0) nodes are drawn, as also K-surfaces for (6,0,0) and (0,0,6) relps projected on [001] and [010] respectively. The relative values of the elastic constants obtained from the equiscattering contours and K-surfaces are consistent with the experimentally determined elastic constants by X-ray diffuse scattering. A discussion of the accuracy of results due to the various sources of error is then presented. The accuracy of C_{11}, C_{22}, C_{33} is $\pm$ 10%, of C_{44}, C_{55}, C_{66} is $\pm$ 8% and of C_{12}, C_{13}, C_{23} is $\pm$ 12%. From the values of the elastic constants the Debye temperature of $KNbO_3$ is estimated to be 302°K (Appendix IV). A qualitative correlation is indicated between thermal expansion and the thermal diffuse scattering of Potassium Niobate. It shows that the directions for which a large spread of diffuse intensity is observed (i.e. for which large amplitude of vibrations of atoms exists), are the same as the ones with a large thermal expansion.

1. INTRODUCTION

The elasticity theories, both the old (Voigt's) and the new (Laval's), are briefly reviewed, followed by a discussion of the experimental methods available for the determination of the elastic constants. Of these methods, X-ray diffuse scattering method is examined in detail. The major characteristics of ferroelectric Potassium Niobate are summarized. A discussion of the dynamical theory of ferroelectricity is also included.

1.1 Theory of Elasticity

1.1.1 Old (Voigt's) theory:

The usual starting point for elasticity theory is the postulation of Hooke's law, which states that stress T_r is proportional to strain U_s for sufficiently small strains. Its generalized statement for an anisotropic medium may be taken as

$$T_r = \sum_{s=1}^{6} C_{rs} U_s \qquad \ldots \quad (1.1)$$

The constants of proportionality (C_{rs}) are called the elastic constants, stiffness constants or moduli of elasticity. The set of linear homogeneous, independent equations represented by Eq. (1.1) can be solved for U's in terms of the T's, given by the relations

$$U_r = \sum_{s=1}^{6} S_{rs} T_s \qquad \ldots \quad (1.2)$$

The components of inverse matrix S_{rs} are called the moduli of compliance. The C_{rs} have dimensions of force per unit area, or energy per unit volume and expressed in units of dynes/cm^2. and S_{rs} have units of cm^2/dynes.

First Cauchy and later Born (1915) have developed elasticity theory on the basis of an atomistic approach and treating interatomic forces as central forces. On the other hand, Voigt (1910) treated the crystalline medium as homogeneous to all scales. Both approaches led to the same conclusion, viz, the stress and strain tensors are symmetrical. As a consequence the nine stress and nine strain components would reduce to six each. The six by six array of constants would contain 36 independent quantities in the most general case. This number is, however, reduced to 21 by the requirement that the matrices be symmetric on interchange of the double indices ($C_{rs} = C_{sr}$). This condition follows from the existence of the strain energy density W. The symmetry of the C_{rs} with respect to interchange of the subscripts is proved by applying the conditions of compatibility

$$\delta W = \sum_{r \geq s} T_{rs}\, \delta U_{rs} \qquad (1.3)$$

since δW is a perfect differential we have

$$T_{rs} = \frac{\partial W}{\partial U_{rs}} \qquad (1.4)$$

from Eqs. (1.4) and (1.1)

$$C_{rs} = \frac{\partial T_r}{\partial U_s} = \frac{\partial^2 W}{\partial U_s \partial U_r} = \frac{\partial^2 W}{\partial U_r \partial U_s} = \frac{\partial T_s}{\partial U_r} = C_{sr}$$

Assumption of linearity between stress and strain allows Eq.(1.3) to be integrated directly giving

$$W = \frac{1}{2} \sum_{s \geq 1} T_{rs} U_{sr} \qquad (1.5)$$

The number of independent elastic constants will be further reduced by the symmetry operations of the respective crystal class (e.g. there are only 9 independent constants for the orthorhombic classes, Bhagavantam, 1966). To investigate the effect of a particular symmetry operation on the elastic matrix one develops expressions for the strains in a transformed coordinate system obtained from the original by the symmetry operation. The expression for the elastic energy W (Eq. 1.5) in terms of the transformed strains is then equated identically to the original W. The resulting equation between the coefficients of corresponding strain products give the relations which reduce the number of independent elastic constants. The conventional formulation of classical elasticity suffers from the disadvantage that the strains are not presented in tensor form. As a result any transformation of the co-ordinates requires an involved treatment. An alternative formulation is due to Sokolnikoff (1946) and others. (Wooster, 1938, Love, 1944; Nye, 1957; Krishnan, 1958, Huntington, 1958; and Bhagavantam, 1966). Their

formulation utilizes the conciseness and economy of the tensor representation.

The expression for strains is

$$U_{rs} = \frac{1}{2}\left(\frac{\partial u_r}{\partial x_s} + \frac{\partial u_s}{\partial x_r}\right) \qquad (1.6)$$

To express Hooke's law in tensor notation it is necessary to treat the elastic moduli as the components of tensor of fourth order,

$$T_{rs} = C_{rskl}\, \epsilon_{kl} \qquad (1.7)$$

The transformation law for such a tensor is in the case of simple rotation

$$C_{rskl} = C_{pqtv}\, L_{rp}\, L_{sq}\, L_{kt}\, L_{lv}.$$

This expression which represents quite an involved relation provides much simpler method for determining the components of C's in new coordinate system. In equations of motion for an elastic medium, the forces on an element of volume are given by the divergence of the stress field,

$$\rho \frac{\partial^2 u_r}{\partial t^2} = \frac{\partial T_{rs}}{\partial x_r} = \frac{\partial}{\partial x_r}\left\{ C_{rskl}\, \frac{1}{2}\left(\frac{\partial u_k}{\partial x_l} + \frac{\partial u_l}{\partial x_k}\right)\right\} \qquad (1.8)$$

where ρ is density of the material. For the particular case of an elastic plane wave one can take $u_k = A_k \exp.i(\omega t - k.x)$ where A_k are amplitudes of the vibration components, ω is the angular frequency and k is the wave-number vector corresponding

to the wavelength, $\lambda = 2\pi/|k|$. The resulting equations of motion, which are called the Christoffel equations, follow

$$\rho\omega^2 A_r = C_{rmsn} A_s K_m K_n$$

In this form the equations constitute the basis for 'Long Wave' method employed by Born to develop the elastic constants from a lattice theory.

For applications to the actual situations in which the elastic constants are determined from plane wave propagation (dynamic method), it is usually preferable to transform to a co-ordinate system in which the direction of propagation is one of the axes, say X_1. In this situation all terms in Christoffel equation which involve differentiation with respect to coordinates other than that along the propagation direction drop out. The result is

$$\rho v^2 A_r = C'_{rlsl} A_s \qquad (1.9)$$

where C'_{rs} are the elastic constants in the transformed co-ordinate system and v is the velocity of propagation. Values for v can be obtained solving the secular determinant of Eq. (1.9). The elastic matrix for the old theory is given by Eq. (1.10),

$$\begin{bmatrix} A_{11} \\ A_{22} \\ A_{33} \\ A_{23} \\ A_{31} \\ A_{12} \end{bmatrix} = \begin{bmatrix} C_{11} & C_{66} & C_{55} & C_{56} & C_{15} & C_{16} \\ C_{66} & C_{22} & C_{44} & C_{24} & C_{46} & C_{26} \\ C_{55} & C_{44} & C_{33} & C_{43} & C_{35} & C_{45} \\ C_{56} & C_{24} & C_{34} & \frac{1}{2}(C_{23}+C_{44}) & \frac{1}{2}(C_{45}+C_{36}) & \frac{1}{2}(C_{46}+C_{25}) \\ C_{15} & C_{46} & C_{35} & \frac{1}{2}(C_{45}+C_{36}) & \frac{1}{2}(C_{13}+C_{55}) & \frac{1}{2}(C_{65}+C_{14}) \\ C_{16} & C_{26} & C_{45} & \frac{1}{2}(C_{64}+C_{25}) & \frac{1}{2}(C_{56}+C_{14}) & \frac{1}{2}(C_{12}+C_{66}) \end{bmatrix} \begin{bmatrix} u^2 \\ v^2 \\ w^2 \\ 2vw \\ 2wu \\ 2uv \end{bmatrix} \qquad (1.10)$$

where C_{rs} are the elastic constants.

1.1.2 New (Laval's) theory:

Born assumes the existence of central forces i.e. the atoms inside a crystalline medium are rigid impenetrable spheres. On the other hand, Laval (1951 a, b,) considers a crystalline solid to consist of positive ions, which are sensibly spherical and rigid, distributed in a periodic array in a continuous fluid of valence or conduction electrons. Since the positive ions constitute almost whole of the mass of the crystal, it is the forces which act on them that chiefly determine the elastic properties. These forces in the first approximation may be considered to be constituted of two parts. The first is produced by relative displacement of the ions and the second is the interaction of the ions with the surrounding deformed electronic medium. Only the first part may be taken to be sensibly central but not the second one.

Taking these considerations into account Laval (1951 a, b) developed an atomistic theory of elasticity and concluded that the stress and strain tensors will not be symmetrical, i.e. $T_{xy} \neq T_{yx}$ and $U_{xy} \neq U_{yx}$ (unlike in the old theory Sec. 1.1.1.), so in general there will be nine components of each of the above stress and strain tensors. Since elastic constants C'_{rs} are given by the relation, Eq. (1.1)

$$T'_r = \sum_s C'_{rs} U'_s \quad \text{where} \quad r, s = 1, 2, \ldots 9$$

there will be 81 constants for a most general case, which will be reduced to 45 due to the relation $C'_{rs} = C'_{sr}$. Similar results were obtained by Viswanathan (1954) and Raman and Viswanathan (1955). It should be mentioned here that the notations used by Raman are different from those of Laval (as given by Le Corre, 1953). Both the notations are given below for comparison.

	XX	YY	ZZ	YZ	ZX	XY	ZY	XZ	YX
Laval's notation	1	2	3	4	5	6	7	8	9
Raman's notation	1	2	3	4	6	8	5	7	9

We shall here after refer to Laval's theory as the new theory of elasticity.

The matrix of Eq. (1.10) according to old (Voigt's) theory when expressed in terms of the new theory (using Laval's notation) takes the following form,

$$\begin{bmatrix} A_{11} \\ A_{22} \\ A_{33} \\ A_{23} \\ A_{31} \\ A_{12} \end{bmatrix} = \begin{bmatrix} C'_{11} & C'_{66} & C'_{88} & 2C'_{86} & 2C'_{18} & 2C'_{16} \\ C'_{99} & C'_{22} & C'_{44} & 2C'_{24} & 2C'_{49} & 2C'_{29} \\ C'_{55} & C'_{77} & C'_{33} & 2C'_{37} & 2C'_{35} & 2C'_{75} \\ C'_{59} & C'_{27} & C'_{34} & (C'_{23}+C'_{47}) & (C'_{39}+C'_{45}) & (C'_{79}+C'_{25}) \\ C'_{15} & C'_{76} & C'_{38} & (C'_{78}+C'_{36}) & (C'_{58}+C'_{13}) & (C'_{17}+C'_{56}) \\ C'_{19} & C'_{26} & C'_{48} & (C'_{28}+C'_{46}) & (C'_{14}+C'_{89}) & (C'_{12}+C'_{69}) \end{bmatrix} \begin{bmatrix} u^2 \\ v^2 \\ w^2 \\ vw \\ uw \\ uv \end{bmatrix} \qquad (1.11)$$

From the matrix Eq. (1.11) matrix A^{-1} can be calculated and A_{11}^{-1}, A_{22}^{-1}, etc. can be derived in terms of the new theory of elasticity.

Thus the new theory of elasticity put forward by Laval (1951-1957) and Viswanathan (1955) based on the principle of homogeneous deformation led to 45 elastic constants. More recently there has been intense discussion about the real difference between the old and the new theories, e.g. Laval (1957) questioned the soundness of the rotational invariance condition which was overlooked by Viswanathan. Le Corre (1953, 1956, 1958), Raman and Viswanathan (1955) and Joel and Wooster (1957, 1958) have modified the continuum theory in order to reconcile it with the lattice theory and suggested the necessity of taking volume couples into consideration. The use of unsymmetrical stress and strain components leads to the situation that strain energy can be altered by rigidly rotating crystal. Krishman *et al* (1958) and Rajgopal (1961) have pointed out that the presence of volume couples does not lead to any departure from classical behaviour.

Experimental verification of the differences in elastic constants according to the old and new theories of elasticity have also run into difficulties. For example, experimental confirmation of deviation from classical theory of elasticity rested largely on observation of light diffraction by ultrasonic waves in Ammonium dihydrogen phosphate (ADP, a piezoelectric crystal). For this crystal Le Corre (1954) claimed a value of 1.36 ± 0.11 for the ratio C_{44}/C_{55}, while Joel and Wooster (1960) derived a value of 1.06 ± 0.02 (Bergmann's method, 1954) by analysis of an elastogram. Jaffe and Smith (1961) have measured C_{44} and C_{55} of ADP by the direct piezoelectric resonance and pulse echo methods. These reliable measurements indicate that C_{44} and C_{55} are equal, well within the experimental error limits of 0.1%. Further, the results reported on ferroelectric Rochelle Salt (Huntington, 1958) by various workers are in poor agreement. More recently, Radha and Rajgopal (1968) observed the C_{44} and C_{55} of $NaBrO_3$ crystal to be equal within 0.1%, which is less than their experimental error. It therefore seems that unequivocal results to verify the new theory are not yet available.

1.2 Experimental Methods

1.2.1 Static measurements:

The first systematic measurements of elastic constants of crystals were made by Voigt (1928) using static methods. Most of the investigators immediately succeeding him used similar

techniques. However static method is not favoured in recent times compared to the dynamic method because of the low accuracy in measuring small strains instead of resonant frequencies, which can be measured more accurately. Static method gives the isothermal moduli, while the dynamic measurements based on resonance techniques give the adiabatic moduli.

1.2.2 Dynamic measurement :

An excellent summary of the dynamic methods for measurement of elastic constants is given by Fine (1952). In the sonic and low ultrasonic range (below 1 MHz) they are generally characterized by the establishment of a standing wave resonance in a system composed, in whole or in part, of the specimen under study.

High precision can be attained comparatively easily in the dynamic methods, since they involve measurements of the resonance frequency and not the displacements (as in static measurements). For the freely vibrating system the determination of the period and the dimensions of the specimen are needed to give the acoustic velocity in the direction of propagation. More usually, the system is put under forced vibration and the frequency of maximum response is found. In both kinds of dynamic experiment, information on the damping of the mechanical system can be obtained almost in the same operation. Formula for the velocity of propagation are less simple and depend on the specimen shape. Special correction factors are involved in

obtaining wave lengths which change in accordance with the mode of oscillation and boundary conditions at the ends of the specimen i.e. whether one end is clamped or both are free (Fine, 1952). Vibrational studies of plates have also been used to measure elastic parameters, mostly of piezoelectric materials. The possibilities here are more numerous and mathematically more complex. Experimentally there is a greater likelihood for mode coupling. For dynamic measurements, as in static methods, big crystals are required which are in many cases to be cut in different directions with respect to symmetry axes; studies as a function of temperature are also very difficult. These are the limitations for its successful application.

1.2.3 Lattice Interaction with Radiation:

The methods considered so far are limited to the frequency range of mechanical vibrations controllable in the laboratory $\leq$ 1000 Mc/Sec. This is far below the region where dispersion begins. Information regarding elastic spectrum can be gained from interactions of the specimen with external radiation. Experiments with X-ray diffraction, neutron diffraction, infrared, Raman and Brillouin scattering are some examples of interaction of specimen with radiation. Of these experiments only X-rays and neutrons have been employed to give systematic quantitative data on elastic constants or non-dispersive part of the spectrum. Neutron diffraction methods also require very large specimen (1-2 cm^3); this limits the usefulness of this method whenever

it is difficult to grow large single crystals or machining them for various orientations.

Coherent diffuse scattering of X-rays, scattered by interaction with the thermal waves of the lattice, is a very useful tool to study lattice dynamics and to give information on the atomic force constants in solids. One unique advantage of this method over other methods is that only a single absolute value of the elastic constants suffices to estimate all other independent constants on the absolute scale (Prasad and Wooster, 1955). For example, in an orthorhombic crystal , there are six independent constants according to old theory (C_{11}, C_{22}, C_{33}, C_{44}, C_{55}, C_{66}). If we know the absolute value of C_{11} by some other method, from the ratios (such as C_{22}/C_{11}, C_{33}/C_{11} etc.) which are very correctly known, one can find out C_{22}, C_{33} etc. as accurately as C_{11}. Another advantage of this method is that the sample remains unstrained throughout the experiment (Ramachandran and Wooster, 1951) unlike in the other methods. The theory of the X-ray diffuse scattering is now described in detail in the following section (1.2.4).

1.2.4 X-ray Diffuse Scattering (Theory):

Excellent summaries of the theory of X-ray diffuse scattering are presented by Born (1942-43), James (1950), Slater (1958), Wooster (1962) and Cochran (1969) and of the experimental work by Laval (1938-1957), Lonsdale and Smith (1941-42), Sen (1955) and Chakraborty (1958).

The idea of determination of elastic constants from the study of diffuse X-ray reflection originates from the thermal theory of Waller (1923, 1925, 1928) and Faxen (1923). According to this theory, atoms constituting the crystalline medium vibrate continuously at all temperatures, the amplitude of vibration increases with an increase in temperature. These vibrations resolve into thermal waves which are superimposed on the static periodicity of the crystal. Consequently, regular periodicity of the crystal is modulated by each thermal wave and gives rise to a series of dynamic stratifications corresponding to each set of (h k l) planes. Coherent reflections from these dynamic stratifications will be possible at angles slightly different from the Bragg angle with respect to the static plane. The intensity of such a reflection will depend on the amplitude of modulation which is given by the amplitude of the corresponding thermal wave. The amplitude of the thermal wave will be smaller if the frequency is higher. Thus the intensity of a dynamic reflection corresponding to a particular thermal wave can be indirectly employed to give its frequency whereas the wave length, which is reciprocal of the wave vector, depends on the geometry i.e. the angle of incidence and reflection (dynamic reflection). The wave length and the frequency of a particular thermal wave being known, its velocity can be determined. Since the thermal waves corresponding to small wave vectors can be identified with the acoustic waves, their velocity in a particular direction can be related

to the elastic constants of the crystal. Now for the above principle to be applied to practical cases for the determination of elastic constants, the thermal theory was required in a form such that it could explicitly express the intensity of diffuse reflections in terms of elastic constants. This was available from the elegant mathematical treatment of the problem by Laval (1943). Essential features of this treatment are described in the following paragraphs.

Thermal vibrations of a crystal consisting of N unit cells and g atoms per unit cell can be resolved into 3 Ng independent waves. Assuming the thermal waves to be plane, the displacement $\vec{U}_j$ of an atom situated at the extremity of a vector $(\vec{I} + \vec{J})$ can be expressed as,

$$\vec{U}_j = \sum_{\alpha=1}^{3Ng} \vec{A}_{j\alpha} \cos 2\pi (\nu_\alpha t - \vec{q}_\alpha (\vec{I} + \vec{J}) + n_{j\alpha}) \qquad (1.12)$$

where,

$\vec{I} = I_1\vec{a}_1 + I_2\vec{a}_2 + I_3\vec{a}_3$; $(I_1, I_2, I_3 = 0, 1, 2, \ldots)$

$\vec{J} = J_1\vec{a}_1 + J_2\vec{a}_2 + J_3\vec{a}_3$; $(J_1, J_2, J_3 < 1)$

$\vec{a}_1$, $\vec{a}_2$, $\vec{a}_3$ are the lattice parameters,

ν_α is the frequency of a thermal wave,

$\vec{q}_\alpha$ is the wave vector of the thermal wave α,

$n_{j\alpha}$ is the phase angle at time t and

$A_{j\alpha}$ is the amplitude of vibration.

Neglecting the absorption and dispersion and excluding the Compton scattering, the total amplitude scattered by a

crystal vibrating under the influence of 3Ng thermal waves is given by the expression,

$$\epsilon \sum_I \sum_j f_j \exp. 2\pi i \left\{ \nu t + \vec{X}(\vec{I}+\vec{J}) + \sum_{\alpha=1}^{3Ng} \vec{X} A_{j\alpha} \operatorname{Cos} 2\pi \left[\nu_\alpha t - \vec{q}_\alpha (\vec{I}+\vec{J}) + n_{j\alpha} \right] \right\}$$

$$= \epsilon \sum_I \sum_j f_j \exp. 2\pi i \left\{ \nu t + \vec{X}(\vec{I}+\vec{J}) \right\} \prod_{\alpha=1}^{3Ng} \exp. 2\pi i \vec{X} \vec{A}_{j\alpha} \operatorname{Cos} 2\pi \left[\nu_\alpha t - \vec{q}_\alpha (\vec{I}+\vec{J}) + n_{j\alpha} \right] \quad (1.13)$$

where f_j is atomic scattering factor,

$\vec{X} = \dfrac{\vec{S} - \vec{S}_o}{\lambda}$; $\vec{S}$ and $\vec{S}_o$ being unit vectors along the directions of reflection and incidence, λ is the wave length of the incident radiation, ϵ is the amplitude of the wave scattered by a free electron and is given by Thomson's formula

$$\epsilon = \frac{e^2}{mc^2 r} (A^2 + B^2 \operatorname{Cos}^2 \phi)^{1/2}$$

where e and m are respectively the charge and mass of the electron, ϕ, diffraction angle, c the velocity of light, r the distance of the point of observations from the electron, A and B are the components of incident electric field perpendicular and parallel to the plane of diffraction respectively.

Let us put $2\pi \vec{X}. A_{j\alpha} = Z$

and $2\pi \left[\nu_\alpha t - \vec{q}_\alpha (\vec{I}+\vec{J}) + n_{j\alpha} \right] = \omega$

we then get

$$\exp.\ 2\pi\, i\, \vec{X}\, \vec{A}_{j\alpha}\ \mathrm{Cos}\ 2\pi \left[\nu_\alpha t - \vec{q}_\alpha\ (\vec{I} + \vec{J}) + n_{j\alpha}\right]$$

$$= e^{iZ\ \mathrm{Cos}\omega}$$

$$= J_o(Z) + iJ_1(Z)\ (e^{i\omega} + e^{-i\omega}) + i^2 J_2(Z)(e^{i2\omega} + e^{-i2\omega})$$

$$+ \ldots\ldots + i^n\, J_n(Z)(e^{in\omega} + e^{-in\omega})$$

where, J_n is the Bessel function of the order n. Now, the total radiation scattered consists of the following components:

i) The Laue-Bragg diffraction having the same frequency as that of incident beam and given by the expression

$$\epsilon\ F_o\ e^{i2\pi\nu t} \sum_I e^{i2\pi \vec{X}\vec{I}}$$

where, $F_o = \Sigma\ f_j\ H_j\ e^{i2\vec{X}\vec{J}}$

and $H_j = \prod_{\alpha=1}^{3Ng} J_o\ (2\pi\ \vec{X}\ \vec{A}_{j\alpha})$, a factor which arises due to thermal vibrations and reduces the scattering factor f_j.

ii) Laval considered general case of n^{th} order radiation due to thermal agitation and gave the following expression for the total intensity scattered (I_1) in the first order.

$$I_1 = \epsilon^2 N^2 \left\{ \sum_{\alpha=1}^{3g} |F_{\alpha M}|^2 + \sum_{\alpha=1}^{3g} |F_{-\alpha M}|^2 \right\} \qquad (1.14)$$

where $F_{\alpha M} = \sum_j f_j\ H_j\ \dfrac{J_1(2\pi \vec{X}\vec{A}_{j\alpha})}{J_o(2\pi \vec{X}\vec{A}_{j\alpha})} \cdot e^{i2\pi(\vec{M}\vec{J} + n_{j\alpha})}$

and $F_{-\alpha M} = \sum_j f_j\ H_j\ \dfrac{J_1(2\pi \vec{X}\vec{A}_{j\alpha})}{J_o(2\pi \vec{X}\vec{A}_{j\alpha})} \cdot e^{i2\pi(\vec{M}\vec{J} - n_{j\alpha})}$

and $\vec{M} = (\vec{X} \mp \vec{q})$. This has been represented by a vector diagram (Fig. 1.1).

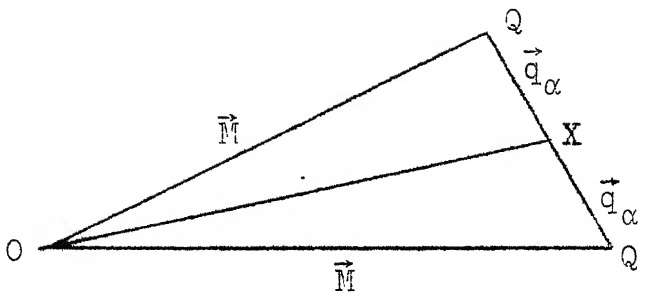

Fig. 1.1: Q is the pole of the diffusion; X reciprocal lattice point nearest to it.

All other radiations of the first order which do not have wave vectors equal to $\pm$ QX do not produce any diffuse scattering in the particular direction under consideration. For poles very near to the corresponding nodes, the fraction of the incident intensity scattered in the first order due to wave vector $\vec{q}_\alpha$, is expressed by

$$\overline{\sigma_1} = \frac{\epsilon^2 N |\vec{X}|^2}{m} \sum_{\alpha=1}^{3Ng} \frac{E_\alpha}{\nu_\alpha^2} \sum_j f_j H_j C_{j\alpha} e^{2\pi i(\vec{M}\vec{J} + n_{j\alpha})} \cos |\vec{X}.\vec{A}_{j\alpha}|^2 \qquad (1.15)$$

where $E = \dfrac{h\nu_\alpha}{e^{h\nu_\alpha/kT} - 1} + \dfrac{1}{2} h\nu_\alpha$, is the mean energy of vibration, m is the mass of the crystalline motif and $C_{j\alpha}$ are coefficients proportional to $A_{j\alpha}$ such that,

$$\frac{|\vec{A}_{j\alpha}|}{C_{j\alpha}} = \frac{|\vec{A}'_{j\alpha}|}{C'_{j\alpha}} = \frac{|\vec{A}''_{j\alpha}|}{C''_{j\alpha}} = A_\alpha$$

$\vec{A}_\alpha$ being the mean amplitude, and $\Sigma\, m_j C_{j\alpha} = m$

For polyatomic lattices one wave vector corresponds to a number of thermal waves having different frequencies. So no exact information about the frequencies can be obtained from the intensity of diffuse reflections. But for very long waves i.e. short wave vectors ($\vec{q} \to 0$), however only three acoustical waves are primarily effective in producing diffuse reflections. Since $\vec{q} \to 0$ the frequency of the three acoustical waves (one longitudinal and two transverse) approach zero while that of optical branch remains still high. The amplitude scattered by optical branch becomes inappreciably low whereas that due to acoustical branch remains high (Fig. 1.2).

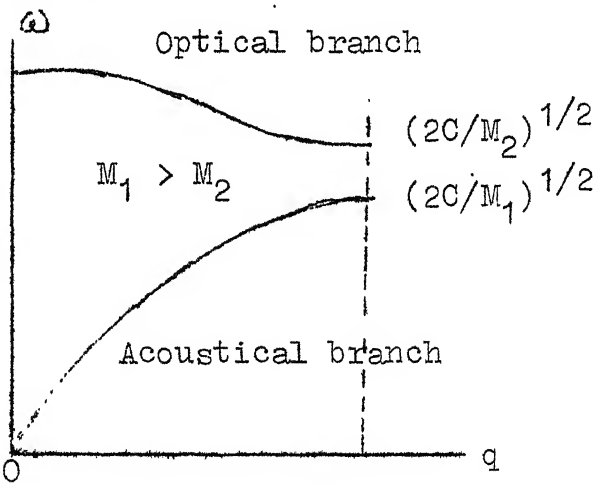

Fig. 1.2: Optical and acoustical branches of the dispersion relation for a diatomic linear lattice showing the limiting frequencies at $q = 0$ and $q = q_{max} = \pi/2a$. The lattice constant is $2a$ and M_1, M_2 are the masses of the two atoms.

For long waves $C_{j\alpha}$ can be approximately taken to be unity, and $(n'_{j\alpha} - n''_{j\alpha})$ etc. become zero as the amplitude of vibrations of different atoms due to wave α can be taken to be same in this case. Then the expression (1.15) reduces to,

$$\sigma_1 = \frac{N.F_T^2 \cdot kT\ \vec{X}^2}{m} \sum_{\alpha=1}^{3} \frac{\cos^2 |\vec{X}.\vec{A}|}{\nu_\alpha}$$

Since, $E_\alpha = kT$ as $h\nu_\alpha << kT$

or
$$\sigma_1 = \frac{\epsilon^2 N\ F_T^2\ kT}{V} \cdot \frac{\vec{X}^2}{\vec{q}^2} \sum_{\alpha=1}^{3} \frac{\cos^2 |\vec{X}.A_\alpha|}{\rho\ \vec{V}_\alpha^{\,2}} \qquad (1.16)$$

where F_T is structure factor of the plane (h k l) under consideration

ρ is density of the crystal,

V is volume of the unit cell,

V_α is the velocity of thermal wave vector $\vec{q}_\alpha$ and

α is the thermal wave.

As explained above the contribution of the optical branch of thermal vibrations to the diffuse intensity is negligible for $\vec{q} \to 0$ as compared to the contribution of the acoustic waves, the velocities of which can be expressed in terms of the elastic constants of the crystal.

Since,

$$\begin{aligned}
\rho V_\alpha^2 P_X^\alpha &= A_{11} P_X^\alpha + A_{12} P_Y^\alpha + A_{13} P_Z^\alpha \\
\rho V_\alpha^2 P_Y^\alpha &= A_{12} P_X^\alpha + A_{22} P_Y^\alpha + A_{23} P_Z^\alpha \qquad (1.17) \\
\rho V_\alpha^2 P_Z^\alpha &= A_{13} P_X^\alpha + A_{23} P_Y^\alpha + A_{33} P_Z^\alpha
\end{aligned}$$

where, P_X^α, P_Y^α, P_Z^α are the polarization vectors of the wave, i.e. the components of the unit displacement vector for the wave α. The elements A_{11}, A_{22} etc. are given by the equation (1.10).

Now,

$$\frac{\text{Cos}^2\,|\vec{X}.\vec{A}_\alpha|}{\varsigma V_\alpha^2} = \frac{1}{\varsigma V_\alpha^2}\left[(LP_X^\alpha)^2 + (MP_Y^\alpha)^2 + (NP_Z^\alpha)^2 + 2\,MNP_Y^\alpha P_Z^\alpha\right.$$

$$\left. + 2\,NLP_Z^\alpha P_X^\alpha + 2\,LMP_X^\alpha P_Y^\alpha \quad \ldots \quad \ldots\right] \qquad (1.18)$$

where L, M, N are the direction cosines of the vector $\vec{X}$ and u, v, w are the direction cosines of a thermal wave vector $\vec{q}$, with respect to the orthogonal system of the reference axes. Solving for the expressions,

$$\frac{(LP_X^\alpha)^2}{\varsigma V_\alpha^2}\ ,\ \frac{LMP_X^\alpha P_Y^\alpha}{\varsigma V_\alpha^2} \quad \ldots \quad \ldots \quad \text{etc. from Eqs. (1.17) and}$$

(1.18) we get,

$$\sum_1^3 \frac{\text{Cos}^2|\vec{X}.\vec{A}_\alpha|}{\varsigma V_\alpha^2} = L^2 A_{11}^{-1} + M^2 A_{22}^{-1} + N^2 A_{33}^{-1} + 2\,MNA_{23}^{-1}$$

$$+ 2NLA_{31}^{-1} + 2LMA_{12}^{-1} \qquad (1.19)$$

$$= K\left[u,\ v,\ w\right]_{hkl}$$

where A_{ij}^{-1} are the elements of the matrix A^{-1} which is inverse to the matrix

$$A = \begin{bmatrix} A_{11} & A_{12} & A_{13} \\ A_{12} & A_{22} & A_{23} \\ A_{13} & A_{23} & A_{33} \end{bmatrix}$$

So we have from (1.16) and (1.19)

$$\sigma_1 = \frac{\epsilon^2 N\, F_T^2\, kT}{V}\ \frac{\vec{X}^2}{\vec{q}^2}\ .\ K\left[u,\ v,\ w\right]_{hkl} \qquad (1.20)$$

A similar expression has also been derived by Begbie and Born (1947) for $\vec{q} \to 0$ by a quantum mechanical treatment.

We have till now considered the contribution of Ist order diffuse scattering only. Laval has shown that the 2nd order diffuse reflection from a pole of diffusion will be produced if the resultant of the two interacting wave vectors $\vec{q}_\alpha$ and $\vec{q}_\beta$ is equivalent to $\vec{q}$ as illustrated in the diagram (Fig. 1.3).

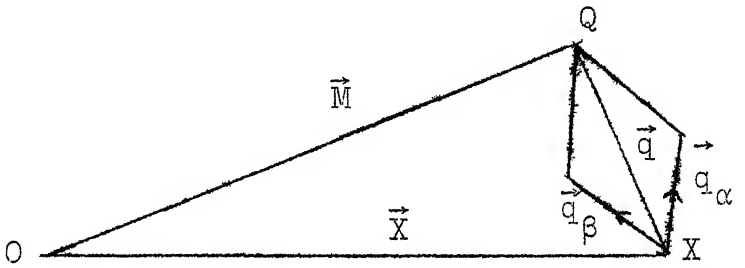

Fig. 1.3: Vector diagram for second order diffuse reflection.

The intensity diffusely scattered in the 2nd order is given by

$$\sigma_2 = \frac{k^2 T^2}{V} \frac{\pi^3}{2\rho^2} \cdot F_T^2 \vec{X}^4 \sum_\alpha \sum_\beta \frac{\mathrm{Cos}^2 (\vec{X}.\vec{A}_\alpha)}{V_\alpha^2 \vec{q}_\alpha^2} \cdot \frac{\mathrm{Cos}^2 (\vec{X}.\vec{A}_\beta)}{V_\beta^2 \vec{q}_\beta^2} \quad \ldots \quad (1.21)$$

Ramachandran and Wooster (1951) made certain approximations in view of the fact that $\sigma_2 \ll \sigma_1$ and deduced the following expression from Eq. (1.21),

$$\sigma_2 = \frac{\pi^3}{2\rho^2} \frac{N(kT)^2}{V} F_T^2 \frac{\vec{X}^4}{\vec{q}} \frac{\mathrm{Cos}^4 (\vec{X}.A_\alpha)}{V_\alpha^4} \quad (1.22)$$

$\sum_1^3 \frac{\mathrm{Cos}^4 (\vec{X}.\vec{A}_\alpha)}{\rho^2 V_\alpha^4}$ can be expressed as a function of elastic constants just as Eq. (1.19) and we may denote it by

$K'[u, v, w]_{hkl}$.

Then one gets,

$$\sigma_2 = \frac{\pi^3}{2\rho^2} \frac{N(kT)^2}{V} F_T^2 \frac{\vec{x}^4}{\vec{q}} \cdot K'[u, v, w]_{hkl} \qquad (1.23)$$

This expression can be used (if required) for correcting the observed intensity for the second order effect before evaluating the elastic constants from Eq. (1.20). This point will be discussed further in Section 4.5.6.

The matrix Eq. (1.10) has been expressed in terms of classical theory (Voigt's) of elasticity. Now according to new theory of elasticity (Sec. 1.2) the matrix Eq. (1.10) takes the form as expressed by the Eq. (1.11). From this Eq. (1.11), the matrix A^{-1} can be calculated and A_{11}^{-1} , A_{22}^{-1} , etc. can be derived in terms of the new theory of elasticity and on substitution in Eq. (1.19), it can be combined with Eq. (1.10) to express the intensity of diffuse reflection corresponding to particular direction of propagation of thermal wave and particular reciprocal lattice point. The expression in Eq. (1.19) is generally simplified (involving very small number of elastic constants, even one or two in some cases) for certain nodes and simple directions of propagation of thermal wave. Observations on intensity of diffuse reflections along such directions would yield elastic constants.

1.2.5 The X-ray diffuse scattering (Experimental):

The method was for the first time successfully employed by Ramachandran and Wooster (1951) for the determination of elastic constants of some cubic crystals. They used a Geiger counter spectrometer suitably modified for the measurement of feeble X-ray intensities. The method was later on used by Wooster and his collaborators (Prince and Wooster 1951, 1953, Prasad and Wooster 1955, 1956 etc.) for determining the elastic constants of a number of crystals (mostly inorganic cubic and more symmetrical tetragonal i.e. 4 2, $\bar{4}$ 2m,4/mm - crystal classes). They have also determined the ratios of the elastic constants (Hoerni and Wooster 1952, Prasad and Wooster 1956) by photographic method of measuring intensities. To derive absolute values of elastic constants Wooster and collaborators have used bulk modulus data taken from other sources (Bridgman, 1938, 1945) or Compton scattering from diamond (Compton and Allison 1935).

Sen (1955), Chakraborty (1958) and Chakraborty and Sen (1958) have developed and standardised a method (of the quantitative study of absolute measurements of the intensity of diffuse reflections by photographic photometry and also determine the elastic constants of Benzil (crystal class D_3) from X-ray study only.

1.3 Potassium Niobate ($KNbO_3$)

$KNbO_3$ is an orthorhombic perovskite type crystal at room temperature. It exhibits ferroelectricity (Matthias 1949), a property of the crystal having spontaneous polarization which can be reversed by means of an electric field. (Ferroelectricity was ably summarized by Jona and Shirane (1962), Fatuzzo and Merz (1967)).

1.3.1 Phase transitions in $KNbO_3$ crystal:

A crystal of Potassium Niobate undergoes the following phase transitions (Shirane et al (1954), Schenk (1969)) in the same order as in $BaTiO_3$.

Rohombohedral $\xrightarrow{-10^{\circ}C}$ orthorhombic $\xrightarrow{225^{\circ}C}$ Tetragonal $\xrightarrow{435^{\circ}C}$ cubic. The Curie temperature of $KNbO_3$ lies at $435^{\circ}C$. All these phase transitions are of first order and connected with detectable temperature hysteresis (Shirane et al (1954)).

1.3.2 Single crystal growth:

Single crystals of $KNbO_3$ were first produced from binary melts using an excess of K_2CO_3 as a flux (Wood, 1951) Molten mixture of 1.2 mole of K_2CO_3 and 1 mole Nb_2O_5, gives quite large flawless crystals (Miller, 1958). The phase relationships in the system K_2CO_3-Nb_2O_5 were studied by Reisman and Holtzberg (1955, 1956). The melting point of $KNbO_3$ is about $1050^{\circ}C$.

1.3.3 Dielectric properties:

The dielectric constant of multidomain crystals of $KNbO_3$ as a function of temperature were studied by Wood (1951), Timofeeva et al (1962) and in more detail by Shirane et al (1954). The dielectric constant vs. temperature curve obtained by Shirane et al, shows a marked resemblance to the higher branch of the curve for $BaTiO_3$ (Merz, 1949). The temperature dependence of the spontaneous polarization was measured by Triebwasser *et al* (1956). The value of P_s just below Curie temperature is 26×10^{-6} C/cm^2.

1.3.4 Thermal Expansion:

The temperature dependence of the lattice parameters of $KNbO_3$ was studied first by Wood (1951) and in more detail by Shirane et al (1954). The general appearance of the curve is again quite similar to the corresponding curve of $BaTiO_3$ (Kay and Vousden, 1949), but the spontaneous strain in $KNbO_3$ is larger in all the three phases. This is quite expected since the Curie temperature which is generally indicative of the strength of interactions, is larger in the case of $KNbO_3$ than that of $BaTiO_3$. Accordingly transition energies are considerably larger for $KNbO_3$ than for $BaTiO_3$ at each of the three phase changes. (Shirane et al 1954, Triebwasser et al 1955).

1.3.5 Piezoelectric and Elastic properties:

The dielectric anamolies and phase transitions in single crystals of Potassium niobate are discussed in sections 1.3.3 and 1.3.1. We may proceed a step further and enquire which of

the piezoelectric and elastic coefficients behave anamolously as the transition temperature is approached? Unfortunately, for this particular crystal no detailed studies have been made in this direction. Dielectric and piezoelectric properties have been reported by Timofeeva and Popova (1962). They have reported only one piezoelectric constant d_{33} and its temperature dependence. No elastic constant data have been reported to date on single crystals of Potassium Niobate (as far as author is aware). Egerton and Dillon (1959), Jaeger and Egerton (1962) have studied ceramic samples of $Na_{0.50}K_{0.50}NbO_3$. They have reported Young's modulus and two piezoelectric constants d_{31} and d_{33} respectively. Their study would have been useful for extrapolating constants for pure $KNbO_3$. Unfortunately they have not reported the data for other compositions in detail. From theoretical point of view, this system (Na, K) NbO_3 was studied in detail by Cross (1956), who applied the thermodynamic treatment developed by Devonshire (1949) for $BaTiO_3$ to both $NaNbO_3$ and the system (Na, K)NbO_3. His theory explains only dielectric properties and the various transition temperatures observed in the system.

1.3.6 Crystal Structure:

The structure of Potassium Niobate at room temperature has been investigated in detail by Katz and Megaw (1967). The structure is strictly isomorphous with orthorhombic $BaTiO_3$, with the space group Bmm2 and 2 molecules per unit cell, but all deviations from perovskite aristotype are rather larger in

$KNbO_3$. A good comparison regarding the structure of $KNbO_3$ and $BaTiO_3$ in orthorhombic phase is given by the above authors. Cell dimensions given by Katz and Megaw at room temperature are a = 5.697 Å, b = 3.971 Å, c = 5.721 Å in agreement within about 0.001 Å with those of Vousden (1951), Shirane, Newnham and Pepinsky (1954). Zr filtered MoKα radiation was used in the above investigation. Structure factor data used in the present investigation are taken from Katz and Megaw (1967) and Dwivedi and Srivastava (1969).

1.3.7 Comparison of $KNbO_3$ and $BaTiO_3$

It is worth mentioning that to date $KNbO_3$ is the only perovskite ferroelectric crystal that exhibits the same phase symmetries and same sequence of transitions as $BaTiO_3$. A comparison between some of the pertinent data of the two crystal, taken from Jona and Shirane (1962), are shown in Table 1.1.

1.4 Lattice dynamical theory of ferroelectricity:

A very successful attempt has been made by Anderson (1960) and in more detail by Cochran (1960,61, 67,69) and Cowley (1963) to provide a microscopic theory (based on Dick and Overhouser model, 1958) of ferroelectricity for certain crystals (Perovskite type, displacive ferroelectrics etc). This is based on the assumption that ferroelectric transitions are the result of an instability for a particular normal mode of vibration, and they can be treated as a problem in lattice dynamics. Details of this theory are presented by Fatuzzo and Merz (1967).

Table 1.1

Comparison between $KNbO_3$ and $BaTiO_3$

	$KNbO_3$	$BaTiO_3$
Transition temperatures ^oC	435, 225, -10	120, 5, -90
Transition energies (Cal/Mole)	190, 85, 32	49, 21, 11
Maximum tetragonal distortion c/a	1.017	1.01
Spontaneous polarization at the Curie point (10^{-6} C/cm^2)	26	18
Curie constant $C(^oK)$ as defined from $\epsilon = C/T-T_o$	2.4×10^5	1.7×10^5
$T_c - T_o$ (^oC)	58	11
Coefficients $\xi_{11}X$ and $\zeta_{111}X$ of the free energy expansion $A = \frac{1}{2} \times XP^2 + \frac{1}{2}\xi_{11}XP^4 + \frac{1}{6}\zeta_{111}XP^6$	$\xi_{11}X = -10\times10^{-13}$ c.g.s. $\zeta_{111}X = 54\times10^{-23}$ c.g.s.	-20×10^{-13} c.g.s. 25×10^{-23} c.g.s.

Essentially, the theory is based on the argument that if a crystal is wholly or partly ionic, lattice vibrations are accompanied by polarization oscillations of equal frequencies which create a local field interacting with ions through long-range Coulomb forces. If for one particular mode of vibration, these long range Coulomb forces and short range forces balance out, then the crystal becomes unstable for this mode.

The detailed mathematical treatment is not given here. Only the final results, as a consequences of the theory, are quoted below.

The dielectric constant ϵ_s is connected to the frequency ν_F of a critical mode by Eq. (1.24)

$$\epsilon_s = K \nu_F^2 \qquad (1.24)$$

where K is a proportionality constant and is independent of temperature. As the temperature approaches the Curie point, ϵ_s becomes extremely large and ν_F tends to decrease rapidly. The occurrence of ferroelectricity and the crystal instability can be connected by Lyddane, Sachs, Teller (L.S.T.) relation (1941).

$$\frac{\omega_L^2}{\omega_T^2} = \frac{\epsilon_s}{\epsilon_e} \qquad (1.25)$$

ϵ_s the static dielectric constant,

and ϵ_e the optical dielectric constant is equal to the square of the refractive index. ω_L is longitudinal frequency and ω_T the transverse optical frequency at $q = 0$ (wave vector).

This L.S.T. relation is written for two atoms per unit cell. Cochran (1960) has extended this treatment for a more general case of n atoms in the elementary cell,

$$\epsilon_s/\epsilon_e = \prod_{j=2}^{n} \frac{(\omega_j^2)_L}{(\omega_j^2)_T} \qquad (1.26)$$

$(\omega_j)_L$ and $(\omega_j)_T$ have the usual meaning as stated above. This relation is obtained from lattice dynamical equation (Cochran 1960). The equation (1.26) is derived on many physically unrealistic assumptions; one of them is that this relation is true only for diagonally cubic crystals i.e. ones in which every atom has surroundings of the tetrahedral symmetry. However, no ferroelectric crystal having this symmetry has yet been discovered (Fatuzzo and Merz 1967). Further shell model treatment is not adequate in the electronic frequency range (though these frequencies do not appear in the final results). Further we assume that the Eq. (1.26) (although this has not been proved conclusively) is valid for every cubic crystal. If one of the transverse optical branches vanishes in the neighbourhood of $q = 0$, at a certain temperature, then the static dielectric constant (Eq. 1.26) becomes infinite at that temperature which is precisely what happens at the transition from ferroelectric to paraelectric state, i.e. frequency $\omega_F(2\pi\nu_F)$ of a ferroelectric mode varies with $(T - T_o)$ as

$$\omega_F^2 \alpha (T - T_o) \qquad (1.27)$$

To is Curie temperature. This equation is generally considered a fundamental consequence of Cochran's theory (1960,61) and one which provides a good check for its validity.

Since the 'ferroelectric soft mode' of abnormally low frequency lies in the far infrared following experiments have been used to search for such a mode.

i. Far infrared (Reflectivity expt. also)

ii. Raman spectrum

iii. Dielectric dispersion

iv. Neutron diffraction

There are some experimental difficulties which one comes across in verifying the existence of soft ferroelectric mode (Cochran's mode) for example, undoubtedly Raman and Infrared experiments could clarify the occurrence of low frequency transverse optical mode (Cochran's mode) but because of the limitations of the experiments, it is difficult to find the ferroelectric mode in perovskites by analysing their far infrared data (Barker 1966). Details are described by Dvorak (1967). Now low frequency mode in millimeter range is experimentally very difficult to handle and if a crystal possesses a high conductivity (as in the case of $KNbO_3$) near the transition temperature the dielectric dispersion study becomes impossible. Neutron dispersion, may be comparatively easy if special care is taken for several important corrections, further this requires very

large single crystals. Experimentally the existence of this soft phonon mode and its strong temperature dependence have been observed in $SrTiO_3$ and $KTaO_3$ (Yamada and Shirane 1969). These are both perovskite type crystals which show an anomalous temperature-dependent dielectric constant, but neither of these materials actually undergo a ferroelectric transition. On the other hand, in the case of $BaTiO_3$ which undergoes a ferroelectric transition around 125°C, the results on the existence of a soft phonon mode as determined by different experimental techniques are found to be in disagreement with each other (e.g. Barker, 1966 and Ballantyne, 1962). Recently, Harada et al (1967) deduced a soft phonon mode energy from X-ray diffuse scattering studies. The significance of these X-ray results is the fact that this optic mode energy, lies much below the energy of the acoustic mode. This has been confirmed by the thermal neutron study of Shirane et al (1969). It is interesting to note that Bell and Ruppercht (1963) have observed a minimum in the elastic constant vs. temperature curve of $SrTiO_3$, but no corresponding maximum or even change of the slope in the dielectric constant vs. temperature curve. If the particular short range lattice forces that determine the elastic properties are also connected with the frequency of the soft mode, a discontinuity of dielectric constant would be expected. These results how that the short range forces responsible in $SrTiO_3$ for sound opagation are not connected with dielectric properties. It is ly surprising to see that a marked change in the elastic

constant vs. temperature graph can occur with little or no observable effect on the dielectric constant. Similar observations have been reported by Cummins (1970) on $Gd_2(MoO_4)_3$.

Recent work due to Shapiro and Cummins (1968) on phase transition in Quartz, Amoros (1968) on $NaNO_2$ and triglycine sulphate, by Honjo and Harada (1969) on α, and β, Quartz, shows that optical mode of low frequency is not responsible for the ferroelectric transitions. (Cross et al 1968) (T,G.S. and Quartz are the examples cited by Cochran (1960-61) in his theory of displasive ion model). Very recently, a disorder theory for $BaTiO_3$ and $KNbO_3$ is proposed by Lambert, Comes and Guinier (1969) and Comes et al (196 in which they claim to account for the ferroelectric transition in a better manner than the alternative explanation of soft mode by Cochran (1960-61).

The theory of ferroelectricity developed by Cochran has been briefly summarized above. Now we shall discuss how the elastic constants of $KNbO_3$ determined from the X-ray diffuse scattering studies are likely to be affected in the light of Cochran's theory.

If one recalls the expression for the diffuse intensity, it is comprised of two parts, intensity of acoustic vibrations and the intensity due to the optical vibrations.

$$I_{diffuse} = I_{ac} + I_{opt.} \qquad (1.28)$$

Generally the optical contribution is negligibly small (owing to high frequency) and hence is eliminated as general scattering correction. If the elastic constants of this crystal ($KNbO_3$) are known by methods other than X-ray diffuse scattering, one can easily find out the contribution of the low lying optical frequency and from this the corrected elastic constants. But to date no such elastic constants data are available (as far as author is aware). Secondly if the infrared or Raman spectrum of this compound is available then one can try to find out the optical frequency contribution to the total diffuse intensity. Recently Perry et al (1969) have reported the Raman laser spectrum of Potassium Niobate, in all the four phases. They also studied the temperature variation in the rhombohedral and orthorhombic phases. But in their spectrum no such low frequency mode has been observed. The temperature dependence of phonon associated with different frequencies is hardly 1%. The lowest frequency in the orthorhombic phase which they have reported is 298 cm^{-1}. Potassium Niobate has a high Curie temperature, around 708°K. Then if we recall the famous Cochran's equation (1.27) we see the difference $T-T_0$ is very large at room temperature and would be definitely finite and hence the elastic constants will not diverge from their normal value. If one makes a very crude approximation that $KNbO_3$ is cubic at room temperature and finds the corrections to the elastic constants as shown by Cowley (1964), the correction does not exceed normally 1-3% . Due account

can be taken of such corrections for low frequency optical mode. That is, the values of the elastic constants of a single crystal of Potassium Niobate would be hardly affected at room temperature due to this transverse phonon mode (Cochran's mode) of low frequency.

1. REFERENCES

Amoros, J.L. and Amoros, M.	Molecular Crystals, John Wiley and Sons (1968).
Anderson, P.	Fizika Dielectrikov, ed G.I.Skanavi, (Akad.Nauk SSSR, Fiz.Inst.im.P.N. Lebedeva, Moscow, 1960).
Ballantyne, B.M.	Phys. Rev. 126, 1710 (1962).
Barker, A.S.	Phys. Rev. 145, 391 (1966)
	Proc. Symp. Ferroelectricity, Michigan, 213-250, Ed.Weller Elsevier Pub. Co. (1967).
Begbie, G.H. and Born M.	Proc. Roy. Soc., A188, 179, 189 (1947).
Bell, R.O. and Rupprecht, G.	Phys. Rev. 129, 90, (1963).
Bergmann, L.	Der Ultraschall, 5th ed.Stuttgart (1954).
Bhagavantam, S.	Crystal Symmetry and Physical Properties, Acad. Press, (1966).
Born, M.	Atom theorie des festen Zustandes Ency. Math. Wiss, (1909-1915-1926).
	Rep. Prog. Phys. 9, 294, (1942-43).
Bridgman, P.W.	Proc. Amer. Acad. Arts Sci., 72, 207, (1938).
	Ibid, 76, 9, (1945).
Chakraborty, S.C.	D.Phil Thesis, Allahabad Univ. (1958).
Chakraborty, S.C. and Sen, R.K.	Proc. Symp. Cryst. Phy. Nat.Inst.Sci. Ind. Bull. 14, 20-35, (1958).
Cochran, W.	Advan, Phys. 9, 387, (1960).
	Ibid, 10, 401, (1961).
	Symp. Ferroelectricity, 62-71, Ed. Weller, Elsevier, Pub.Co. (1967).

	Lattice Dynamics, 93-137, Benjamin (1969).
Cochran, W. and Cowley, R.A.	Handb. Phys. 35/2A, 59, Berlin Springer, (1967).
Comes, R., Lambert, M. and Guinier, A.	Solid, State. Commun. 6, 715 (1968)
	Secd. Int. Conf. Ferroelectricity, 123, Kyoto, Japan (1969).
Compton, A.H. and Allison, S.K.	X-rays in Theory and Experiments Van Nostrand (1935).
Cowley, R.A. and Cochran, W. et.al.	Phys. Rev. 131, 1030, (1963).
Cowley, R.A.	Ibid, 134, A981-997, (1964).
Cross, L.E.	Phil. Mag. Ser. 8, 1, 76, (1956).
Cross, L.E., Fouskova, A. and Cummins, S.	Phys. Rev. Letters, 21, 812, (1968).
Cummins, S.E.	Ferroelectrics, 1, 16, (1970).
Dick, B.G.Jr. and Overhauser, A.W.	Phys. Rev. 112, 90, (1958).
Devonshire, A.F.	Phil. Mag. 40, 1040, (1949).
Dvorak, V.	Phy. Rev. 159, 652, (1967).
Dwivedi, G.L. and Srivastava, R.C.	Unpublished work (1969).
Egerton, L. and Dillon, D.M.	J. Am. Ceram. Soc. 42, 438, (1959).
Fatuzzo, E. and Merz, W.J.	Ferroelectricity, 7, North Holland Pub. Co. (1967).
Faxen, H.	Z. Phys. 17, 266, (1923).
Fine, M.E.	A.S.T.M. Bull, 181, 20, (1952).
Harada, J., Honjo, G., Mitsui, T. and Hoshino, S.	J.Phy.Soc. Japan, 22, 1515, (1967).
Honjo, G. and Harada, J	J.Phy.Soc. Japan, 23, 1558 (1969).
Huntington, H.B.	Solid State Physics 7, 213-351, Acad. Press (1958).

Hoerni, J. and Wooster, W.A.	Acta Cryst. 5, 386 (1952).
Jaeger, R.E. and Egerton, L.	J. Am. Ceram. Soc. 45, 209-13 (1962).
Jaffee, H. and Smith, C.S.	Phys. Rev. 121, 1604 (1961)
Jona, F. and Shirane, G.	Ferroelectric Crystals, Pergomon Press (1962).
James, W.	Optical Principles of X-ray Diffraction, G.Bell and Son, London (1950).
Joel, N. and Wooster, W.A.	Nature, Lond. 180, 430, (1957).
	Acta Cryst. 11, 573, (1958).
	Ibid., 13, 516, (1960).
Katz, L. and Megaw, H.D.	Acta. Cryst. 22, 639, (1967).
Kay, H.F. and Vousden, P.	Phil.Mag. 40, 1019 (1949).
Krishnan, R.S.	Prog. in Crystal Phys. 1, 73-101 (1958). S. Viswanathan, Ma
Krishnan, R.S. Chandrasekhran, V. and Rajagopal, E.S.	Nature Lond. 182, 518, (1958).
Lambert, M., Comes, R. and Guinier, A.	Service de Physique des Solides Faculte des Sciences 91-ORSAY, Phy.Sol.69/81, (1969).
	Solid State. Commun. 7, 305, (1969).
Laval, J.	C.R. Acad. Sci. Paris 207, 169, (1938).
	Bull. Soc. France, Miner. Cryst. 69, 137, (1939).
	Ibid, 64, 1 (1941).
	J. Rad. Phys. 4, 1, (1943).
	C.R. Acad. Sci. Paris, 232, 1947, (1951a)
	L'etate Solide Rapporte et discussions Congre's Solvay, Bruxselis, Stoops (1951b).
	J.Phy.Rad. 18, 247, 289, 369, (1957).

Le Corre,	Bull. Soc. France. Miner. Cryst. 76, 464 (1953).
	C.R. Acad. Sci. Paris, 236, 1903,(1953).
	Bull. Soc. France.Miner. Cryst. 77, 1363, 1393, (1954).
	Ibid, 78, 33, (1955).
	J. Phys. Rad. 17, 924, (1956).
	J. Phys. Rad. 19, 541, (1958).
Lonsdale, K. and Smith H.	Proc. Roy. Soc. A 179, 8, (1941).
	Nature Lond. 148, 628, (1941).
	Ibid, 149, 21, (1942).
Love, A.E.H.	Mathematical Theory of Elasticity Dover, (1944).
Lyddane, R.H., Sachs,R.G. and Teller, E.	Phys. Rev..59, 673, (1941).
Matthias, B.T.	Phys. Rev. 75, 1771, (1949).
Merz, W.J.	Phys. Rev. 76, 1221, (1949).
Miller, C.E.	J. Appl. Phys. 29, 233, (1958).
Nye, J.F.	Physical Properties of Crystals, Clarendon Press, Oxford (1957).
Perry, C.H. and Tornberg, N.E.	Proc. Int. Conf. Light Scattering Spectra of Solids, 467-76, New York, Springer vVerlag (1969).
Prasad, S.C. and Wooster, W.A.	Acta Cryst. 8, 361, 507, 614, 682, (1955).
	Ibid, 9, 35, 38, 169, 304, (1956),
Prince, E. and Wooster, W.A.	Acta Cryst. 4, 191 (1951).
	Ibid, 6, 450, (1953).
Radha, V. and Raja Gopal, E.S.	J. Ind. Inst. Sci. 50, 26, (1968).
Rajagopal, E.S.	J. Sci. Industr. Re. 20B, 50, (1961).

Ramachandran, G.N. and Wooster, W.A.	Acta Cryst. 4, 335, (1951).
	Ibid, 4, 437, (1951).
Raman, C.V., and Viswanathan, K.	Proc. Ind. Acad. Sci. 42A, 1, 51, (1955).
Reisman, A, and Holtzberg, F.	J. Am. Chem. Soc. 77, 2115 (1955)
Reisman, A., Holtzberg, F., Triebwasser, S. and Berkenblit, M.	J. Am. Chem. Soc. 78, 719, (1956).
Schenk, M.	Phys. Stat. Sol. 36, K31, (1969).
Sen, R.K.	D.Sc. Thesis, Allahabad Univ. (1955).
Shapiro, S.M. and Cummins, H.Z.	Phy. Rev. Letters, 21, 1578 (1968).
Shirane, G. Danner, Pavlovic and Pepinsky, R.	Phys. Rev. 93, 672 (1954).
Shirane, G., Newnham, R. and Pepinsky, R.	Phys. Rev. , 96, 581, (1954).
Shirane, G. and Yamada, Y.	Ibid, 177, 858, (1969).
Slater, J.C.	Rev. Mod. Phys. 30, 197 (1958).
* Timofeeva, V.A., and Popova, A.S.	Soviet Phys. Cryst. 7, 235, (1962).
Triebwasser, S. and Halpern, J.	Phys. Rev. 98, 1562, (1955).
	Ibid, 101, 993, (1956).
Viswanathan, K.	Proc. Ind. Acad. Sci. A39, 196, (1954).
	Ibid, A41, 98 (1955).
Voigt, W.	Lehrbuch der Kristall Physik, Leipzig, Teubner (1910-1928).
Vousden, P.	Acta Cryst. 4, 373, (1951).
* Sokolnikoff, I.S.	Mathematical Theory of Elasticity,

Waller, I.	Z. Phys. 17, 398, (1923).
	Dissertation, Uppsala (1925).
	Z. Phys. 51, 213, (1928).
Wood, E.A.	Acta Cryst. 4, 353, (1951).
Wooster, W.A.	Crystal Physics, Camb.Univ. Press (1938).
	Acta Cryst. 14, 571, (1961).
	Diffuse X-ray Reflections from Crystals, Clarendon Press, Oxford, (1962).
Yamada, Y. and Shirane, G.	Phys. Rev. 177, 848, (1969).

2. STATEMENT OF THE PROBLEM

The behaviour of a ferroelectric crystal is characterized by its dielectric, elastic and piezoelectric constants. Such complete data are available on very few ferroelectric materials. Potassium Niobate with its high Curie temperature ($708^{\circ}K$) is a potentially useful ferroelectric. The interest in this compound is further enhanced by its close similarity to the much studied ferroelectric Barium Titanate (Table 1.1). However as pointed out in Sec. 1.3.3, fairly detailed dielectric data are available, while knowledge of the elastic and piezoelectric constants of Potassium Niobate is lacking. The main purpose of this investigation therefore is to evaluate the elastic constants of Potassium Niobate ($KNbO_3$) at room temperature i.e. in the orthorhombic phase. X-ray diffuse scattering method has been employed for this purpose in the present study, both by photographic and diffractometer technique.

A crystal of Potassium Niobate belongs to an orthorhombic {mm2} class and has 9 elastic constants according to old (Voigt's) theory and 15 elastic constants according to new (Laval's) theory. In order to measure all the nine elastic constants (old theory) a crystal under investigation has to be mounted along all the three mutually perpendicular axes. The study of the following Bragg reflections were made on the XRD-6 (G.E.) counter diffractometer with CA-7 MoKα target, operated at 35 KVP/25 mA.

Relp (Reciprocal Lattice Point) (6,0,0) with c-axis vertical (i.e. perpendicular to the equatorial plane of the diffractometer.) gives the constants C_{11} and C_{66} independently and the dependence of constant C_{12} on other constants.

The relp (0,0,6) with b-axis along the vertical gives the constants C_{33} and C_{55} independently and the dependence of C_{13} on other constants (Tables 3.1 , 3.2 and 3.3).

The relp (0,4,0) with a-axis vertical gives the constants C_{22} and C_{44} independently and the dependence of C_{23} on other constants.

The choice of the above planes (relps) for the study is explained in Section 4.5.10.

In this way all the constants (of the old theory) have been obtained (Tables 3.1, 3.2, 3.3). Additional constants of the new theory also have been evaluated and shown to be similar to the ones obtained from the old (Voigt's) theory. In each relp normally three rekhas (any line drawn through the given relp) have been studied on either side of the relp. For each rekha 5 to 7 sets of observation are recorded on the proportional (Xe-filled) counter. For each observation, time for 10,000 counts was recorded. Zr-Y balanced pair of filters have been used during the entire diffractometer observations. On the other hand photographic data were obtained on rotation, oscillation and Laue camera with crystal (LiF) reflected monochromatic

MoKα radiation (operated at 35 KVP/25mA). Each exposure for diffuse spots, ran for 35 to 40 hours. Type F X-ray films were employed.

In addition to this the relps (4,0,0) and (0,0,4) with b-axis vertical have been studied on the XRD-6 diffractometer. The crystal used for these relps was very small (Vol. 1.782 x 10^{-4} cc). The results obtained from these relps are compared with those obtained by photographic technique on an equally small crystal (Vol. 0.996 x 10^{-4} cc) from the relp (4,0,0) with b-axis vertical. The constants obtained by these two different techniques are in very good agreement, suggesting that one can also work on the diffractometer with such a small crystal, as the one used in the present investigation. The diffractometer technique is obviously more convenient and handy, besides giving better accuracy.

Some of the thermodynamic parameters can be obtained from the observed elastic constants. One such parameter viz. the Debye temperature is obtained. An attempt is made to inter-relate the elastic constants and thermal expansion as to correlate the same with the crystal structure.

3. A SIMPLIFIED FORMULA FOR THE DIFFUSE INTENSITY AND THE ELASTIC CONSTANTS

The general formula for the ratio of the intensity of diffuse X-ray reflection I_d (Ist order only, second order correction is neglected for the present) to that of the incident beam I_o corresponding to thermal wave vector $\vec{q}$ and the reciprocal lattice point (h,k,l) is given by Eq. (1.20). The corresponding formula for the diffractometer and photographic methods are given by Eq. 3.1 and 3.2 respectively.

3.1 Formulae

Diffractometer method (Ramachandran and Wooster, 1951)

$$\sigma_1 = \frac{I_d}{I_o} = \frac{\epsilon^2 kT \Omega}{2\mu_c V^2} F_T^2 \frac{\vec{X}^2}{\vec{q}^2} K[u, v, w]_{hkl} \qquad (3.1)$$

per unit cell.

where $\epsilon^2 = \left(\frac{e^2}{m.c^2}\right)^2 (A^2 + B^2 \cos^2 \phi)$

Symbols have been explained in Sec. 1.2.1.

Photographic method (Srivastava, 1960, Joshi 1964, Kashyap, 1964)

$$\sigma_1 = \frac{I_d}{I_o} = \frac{\epsilon^2 \delta V kT}{V^2} F_T^2 \frac{\vec{X}^2}{\vec{q}^2} K[u,v,w]_{hkl} \qquad (3.2)$$

where $\epsilon^2 = \left(\frac{e^2}{mc^2 r}\right)^2 (A^2+B^2 \cos^2 \phi)$

r is the radius of the camera (r = 5.70 cms.)

μ_c is the linear absorption coefficient of the crystal

δV is the volume of the crystal

V is the volume of the unit cell

T is the absolute temperature at which observations are made.

k is the Boltzmann constant

Ω is the solid angle subtended at the crystal by the counter collimator slit

I_o is the direct beam intensity

F_T is the structure factor of the plane (h,k,l) at temperature T.

$\vec{q}$ is the thermal wave vector

$\vec{X}$ is the rel vector (a line joining a given point (relp) to the origin of the reciprocal lattice) corresponding to the given relp (h,k,l)

and

$$K[u,v,w]_{hkl} = L^2A^{-1}_{11} + M^2A^{-1}_{22} + N^2A^{-1}_{33} + 2MNA^{-1}_{23} + 2NLA^{-1}_{31} + 2LMA^{-1}_{12} \qquad (3.3)$$

where L, M, N and u, v, w are the direction cosines of $\vec{X}$ and $\vec{q}$ respectively corresponding to the orthogonal elastic axes. A^{-1}_{ij} are the matrix elements of the matrix A^{-1};

where,

$$A^{-1} = \frac{\text{adj.A}}{\text{det.A}} \text{ ; and det } A = \begin{vmatrix} A_{11} & A_{12} & A_{13} \\ A_{12} & A_{22} & A_{23} \\ A_{13} & A_{23} & A_{33} \end{vmatrix} \qquad (3.4)$$

where A_{11}, A_{22} etc. are given by the matrix equation. (3.4). The expression $K[u, v, w]_{hkl}$ becomes simpler for crystals of higher symmetry and for particular reciprocal lattice points and particular directions of propagation of the thermal waves. Simple expressions for both theories of elasticity (using matrix Eq. 1.10 for old theory and Eq. 1.11 for the new theory) are derived in sections 3.1.1 and 3.1.2.

The term for the volume of the crystal (δV) is not occuring in the expression (Eq. 3.1) used for the diffractometer method for the reason that I_o, the direct beam intensity, is independently obtained in this method, unlike the photographic method (Eq. 3.2) as explained in detail in Sec. 4.5.5.

3.1.1 Classical theory:

Potassium Niobate belongs to orthorhombic Bmm2 (Katz and Megaw, 1967) crystal class. The elastic constants in this system are given by the following matrix. (Krishnan, 1958, Bhagavantam 1966, Prasad and Wooster, 1956. Wooster, 1962).

$$\begin{matrix} C_{11} & C_{12} & C_{13} & 0 & 0 & 0 \\ & C_{22} & C_{23} & 0 & 0 & 0 \\ & & C_{33} & 0 & 0 & 0 \\ & & & C_{44} & 0 & 0 \\ & & & & C_{55} & 0 \\ & & & & & C_{66} \end{matrix} \qquad (3.5)$$

Now from the matrix equation (1.10) we can get expressions for A_{ij} for a general case as follows (Ramachandran and Wooster, 1951),

$$
\begin{aligned}
A_{11} &= u^2C_{11} + v^2C_{66} + w^2C_{55} + 2vwC_{56} + 2wuC_{15} + 2uvC_{16} \\
A_{22} &= u^2C_{66} + v^2C_{22} + w^2C_{44} + 2vwC_{24} + 2wuC_{46} + 2uvC_{26} \\
A_{33} &= u^2C_{55} + v^2C_{44} + w^2C_{33} + 2vwC_{43} + 2wuC_{35} + 2uvC_{45} \\
A_{23} &= u^2C_{56} + v^2C_{24} + w^2C_{34} + vw(C_{23}+C_{44}) + wu(C_{45}+C_{36}) + uv(C_{46}+C_{25}) \\
A_{31} &= u^2C_{15} + v^2C_{46} + w^2C_{35} + vw(C_{45}+C_{36}) + wu(C_{13}+C_{55}) + uv(C_{65}+C_{14}) \\
A_{12} &= u^2C_{16} + v^2C_{26} + w^2C_{45} + vw(C_{64}+C_{25}) + wu(C_{56}+C_{14}) + uv(C_{12}+C_{66})
\end{aligned}
\qquad \ldots(3.6)
$$

With the help of elastic matrix Eq. (3.5) for C_{2v}, D_2, D_{2h} crystal class the expressions A_{11}, A_{22} etc. are simplified to the following equations:

$$
\begin{aligned}
A_{11} &= u^2C_{11} + v^2C_{66} + w^2C_{55} \\
A_{22} &= u^2C_{66} + v^2C_{22} + w^2C_{44} \\
A_{33} &= u^2C_{55} + v^2C_{44} + w^2C_{33} \\
A_{12} &= (C_{12} + C_{66})\,uv \\
A_{13} &= (C_{13} + C_{55})\,wu \\
A_{23} &= (C_{23} + C_{44})\,vw
\end{aligned}
\qquad (3.7)
$$

With the help of these A_{ij}'s and the Eqs.(3.3) and (3.4) the expressions for different $K[u,v,w]_{hkl}$ for some directions

of propagation of thermal waves have been derived and are given in Tables 3.1, 3.2, 3.3. These relations have been used for evaluation of the elastic constants of Potassium Niobate.

3.1.2 New theory of elasticity:

The elastic properties of crystals belonging to (C_{2v}, D_2, D_{2h}) crystal class are given by the following matrix (following the notation of Laval, 1951).

$$\begin{matrix} C'_{11} & C'_{12} & C'_{13} & 0 & 0 & 0 & 0 & 0 & 0 \\ & C'_{22} & C'_{23} & 0 & 0 & 0 & 0 & 0 & 0 \\ & & C'_{33} & 0 & 0 & 0 & 0 & 0 & 0 \\ & & & C'_{44} & C'_{47} & 0 & 0 & 0 & 0 \\ & & & & C'_{77} & 0 & 0 & 0 & 0 \\ & & & & & C'_{55} & C'_{58} & 0 & 0 \\ & & & & & & C'_{88} & 0 & 0 \\ & & & & & & & C'_{66} & C'_{69} \\ & & & & & & & & C'_{99} \end{matrix} \qquad (3.8)$$

Now from the matrix equation (1.11) we can get the expressions for A_{ij} for a most general case as follows:

$$A_{11} = u^2C'_{11} + v^2C'_{66} + w^2C'_{88} + 2vwC'_{86} + 2uwC'_{18} + 2uvC'_{16}$$

$$A_{22} = u^2C'_{99} + v^2C'_{22} + w^2C'_{44} + 2vwC'_{24} + 2uwC'_{49} + 2uvC'_{29}$$

$$A_{33} = u^2C'_{55} + v^2C'_{77} + w^2C'_{33} + 2vwC'_{37} + 2uwC'_{35} + 2uvC'_{75}$$

contd...

$$A_{23} = u^2C'_{59} + v^2C'_{27} + w^2C'_{34} + vw(C'_{23}+C'_{47}) + uw(C'_{39}+C'_{45}) + uv(C'_{79}+C'_{25})$$

$$A_{13} = u^2C'_{15} + v^2C'_{76} + w^2C'_{38} + vw(C'_{78}+C'_{36}) + uw(C'_{58}+C'_{13}) + uv(C'_{17}+C'_{56})$$

$$A_{12} = u^2C'_{19} + v^2C'_{26} + w^2C'_{48} + vw(C'_{28}+C'_{46}) + uw(C'_{14}+C'_{89}) + uv(C'_{12}+C'_{69})$$

With the help of elastic matrix (3.8) for the particular case, (C_{2v}, D_2, D_{2h}) crystal classes, these relations are simplified to,

$$\begin{aligned} A_{11} &= u^2C'_{11} + v^2C'_{66} + w^2C'_{88} \\ A_{22} &= v^2C'_{99} + v^2C'_{22} + w^2C'_{44} \\ A_{33} &= u^2C'_{55} + v^2C'_{77} + w^2C'_{33} \\ A_{23} &= vw(C'_{23} + C'_{47}) \\ A_{13} &= uw(C'_{58} + C'_{13}) \\ A_{12} &= uv(C'_{12} + C'_{69}) \end{aligned} \qquad (3.9)$$

From these relations (3.3) and (3.4) the expressions for different $K[u,v,w]_{hkl}$ for some directions of propagation of thermal waves have been derived and are given in Tables 3.1, 3.2, 3.3 (Prasad and Wooster 1955). These relations have been used in interpreting the results of the present study in terms of the new theory of elasticity.

3.2 Evaluation of Elastic Constants

3.2.1 Classical theory:

It can be seen from Tables 3.1, 3.2, 3.3 that constants C_{11}, C_{22}, C_{33}, C_{44}, C_{55}, C_{66} can be determined independently from the observations along $[1\,0\,0]_{h00}$, $[0\,1\,0]_{0k0}$, $[0\,0\,1]_{001}$, $[0\,0\,1]_{0k0}$ or $[0\,1\,0]_{001}$, $[0\,0\,1]_{h00}$ or $[1\,0\,0]_{001}$, $[0\,1\,0]_{h00}$ or $|1\,0\,0|_{0k0}$ respectively. The constants C_{12}, C_{23}, C_{13} cannot be determined independently, but can be determined by substituting values of independent constants C_{11}, C_{22}, C_{33} etc. into the expressions for $\left[\pm\frac{1}{\sqrt{2}}, \pm\frac{1}{\sqrt{2}}, 0\right]_{h00}$, $\left[\pm\frac{1}{\sqrt{2}}, 0, \pm\frac{1}{\sqrt{2}}\right]_{001}$ and $\left[0, \pm\frac{1}{\sqrt{2}}, \pm\frac{1}{\sqrt{2}}\right]_{0k0}$ respectively. Following the above method absolute values of all the nine constants of Potassium Niobate crystal (Crystal class C_{2v} or mm2) have been determined from the quantitative study of its diffuse reflections by photographic and diffractometer methods.

3.2.2 New theory:

The new (Laval's) theory of elasticity requires fifteen elastic constants for an orthorhombic crystal class $\{mm2\}$ or C_{2v}. But for all the dynamical methods six of these would combine into pairs and thus we are left with only twelve dynamical constants to be determined viz. C'_{11}, C'_{22}, C'_{33}, C'_{44}, C'_{55}, C'_{66}, C'_{77}, C'_{88}, C'_{99}, $(C'_{12}+C'_{69})$, $(C'_{23}+C'_{47})$, $(C'_{13}+C'_{58})$. The constants C_{11}, C_{22}, C_{33}, C_{44}, C_{55} and C_{66} of the classical (old) theory can be easily identified with C'_{11}, C'_{22}, C'_{33}, C'_{44}, C'_{55} and C'_{66} of the new theory,

the additional constants of the new theory C'_{77}, C'_{88}, C'_{99} are determined independently from observations along $[0\,1\,0]_{00l}$, $[0\,0\,1]_{h00}$, $[1\,0\,0]_{0k0}$ rekhas respectively. The constants which occur in pairs viz. $(C'_{23} + C'_{47})$, $(C'_{12} + C'_{69})$, $(C'_{13} + C'_{58})$ can be determined by substituting the above independent constants C'_{11} etc. into the observations along $[0, \pm \frac{1}{\sqrt{2}}, \pm \frac{1}{\sqrt{2}}]_{0k0}$, $[\pm \frac{1}{\sqrt{2}}, \pm \frac{1}{\sqrt{2}}, 0]_{h00}$ and $[\pm \frac{1}{\sqrt{2}}, 0 \pm \frac{1}{\sqrt{2}}]_{00l}$ respectively. These constants cannot be separated out by the dynamical methods (Wooster 1961).

In this way it is possible in principle to determine the absolute values of all the twelve dynamical elastic constants of the Potassium Niobate crystal belonging to mm2 orthorhombic class, from the study of diffuse reflections only. The above derivations have been employed in interpreting and discussing the results of the present investigations on Potassium Niobate in terms of the new (Laval's) theory of elasticity in Sec. 5.1.2.

TABLE 3.1

a^*b^* Plane

Direction cosines, u,v,w of the direction of propagation of the thermal wave through node (h,k,l)	Expressions for $K\,[u,v,w]_{hkl}$ According to Classical Theory	According to New Theory
$[1\,0\,0]_{h00}$	$\frac{1}{C_{11}}$	$\frac{1}{C'_{11}}$
$[1\,0\,0]_{0k0}$	$\frac{1}{C_{66}}$	$\frac{1}{C'_{99}}$
$[0\,1\,0]_{h00}$	$\frac{1}{C_{66}}$	$\frac{1}{C'_{66}}$
$[\pm\frac{1}{\sqrt{2}}, \pm\frac{1}{\sqrt{2}}\,0]_{h00}$	$\frac{2(C_{22}+C_{66})}{P_1}$	$\frac{2(C'_{22}+C'_{99})}{P'_1}$
$[\pm\frac{1}{\sqrt{2}}, \pm\frac{1}{\sqrt{2}}\,0]_{0k0}$	$\frac{2(C_{11}+C_{66})}{P_1}$	$\frac{2(C'_{11}+C'_{66})}{P'_1}$

$$P_1 = [\,C_{11}(C_{22}+C_{66}) + C_{22}C_{66} - 2C_{12}C_{66} - C_{12}^2\,]$$

$$P'_1 = [\,(C'_{11}+C'_{66})\,(C'_{22}+C'_{99}) - (C'_{12}+C'_{69})^2\,]$$

TABLE 3.2

b*c* Plane

Direction cosines, u,v,w of the direction of propagation of the thermal wave through node (h,k,l)	Expressions for $K\,[u,v,w]_{hkl}$ According to Classical Theory	According to New Theory
$[0\,1\,0]_{0k0}$	$\frac{1}{C_{22}}$	$\frac{1}{C'_{22}}$
$[0\,0\,1]_{0k0}$	$\frac{1}{C_{44}}$	$\frac{1}{C'_{44}}$
$[0\,1\,0]_{00l}$	$\frac{1}{C_{44}}$	$\frac{1}{C'_{77}}$
$[0, \pm\frac{1}{\sqrt{2}}, \pm\frac{1}{\sqrt{2}}]_{0k0}$	$\frac{2(C_{44} + C_{33})}{P_2}$	$\frac{2(C'_{77} + C'_{33})}{P'_2}$
$[0, \pm\frac{1}{\sqrt{2}}, \pm\frac{1}{\sqrt{2}}]_{00l}$	$\frac{2(C_{22} + C_{44})}{P_2}$	$\frac{2(C'_{22} + C'_{44})}{P'_2}$

$$P_2 = [\, C_{22}(C_{44} + C_{33}) + C_{44}C_{33} - 2C_{23}C_{44} - C_{23}^2 \,]$$

$$P'_2 = [\, (C'_{22} + C'_{44})\,(C'_{77} + C'_{33}) - (C'_{23} + C'_{47})^2 \,]$$

TABLE 3.3

a*c* Plane

Direction cosines, u,v,w of the direction of propagation of the thermal wave through node (h,k,l)	Expressions for $K\,[u,v,w]_{hkl}$ According to Classical Theory	According to New Theory
$[100]_{001}$	$\frac{1}{C_{55}}$	$\frac{1}{C'_{55}}$
$[100]_{h00}$	$\frac{1}{C_{11}}$	$\frac{1}{C'_{11}}$
$[001]_{001}$	$\frac{1}{C_{33}}$	$\frac{1}{C'_{33}}$
$[001]_{h00}$	$\frac{1}{C_{55}}$	$\frac{1}{C'_{88}}$
$[\pm\frac{1}{\sqrt{2}}, 0, \pm\frac{1}{\sqrt{2}}]_{001}$	$\frac{2(C_{11}+C_{55})}{P_3}$	$\frac{2(C'_{11}+C'_{88})}{P'_3}$
$[\pm\frac{1}{\sqrt{2}}, 0, \pm\frac{1}{\sqrt{2}}]_{h00}$	$\frac{2(C_{33}+C_{55})}{P_3}$	$\frac{2(C'_{33}+C'_{55})}{P'_3}$

$$P_3 = [C_{11}(C_{33}+C_{55}) + C_{33}C_{55} - 2C_{13}C_{55} - C_{13}^2]$$

$$P'_3 = [(C'_{11}+C'_{88})(C'_{55}+C'_{33}) - (C'_{58}+C'_{13})^2]$$

3. REFERENCES

Bhagavantam, S. — Crystal Symmetry and Physical Properties Acad. Press (1966).

Kashyap, B.M. — Ph.D. Thesis Allahabad Univ. (1964).

Krishnan, R.S. — Progress in Crystal Physics 1, 73-94 (1958).

Joshi, S.K. and Kashyap, B.M. — Acta Cryst. 17, 629 (1964).

Laval, J. — C.R. Acad. Sci., Paris, 232, 1947 (1951).

L'etate Solide, Rapporte et discussions, Congre's Solvay, Bruxsells, Stoops.

Prasad, S.C. and Wooster, W.A. — Acta Cryst. 8 614, (1955).

Ramachandran, G.N. and Wooster, W.A. — Acta Cryst. 4, 335 (1951).

Srivastava, R.C. — Ph.D. Thesis Allahabad Univ. (1960).

Wooster, W.A. — Diffuse X-ray reflections from Crystals Clarendon Press Oxford (1962).

Acta Cryst. 14, 571, (1961).

4. EXPERIMENTAL PROCEDURE

4.1 Specimen Preparation

Small crystals of Potassium Niobate, parallelepiped in shape, were produced from binary melts (of K_2CO_3 and Nb_2O_5) using excess of K_2CO_3 as a flux (Wood 1951). Crystals, light blue, colourless and slight yellowish in colour were obtained with well developed faces and with a preferred cleavage perpendicular to [0 1 0] axis. Larger crystals were grown by the technique described by Miller (1958). Crystals so grown from the above methods however have very large electrical conductivity near the transition temperature (708°K) which makes the dielectric measurements difficult. Nearly single domain crystals of suitable dimensions for the diffuse scattering study were selected from them by a careful examination under a polarizing microscope.

The volume of the crystal was determined either from the dimensions measured by a travelling microscope or from the weight and the density of the crystal. The second method involves less error, if the crystal weighs more than 300 μg (Burbank 1965). Few crystals were finely ground to a cylindrical shape (diameter around 0.5 mm), one each for photographic and diffractometer methods. Crystals were annealed at about 800°C and were examined by Laue photographs and under a polarizing microscope for any strains etc.

4.2 Comparison of Photographic and Counter Methods (Wooster, 1962, 1964)

There are essentially two types of experimental arrangements, one based on photographic and the other on ionization (Geiger, proportional or scintillation) counter, recording of the reflected X-rays.

The apparatus required for photographic work is (i) a Rotation-Oscillation and Laue Camera, with radius of at least 5.7 cms. required for the accurate measurement of angular relationships which are important in determining the direction in which the diffuse X-ray beam has travelled. (ii) A microdensitometer for the measurement of the intensity of diffuse spots.

The apparatus required for the ionization method is (i) a diffractometer, (ii) single crystal orienter, which is the same as used in the single crystal - structure studies.

The following differences between the photographic and ionization methods may be noted:

(a) Even the weakest reflection can be recorded on the photograph by giving long exposures, unlike the diffractometer where the results on any single observation has to be recorded in few minutes;

(b) In the photographic method a large volume of the reciprocal space is recorded simultaneously, enabling a general survey

which is important in selecting proper planes for detailed studies; the diffractometer,on the other hand, covers very small volume for a single observation.

(c) Stability of the incident X-ray beam is very good in the photographic method because of long exposure and simultaneous recording of diffuse and direct beam intensity; while in the diffractometer the intensity of direct and diffuse beams are measured separately. This requires greater stabilization of the X-ray source.

(d) Angular resolution is roughly 100 times higher in the photographic method than in the diffractometer method. The angular resolution in the diffractometer can be improved at the expense of the number of counts.

(e) The accuracy of intensity measurement of X-ray reflection by photographic means is hardly ever better than 5% (Wooster, 1964) and to achieve even this accuracy requires very careful work. The diffractometer, on the other hand,can be arranged to give an accuracy of 1% with the help of very good stabilization, in most cases. Besides this, a diffractometer is very convenient for measurements along given directions accurately passing through reciprocal lattice points. This property is very important in the determination of elastic constants.

The photographic and ionization methods are each particularly valuable in certain types of work. Each of them have

certain advantages and disadvantages. So it is difficult to decide which is better;in fact both the methods are in many ways complimentary. But in the elastic constant determination the ionization method is preferred, since it depends for its accuracy primarily upon the number of counts per unit time which can be measured in any given direction. Owing to random fluctuations, the number of counts which must be measured in order to attain an accuracy of 1% is 10,000. With the modern diffractometers 10,000 counts can be registered in a reasonable time and hence no difficulty in attaining an accuracy of 1% (Arndt and Willis, 1966).

4.3 Photographic Method

4.3.1 Preliminary adjustments:

In the present investigation, Laue photographs were taken on a universal Rotation-Oscillation and Laue Camera of 5.7 cm radius, designed and fabricated in our laboratory. The complete assembly drawings are given in Fig. 4.1 and 4.2 and the experimental arrangement is shown in Fig. 4.3. The cylindrical camera has a collimator of 7 cm length. A conical rod resting on three balls fitted in a steel cup, passing through the axis of rotation of the camera carried a goniometer head which had usual arrangements for making axis of rotation of the crystal parallel and coincident with the axis of rotation of the camera. The rotation of camera could be read on the vernier attached to a

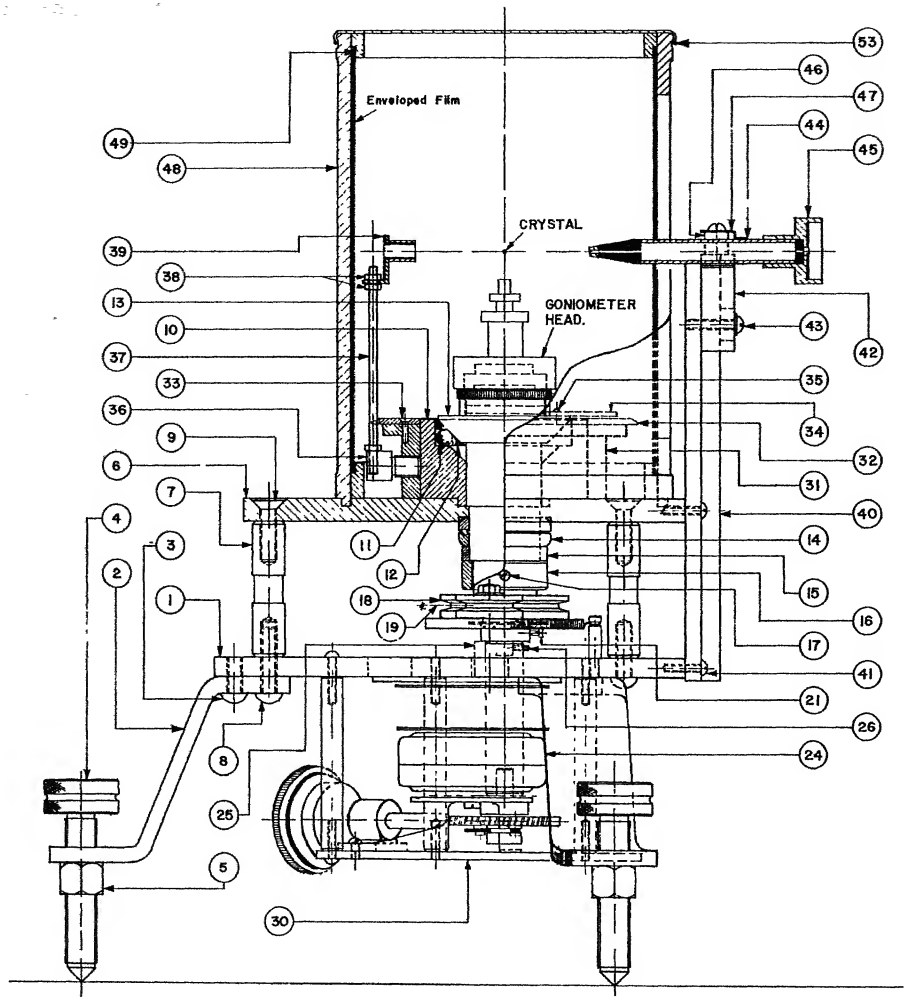

ELEVATION

FIG. 4·1

Sr.No.	DESCRIPTION	MATL	No.Off	REMARKS
53	COVER LID	Al	1	
52	ADJUSTING SCREW	BRASS	2	
51	ROUND HD SCREWS M2 5	"	2	5 LONG
50	FILM CLAMPING STRIP	Ni Stl	2	
49	FILM RETAINING RING	BRASS	2	
48	CYLINDRICAL CAMERA	"	1	
47	HOLDING STRIP (with screws)	"	2	
46	STRIP BLOCK	"	2	
45	COLLIMATOR CUP	"	1	
44	COLLIMATOR(variable size)	"	1	
43	ROUND HD SCREW M4, 20L	"	1	with washer
42	COLLIMATOR ADJUSTING PLATE	M.S.	1	
41	ROUND HD. SCREWS M4	M S	4	16 LONG
40	COLLIMATOR SUPPORTING PLATE	M.S.	1	
39	BEAM STOPPER (WITH FILTER PKT.)		1	
38	CHECK NUTS	BRASS	3	
37	BEAM STOPPER BAR	"	1	
36	HOLDING NUT(BEAM STOPPER BAR)	"	1	
35	CSK HD. SCREWS M2	"	2	5 LONG
34	POINTER	Perspex	1	
33	CSK HD. SCREWS M2 5	STEEL	3	8 LONG
32	DIAL	Perspex	1	
31	HOUSING	Al	1	
30	REDUCTION UNIT 1:50 RATIO	-	1	with accessories
29	CHECK NUT	BRASS	1	
28	DRIVING PULLEY	"	1	with belt
27	HEART CAM	STEEL	1	
26	LOCKING SCREW M2 5	"	1	6 LONG
25	MOTOR SHAFT ADAPTOR	BRASS	1	
24	ELECTRIC MOTOR (1 RPM)	-	1	220V, 50 c/s
23	SPRING HOLDING PIN	STEEL	1	
22	COMPRESSION SPRING	Sp Stl	1	
21	LOCKING SCREW M2 5	STEEL	1	6 LONG
20	CAM ROCKER	BRASS	1	
19	LOCKING SCREW M3	STEEL	1	8 LONG
18	PULLEY (DRIVEN)	BRASS	1	
17	LOCKING SCREW. M3	"	1	8 LONG
16	CHECK NUT	"	1	
15	DISTANCE PIECE	"	1	
14	THRUST BEARING	-	1	cycle bearing
13	MAIN. SPINDLE	SS	1	
12	BALL RETAINING CAGE	BRASS	1	
11	STEEL BALL	—	3	Chrome Stl.
10	CENTRAL CUP	S S	1	
9	CSK HD SCREWS	STEEL	3	20 LONG
8	ROUND HD. SCREWS	"	3	6 ϕ, 25 LONG
7	DISTANCE PINS	"	3	
6	UPPER PLATE	BRASS	1	
5	HEX HD LOCK NUT	BRASS	3	
4	LEVELLING SCREWS 60L	STEEL	3	M12X1 25
3	ROUND HD SCREWS	"	5	6 ϕ, 15 LONG
2	LUGS	M S	3	
1	BOTTOM PLATE	M S	1	

	DATE	NAME
DGN.	17.5 68	S.D. Phatak
DRN	7.2 70	B.L. Arora
TRD	18 2 70	"
CHD		

SCALE: 1:1

TOLERANCE: ±0.02

DEPARTMENT OF PHYSICS

ASSEMBLY DESIGN OF

ROTATION OSCILLATION and LAUE CAMERA

DRAWING OFFICE I I T. K

Appd

DRG. No. 2981/BLA/FEB 70

PLAN

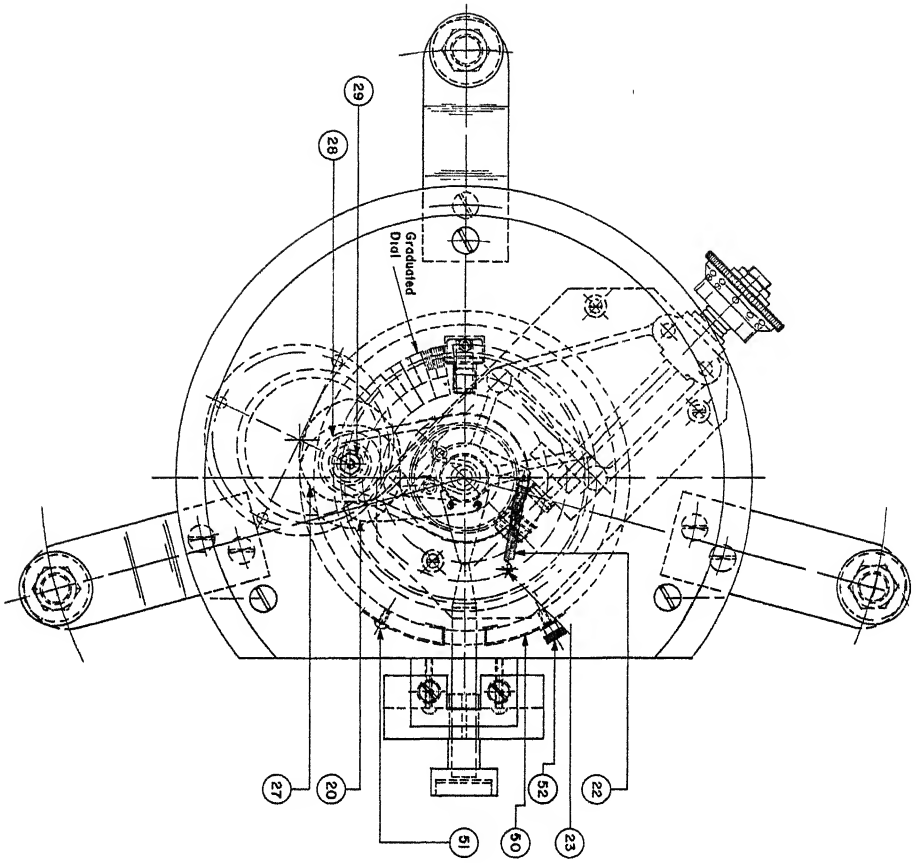

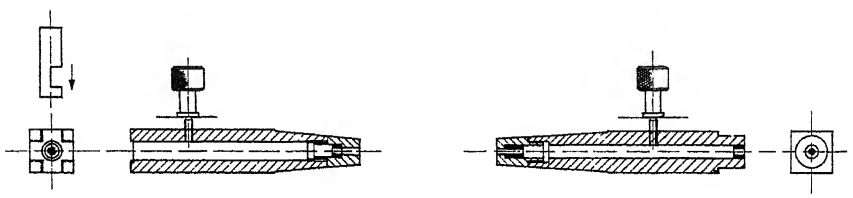

RECEIVING COLLIMATOR
Range. 1mm-4mm

BEAM COLLIMATOR
Range: 0·5mm-2mm

COLLIMATOR PAIR FOR COUNTER DIFFRACTOMETER
XRD VI (G.E.)

FIG. 4·2

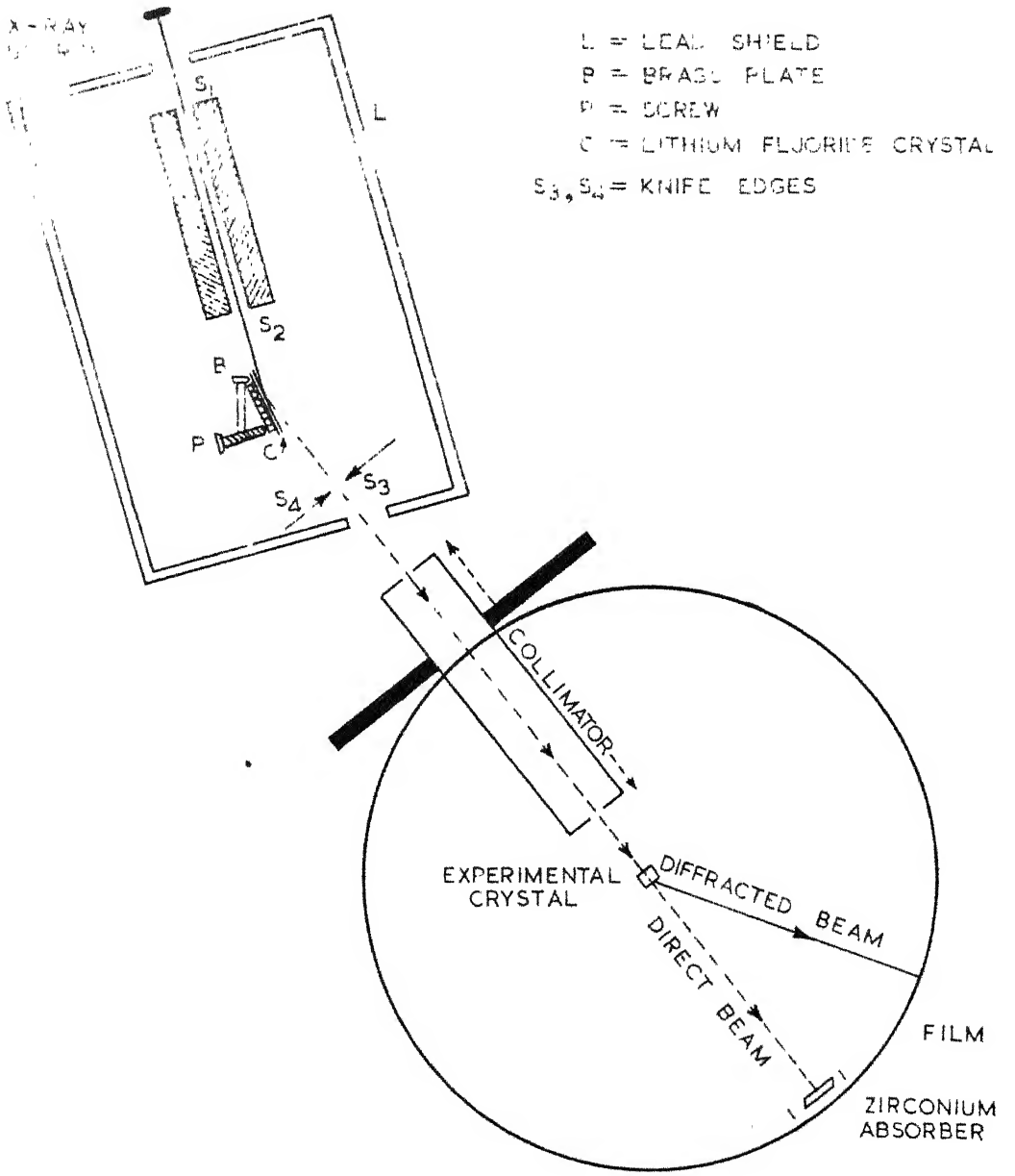

FIG. 4.3: The experimental arrangement for taking Laue pictures with monochromatic MoKα radiation.

graduated disc. with an accuracy of 3'. A screw catch carrying a vernier arrangement could fasten the rod carrying the goniometer head at any position, so as to keep the orientation of the crystal with respect to the incident beam fixed at any desired value.

A crystal of suitable size was mounted on the top of a glass fiber (of diameter much smaller than that of the crystal, to avoid any absorption of intensity due to this), with the help of an adhesive (Araldite or Quick Fix); the whole thing was mounted rigidly on the top of the goniometer head with the help of a brass pin and sealing wax. Some aluminium powder was made into a thick paste in collodion and a small amount of it was put in the centre of the top of the crystal to give powder diffraction lines of Al superimposed on the Laue pattern of the crystal. These lines were used for (i) determination of the correct orientation of a particular plane with respect to incident beam, (ii) the measurement of camera radius and (iii) the calibration of angle of diffraction, $\emptyset$, in Laue pictures taken with monochromatic X-ray beam.

After the preliminary adjustment was done optically, it was checked by taking rotation pictures (Appendix I, Plate 1). The faces being known, different directions in the crystal could be identified easily with the help of diffractometer technique, and so the crystal could now be rotated through a desired angle

orienting it in such a way as to record diffuse reflection from a particular plane (hkl). Finer rotations could be given with the help of a guide and a cam after fastening the rod with the catch.

4.3.2 Orientation (Laue) Photographs:

Since we are interested in small wave vectors only, the crystal was oriented such that the incident beam makes an angle little different from the position of the Bragg reflection of the corresponding plane. After the crystal plane has been oriented the camera is adjusted in the X-ray beam, the tube being operated at 40 kV and 20 mA (Mo radiation). Because of the presence of white radiation, the whole Laue pattern will be recorded and because of the characteristic radiation, the diffuse reflection and powder diffraction pattern of Al will be recorded simultaneously on the film. Typical photographs are given in Appendix I (Plate 2). The indexing of the plane responsible for particular diffuse reflection was ascertained with the help of a reciprocal lattice net and circle of reflection (orientation of the crystal being approximately known) and verified by diffractometer method.

Since angles of diffraction, $\emptyset$, for Al planes are known accurately, the distance on the film can be calibrated in terms of angle $\emptyset$. Thus by measuring the distance between the Al(111) line and a particular Laue spot the angle between the incident X-ray beam and a particular axis of the crystal can be computed. The measurement of distances was done with the help of a

comparator and orientations thus determined are believed to be accurate upto 1'.

4.3.3 Monochromatic Photographs:

For the determination of $K[u,v,w]_{hkl}$ which are ultimately related to elastic constants it is necessary to determine the ratio of the diffusely scattered X-ray intensity I_d by a particular wave vector to the incident intensity I_o. This ratio will be meaningful only when monochromatic radiation is used. (otherwise the diffuse pattern due to one wavelength will be disturbed by the others).

In the present investigation MoKα (0.7107 Å) radiation was used, operated at 35 KVP and 25 mA.

The experimental arrangement used for taking Laue pictures with monochromatic X-rays is shown in Fig. 4.3. For monochromatization a plane crystal monochromator using a lithium fluoride crystal as a reflector was used. G.E. CA-7 sealed Mo tube was used as a source of X-rays. The X-ray beam was first collimated through the rectangular slits S_1, S_2 and then allowed to fall on the lithium fluoride crystal mounted on a plate B, provided with necessary arrangement to have motion in two mutually perpendicular directions. At first the crystal face was made parallel to the slits S_2 and then by rotating the crystal with the help of a screw P, it was brought to Bragg reflection position for (2,0,0) plane (Bragg angle for MoKα is $\theta = 10.15^{\circ}$). The reflected beam

was seen on the fluorescent screen and the LiF crystal was so oriented that the reflected beam was uniform as checked photographically. Spurious radiations at the edges of the reflected beam were eliminated by using straight knife edges S_3 and S_4. The horizontal and vertical divergences of the monochromatized beam were also measured by exposing two films 11.5 cm apart. The divergences were calculated in the usual way by the measurement of the areas blackened in the two films. The horizontal divergence was found to be 8' and the vertical $1^{o}12'$. The latter assumed a much smaller value (22') when collimated through slits of the camera and both are further reduced effectively due to small dimensions of the crystal.

After the crystal has been oriented for a particular diffuse spot and an orientation picture is taken, the camera is collimated in the monochromatic beam for recording the diffuse reflection for intensity measurements. The ratio of the intensity of diffuse reflection to the intensity of the incident beam is of the order of 10^{-6}. Since the intensity measurements by the photographic method are reliable only if the blackening produced on the film lies (falls) in the straight portion of the intensity versus blackening curve, it is necessary to reduce the intensity or the time of exposure for the direct beam such that the blackening that it produces on the film is almost the same as that produced by the diffuse reflection (both impressions being simultaneously developed). The procedure followed in the present

investigation is to interpose suitable number of zirconium foils (.0002" each) of known thickness in the path of the direct beam just before it strikes the film. The thickness of Zr absorber is adjusted such that intensity of direct beam left over after absorption is nearly equal to the intensity of diffuse reflection. Now, the reduced direct beam and the diffused beam both are allowed to fall on the film simultaneously and the film is exposed to both of them for the same length of time. The greatest advantage of this method is that the fluctuations of X-ray output of the tube do not affect the relative intensities.

For interposing Zirconium foils a small pocket of thin paper was made in the centre of the black paper envelope in which the film for taking monochromatic picture was wrapped. In this small pocket, suitable number of Zr foils could be placed. As the intensity of diffuse reflection varies with the degree of misorientation and the structure factor of the plane concerned, the thickness of the absorber was varied accordingly, so that the intensity of reduced incident X-ray beam was nearly equal to that of the diffuse intensity. In the present study the number of foils were varied from 19 to 21 (i.e. the thickness varies from .0038" to .0042"). It may be mentioned here that the absorption coefficient of a substance is different for different wave lengths and in the monochromatized X-ray beam higher harmonics will be normally present. In order to avoid any error due to differential absorption of λ, $\lambda/2$, $\lambda/3$ etc. higher harmonics

were eliminated by running the Mo-target at 35 kV and 25 mA. This increased the exposure time considerably, which varied from 35 hrs. to 50 hrs. in different cases.

Each photograph thus taken would contain the diffuse reflectuion, the impression of the direct beam and the powder diffraction lines of aluminium. To stop the back reflection lines (if any) of Zr from being recorded on the film, a thin sheet of lead was made in the form of a 2mm high, lidless and bottomless box which was hung from the edge of the cylindrical film holder or in the place of beam stopper so as to surround the Zr foils from all sides. (Typical monochromatic pictures are shown in Plate III, Appendix I).

4.3.4 Intensity Measurements:

Following the method described by Sen and Chakraborty (1958) the intensity of the photographic records was measured using Moll recording microphotometer (Kippen Zonen). The film could be mounted on the sliding carriage of the photometer in the desired way. The scanning beam of light traverses the photograph when the carriage is moved. Since only the diffuse reflections in the equatorial layer line were considered in the present investigation, the photographs were mounted such that the scanning spot crossed the middle of the shadow of the crystal in the direct beam impression and the middle of the diffuse spot when the carriage was moved.

The dimensions of scanning spot were adjusted at 0.02 to .02 cm in height and 0.005 cm in breadth, the current for illuminating lamp was supplied by 6 volt accumulator batteries and was kept constant at 3.1 amp. The beam of light is focussed on the film, which has to be scanned. After falling on the film., it is again converged on a vacuum thermopile. The current developed is recorded by a Moll sensitive galvanometer which is mounted on a vibrationless pillar. The time of response of the combination is of the order of 0.25 sec. The mirror attached to the galvanometer fibre reflects a fine beam of light which deflects according to the density of blackening i.e. according to the current generated at the junctions of the vacuum thermopile and after being reflected by a total internal reflection prism is recorded on a strip of photographic paper. The paper is wrapped round a drum, the rotation of which is coupled with film translation by means of a variable gear. The movement of the reflected beam is parallel to the axis of rotation of the drum. The gear ratio used in the present investigations was 1:4. The distance between the two peaks corresponding to Al(111) lines in photometric record was used in converting the distances (abscissa) of the photometric curve into corresponding angular coordinates of the photograph. The intensities were obtained by comparing the ordinate of the photometric curve with the standard wedge following the method of Robinson (1933).The calibration wedge was recorded for each picture separately on the photographic film cut out of the same sheet as used for recording the

monochromatic picture and both were developed together. The time of exposure is linearly proportional to the distance along the length of the wedge and hence the intensity corresponding to any ordinate of the photometric curve is proportional to the distance from the zero intensity point. The photometric curve for the wedge was recorded under the same photometric conditions as the diffuse spot and the direct beam impression. Typical photometric curves for the calibration wedge (Appendix III,c) and also for the diffuse spot and direct beam impression have been reproduced in Appendix III(a,b,c). The intensities of diffuse reflections and the incident beam were thus measured from a photograph on the same arbitrary scale.

4.3.5 Evaluation of relative intensity (I_d'/I_o):

The direct beam impression will have in its centre the shadow of the crystal due to the absorption by the crystal, hence its microphotometer record will have a dip in the centre corresponding to the shadow of the crystal (Appendix III,a).

The intensity corresponding to the ordinate for the dip of the photometric curve of the direct beam impression (the reason for taking the dip has been discussed in Appendix III) may be denoted by I_r' i.e. reduced intensity of the incident beam at the film.

Now $$I_o' = I_r' e^{\mu t_n}$$

I_o' is the intensity of the direct beam at the film, μ the linear absorption coefficient of Zirconium and t_n the thickness of the zirconium foils used for reducing the intensity. From I_o' we can compute I_o, the intensity of the direct beam at the crystal. Let the area over which the direct beam spreads at the crystal and on the film be S_c and S_F respectively. Then it is evident that $I_o = I_o' \frac{S_F}{S_c}$. This factor $\frac{S_F}{S_c}$ can be evaluated from the knowledge of the divergence of the beam and the size of the slit. In the present case it was 1.28. Next comes the consideration of the value of linear absorption coefficient of the zirconium foil for MoKα, which was used to reduce the intensity of the direct beam. In order to avoid any error caused due to variation of the purity of the sample of zirconium foils the value of mass absorption coefficient was determined by the diffractometer method as described by Chakraborty (1958). (see appendix III) It was in full agreement with the one given in the International tables for X-ray crystallography (1963) which shows that the sample is highly pure.

The intensity corresponding to the ordinates of the photometric curve of diffuse reflection is found out from the photometric curve of the calibration wedge. The distance between Al (111) peaks in the microphotometer record was calibrated in terms of the angle of diffraction. Thus the abscissa of photometric curve for diffuse reflection gives Ø and the corresponding ordinates give the observed diffuse intensity I_d' (uncorrected for any factor). I_d'/I_o was plotted against Ø for each case and

these curves were used for determining the value of I_d^1/I_o corresponding to a certain $\emptyset$, which is related to a particular wave vector and was found out by calculation. Some of these curves have been reproduced, shown in Fig.I-14.

4.4 Diffractometer Method

Since the diffractometer with single crystal orienter (Goniostat) permits a continuous survey of a whole hemisphere of a reciprocal lattice with smooth and finely controllable motions, it is ideally suited for holding and manipulating crystal specimens for a detailed study of their diffuse scattering. Without changing the physical arrangement and alignment of the Goniostat and SPG spectrogoniometer (Furnas 1957) as it is used in the single crystal structure studies, remarkably good results can be obtained through the use of balanced filters (for monochromotization) for the X-ray beam. The absolute value of the direct beam intensity (I_o) is obtained from Compton scattering of diamond as intermediate standard (Appendix II).

4.4.1 Method of Monochromatization:

The system of balanced filters (Chipman and Warren (1950), Tanaka et al (1959), Guinier (1945), Peiser et al (1955), Umanskii (1960), Burbank (1965), Arndt and Willis (1966) and Ross (1928)) is an alternative to the monochromatizing crystal. The filters are precisely matched so that they transmit the same proportions of the radiation on either side of the small spectral range which

contains the Kα line of the given X-ray target. The advantage of this method of monochromatization is that the intensity of the monochromatic beam is much higher than it is with crystal reflected radiation. Unfortunately, there is small portion of the white radiation which is transmitted more by one filter than by the other, but this usually only involves a very small correction to the results.

4.4.1.1 Balanced Filters:

The operating principle of balanced filters (Ross 1928) is shown in Fig. 4.4. Two filters are constructed, generally of two elements of atomic numbers Z and Z-1, whose absorption matches at all wave lengths other than over the narrow band between the two absorption edges λ_Z and λ_{Z-1}. If two measurements are made, one with each filter, the difference between the two is due solely to radiation within this narrow 'pass-band'. i.e. monochromatic radiation.

However in the present case we have used Zr and high purity Y_2O_3 powder as a pair of balanced filters for Molybdenum target. The latter filter is used in the form a thin pellet of the oxide of the metal because pure yttrium metal in the form of a thin foil was not available. The balance obtained for (004) reflection is shown in Fig. 4.5.

The balance of the filter pair must be tested at every stage by plotting transmitted intensity as a function of

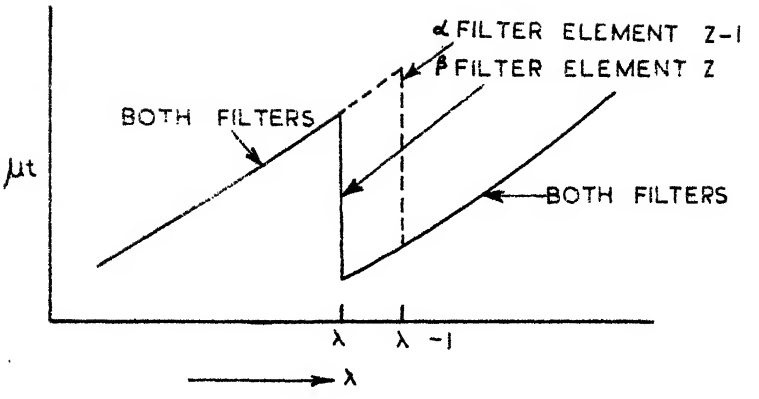

FIG. 4.4: The pass-band of an idealized filter pair is the wavelength range between the two absorption edges. Outside the pass-band, the absorption of the two filters matches completely.

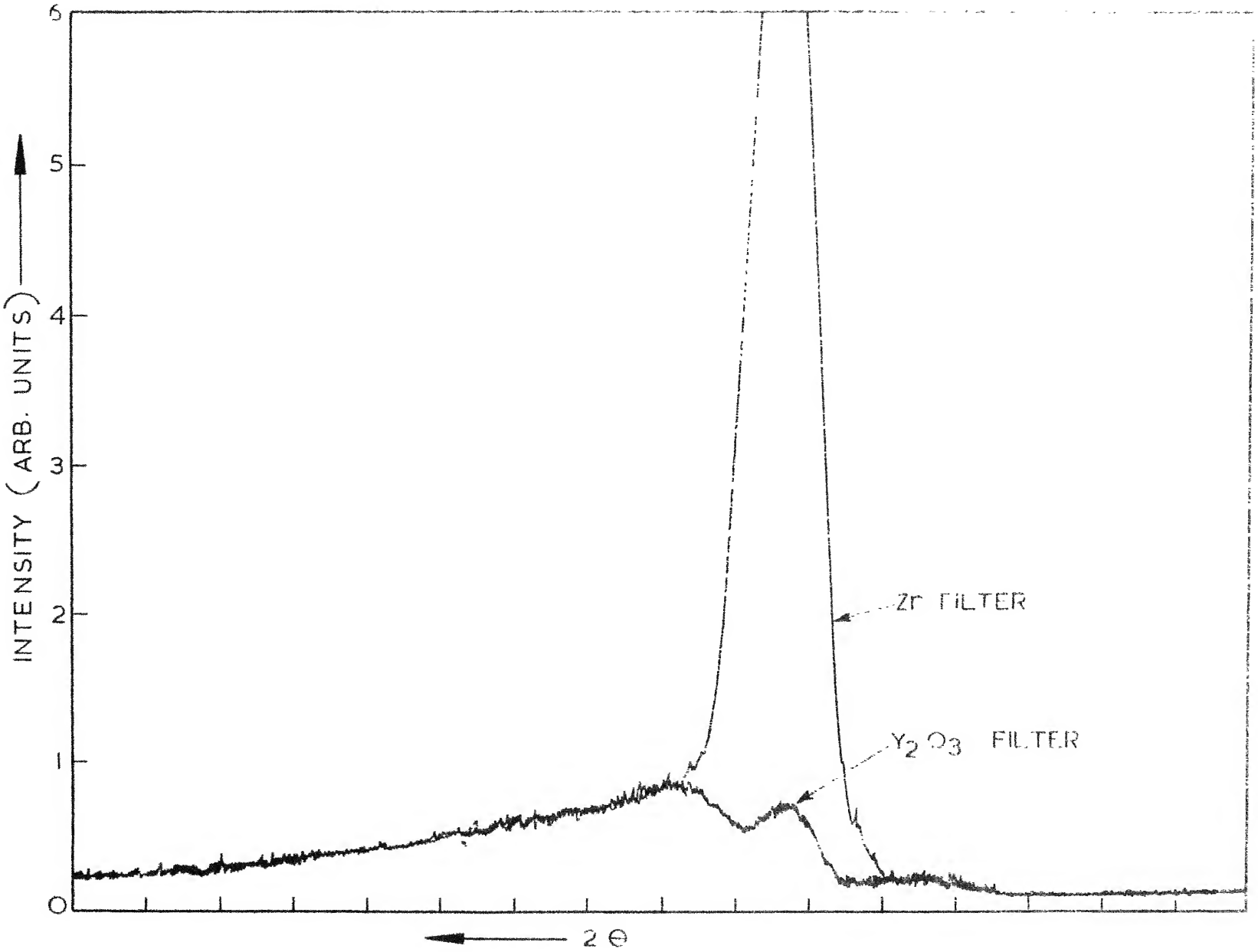

FIG. 4.5: Wavelength scan for a perfectly balanced Y_2O_3/Zr filter pair for (0 0 4) reflection from $KNbO_3$ crystal, using MoKα radiation.

the wavelength for both filters, The wavelength scan can be performed by mounting an analysing crystal on the diffractometer and by varying 2θ and Ø (SPG goniometer motions) in the ratio 2:1 as can be seen in the Fig. 4.5.

4.5 Correction Factors

The crystal used on the diffractometer is fully immersed in the X-ray beam by using a suitable beam collimator; hence many of the corrections involved can be applied in a similar way as in the photographic method.

4.5.1 General Scattering:

In the diffraction process by the diffractometer and the photographic technique a general scattering underlies Bragg and diffuse scattering. The general scattering includes, Compton scattering, flourescent radiation and scattering due to optical waves. The intensity of the general scattering varies to a limited extent over the region of the reciprocal space, covering the observations about one relp.

The correction to be applied to the observed diffuse intensity due to general scattering is the same in both the techniques.

In the diffractometer method such variation in the general scattering can be eliminated by taking the mean value of the intensities of X-rays scattered from reciprocal volumes at equal distances on opposite sides of the relp. The diffuse

intensity I_d due to first-order scattering from elastic waves, is found by plotting observed diffuse intensity, I_d (corrected for skew, polarization, absorption and divergence) against $1/q^2$. (i.e. λ_t^2). The points so plotted lie, within the accuracy of the measurement, on a straight line, which cuts the axis of I_d at a point corresponding to the constant contribution of the Compton, fluorescent and optical scattering. This quantity is subtracted from the observed intensity to obtain the intensity due to the first and second order elastic scattering.

In the case of the photographic technique, intensities due to diffuse reflections are superimposed over the background intensity due to Compton scattering, air scattering etc. By subtracting the extrapolated background intensity from the total, the corrected intensity for the diffuse reflection only has been obtained. The background intensity has been shown as a dotted line in the I_d'/I_o vs. ϕ curves in Fig. I-14 (Appendix I). Thus the values of I_d'/I_o given in the table A-16 (Appendix I) are corrected for general scattering.

4.5.2 Divergence correction:

An ideal collimator gives rise to a perfectly parallel beam of X-rays. However, the finite size of the slits between the crystal and the X-ray tube and also between the crystal and the detector permits X-rays having certain divergence to enter the detector and be counted together. The experimental

observation does not, therefore, correspond only to the intensity of diffuse scattering from a single point in reciprocal space but also covers a certain volume of reciprocal space surrounding the point. The greater the divergence of the X-ray beam the greater the volume of reciprocal space over which the integration is effected.

4.5.2.1 Photographic method:

The divergence of the incident beam in this case is very low (horizontal 8' and vertical 22') because of the very narrow slit employed and the short distance between the crystal and the collimator. ($\sim$ 2 cm). The effective divergence would be further reduced due to the small size of the crystal (0.996 x 10^{-4} cc). The divergence correction was determined in few cases and was found to be negligible.

4.5.2.2 Diffractometer method:(Wooster 1962)

The size of the collimator slits and the crystal used in the diffractometer method is comparatively larger than in the photographic method. As a result the divergence correction becomes appreciable, However in the present study unusually small crystals were used. The total divergence may be divided into three components denoted respectively by i, θ and χ. The i-divergence is the maximum angle between the rays falling on the crystal when they are projected on a horizontal plane. The θ divergence is the maximum angle between the reflected rays,

also projected on a horizontal plane, which can enter the detector at any given setting. The χ-divergence is the maximum angle between the reflected rays, projected on to a vertical plane passing through the crystal and the detector, which can be recorded at the given setting. The magnitude of divergence will vary from one experiment to another, depending on the size of the crystals and the slits; in the present experiment i is about 30', θ about 1° and χ about 5°.

In order to apply the i-divergence correction, the detector and χ-positions are kept fixed. The intensity of the Bragg reflection is measured as a function of the angle i in the vicinity of the Bragg peak position (Fig. 4.6a). The angle i is read on the ϕ circle of the crystal orienter. Then intensity data (D(i)) are collected at a fixed positions of i (such as A in Fig. 4.6b) which are atleast 1° away from the i corresponding to the Bragg peak. The angle i is varied in small intervals (δ i $\sim 0.02^{\circ}$) around point A, to obtain the curve AB in Fig. 4.6b. The diffuse intensity varies slowly with i, whereas the Bragg reflection varies rapidly with i in the neighbourhood of the Bragg setting (Fig. 4.6a,b). Each point on the curve AB can be regarded as being produced by many planes ~~slightly~~ slightly inclined to the reciprocal lattice planes which give the Bragg reflection. At a point A, Fig.4.6b, one lattice plane is in the Bragg setting and its contribution to the intensity is represented by the small copy CD of the Bragg intensity

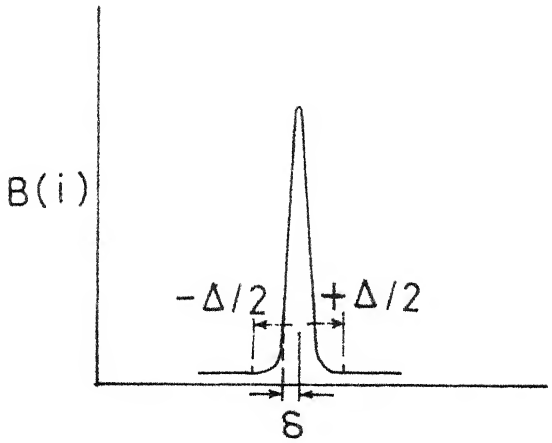

FIG. 4.6(a): The curve [illegible] to the variation of intensity across Bragg reflection. Curve CD is a copy, reduced to an appropriate scale, of the Bragg reflection curve.

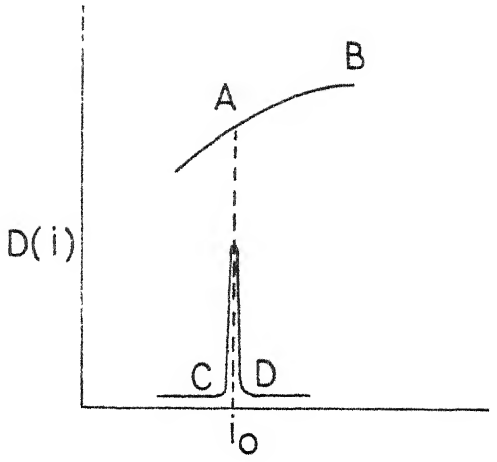

FIG. 4.6(b): The curve AB corresponds to the variation of intensity, D, across the diffuse reflection

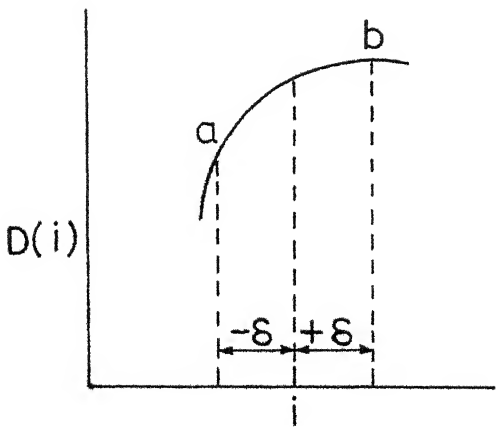

FIG. 4.6(c): Shows the meaning of the quantity δ used in the divergence corrections.

curve drawn at the same angle i as that of point A. This particular plane contributes the maximum possible diffuse intensity at point A. Other planes nearly parallel to the A set, contribute an amount corresponding to the departure of the angle i from that value which corresponds to their maximum contributions. Thus at any point A, the value of D(i) is the sum of contributions, each one of which is the product of the maximum intensity of diffuse scattering from a lattice plane, and an ordinate of the curve CD. Let us denote by D(i) the true intensity curve of the diffuse reflection due to the disturbed lattice without any modification due to the shape of the B(i) curve. The angular breadth of the B(i) curve is denoted by Δ, and the angular separation of any point on the B(i) curve from the central maximum is called δ (Fig. 4.6b). The particular value of i at the point A on curve D(i) is denoted by i_o. The elastic waves corresponding to a Bragg setting $(i_o + \delta)$ give a contribution at A equal to $D'(i_o + \delta)\ B(\delta)$, where $B(\delta)$ is the ordinate of the B(i) curve at a distance δ from the maximum. The total effect is thus the integration of all these contributions from the separate elastic wave trains, namely,

$$D(i_o) = \int_{-\Delta/2}^{+\Delta/2} D'(i_o + \delta)\ B(\delta)\ d\delta \qquad (4.1)$$

It is assumed here that the Bragg reflection curve is symmetrical about its centre. This assumption is usually justified.

If the Bragg reflection curve is not symmetric with respect to its centre then the error due to this assumption is removed by taking the values of B(i) at + δ and - δ (Fig.4.6c). From an experimental curve such as Fig. 4.6c, which gives D(i) as a function of i, we may calculate the quantity G(δ) for each value of δ between 0 and $\pm \Delta/2$ according to the expression

$$G(\delta) = \left\{ \frac{1}{2} \left(D(i_o+\delta) + D(i_o-\delta) \right) - D(i_o) \right\} / D(i_o) \qquad (4.2)$$

The expression G(δ) gives the correction factor at every value of δ which must be applied to the experimental curve. To take into account the shape of the B(i) curve, each value of G(δ) is multiplied by the corresponding B(δ) and integrate the product over the range $\pm \Delta/2$. This is divided by the integral of B(δ) (to normalize) over the same range to obtain the final correction.

$$Z(i_o) = \int_{-\Delta/2}^{+\Delta/2} G(\delta)\, B(\delta)\, d(\delta) \Big/ \int_{-\Delta/2}^{+\Delta/2} B(\delta)\, d\delta \qquad (4.3)$$

The evaluation of this correction is carried out graphically. The observed value of the diffuse intensity at any given point i_o is multiplied by a factor $(1 + Z(i_o))$ to obtain the correct value of diffuse intensity.

θ - divergence and χ -divergence corrections are carried out in a manner similar to i - divergence correction. In the former i and χ are kept in a fixed position and intensity is collected as a function of θ, while in the latter i and θ are kept constant and intensity is studied as function of χ. The

intensity data are analysed in an analogous manner to determine the correction factors. Finally i, θ and χ-divergence corrections are added to obtain the corrected diffuse intensity.

4.5.3 Skew correction:

The skew correction arises because the glancing angles of the incidence and of reflection are not equal. Laval (1939-51) has shown that diffused intensity I_d in such a case is given by

$$I_d = I_d' \times \frac{1}{2} \left\{ 1 + \frac{\text{Sin } i}{\text{Sin } (\phi - i)} \right\} \qquad (4.4)$$

Where I_d' is the observed diffuse intensity i is the angle of incidence and ϕ is the angle of diffraction. The factor $1/2 \left\{ 1 + \text{Sin } i / \text{Sin}(\phi - i) \right\}$ is called skew correction. The observed intensity I_d' must be multiplied by the skew correction to obtain I_d; the intensity which would be observed if the angles of incidence and reflection were equal. It will be seen that when $i > \phi/2$ the skew factor is greater than unity and when $i < \phi/2$ it is less than unity. When $i > \phi/2$ the volume of the crystal irradiated is less than when the Bragg condition is satisfied (i.e. when $i = \phi/2$). For both these reasons I_d' is less than I_d. This correction is the same in the photographic and diffractometer methods and has been applied to each observation.

4.5.4 Polarization factor:

The polarization factor is given by,

$$P = (A^2 + B^2 \text{ Cos}^2 \phi) \qquad (4.5)$$

where, A and B have the same meaning as in Eq.1.13. If a monochromatizing crystal is not used as in the diffractometer, then the radiation is unpolarized and,

$$A = B = 1/\sqrt{2}$$

$$A^2 = 1/1+\mathrm{Cos}^2 2\theta, \quad B^2 = \mathrm{Cos}^2 2\theta/(1+\mathrm{Cos}^2 2\theta)$$

θ is the angle at which X-ray beam is reflected. On the other hand, since the crystal reflected monochromatic beam has been used for recording all the photographs from which intensity measurements have been made, the polarization factor for equatorial reflections takes the form,

$$P = \frac{1 + \mathrm{Cos}^2 2\alpha \, \mathrm{Cos}^2 \phi}{1 + \mathrm{Cos}^2 2\alpha} \qquad (4.5)$$

where, 2α is the angle of diffraction of the monochromatic beam plane and ϕ the angle of diffraction at which the observation is made. A general expression applicable to non-equatorial reflections also has been given by Azaroff (1955).

4.5.5 Absorption correction:

Let I_o be the initial intensity of an X-ray beam incident normally on the absorbing material (crystal) and I the intensity after the beam has travelled through a distance x in the absorber. If dI represents a further diminution of intensity of the beam on its travelling an additional small distance dx, then $-dI/dx$ is the rate of decrease of intensity. If it be assumed that dI/dx is proportional to I, we may write,

$$-\frac{dI}{dx} = \mu I \qquad (4.6)$$

where μ, the constant of proportionality, is called the linear absorption coefficient, which is a characteristic of the absorbe crystal and is a function of the wavelength of incident X-rays. On integration and applying initial conditions, we get,

$$I = I_o e^{-\mu x} \qquad (4.7)$$

If the distances traversed inside the crystal by the inc dent and the diffusely reflected beams are equal, then the inten. sity of both of them will be reduced to the same extent i.e. by a factor $e^{-\mu x}$ and consequently the ratio I_d/I_o remains unaltered. Such will be the case (for equatorial reflections) when the crystal is spherical or cylindrical. This is the reason why μ does not occur in the expression for intensity formula (Eq. 3.2) in the photographic method. Some times it is not possible to obtain cylindrical or spherical crystals because grinding the crystal may lead to fragmentation or twinning; shaping is also difficult if there are strong cleavage planes. Therefore, for an unground crystal, (if the dimensions of the faces bounding the crystal are measured) the distances traversed by the incident and diffuse beams would not in general be equal and correction might be neces. sary in certain cases. For applying this correction (in the photographic and diffractometer methods) the value of μ should be known Simple methods for the determination of μ by the photographic and

diffractometer techniques are described in Appendix III. A graphical method due to Albrecht (1939) for treating absorption in a crystal of any size, shape and absorbing power is briefly described here.

In an actual crystal the path length x is a variable depending on the size and shape of the crystal and on the diffracting plane. The intensity of the diffracted beam is given by,

$$I = I_o \int_v e^{-\mu x} \, dv/v \qquad (4.8)$$

where I_o is the intensity which the diffracted beam would have possessed had it not been for absorption. This integral is difficult to evaluate but an approximate solution can be obtained graphically by dividing the crystal into small volume elements and summing the absorption effects of each, Eq. (4.8) may then be rewritten as,

$$I = \frac{I_o \int e^{-\mu x} \, dv}{v} = \frac{I_o \sum_i e^{-\mu x_i}}{n} \qquad (4.9)$$

where n volume elements are considered. In Fig. 4.7 the absorption by a volume element is given by $I/I_o = e^{-\mu(t_1+t_2)}$, where $t_1 + t_2$ is the path length (in the crystal) of beam diffracted from this volume element. If the incident beam S_o is divided into a number of equal rays as shown in Fig. 4.8, where θ is the Bragg angle for the plane hkl considered here, then S will represent the diffracted beam, divided into rays of the same dimensions as

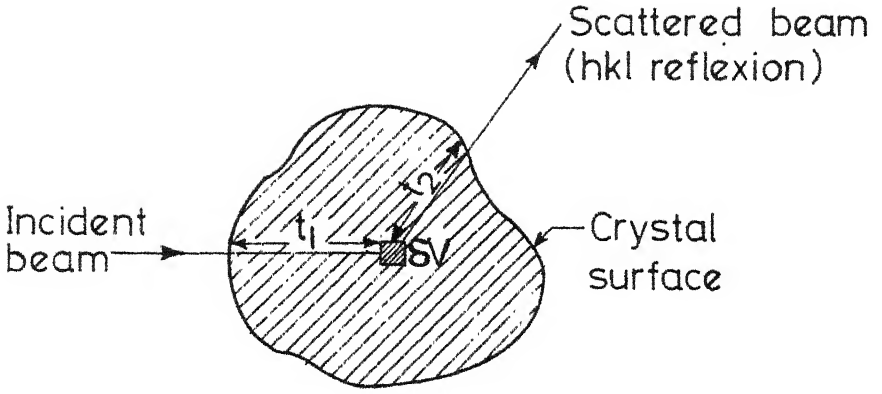

FIG. 4.7: Scattering from volume element δV of crystal.

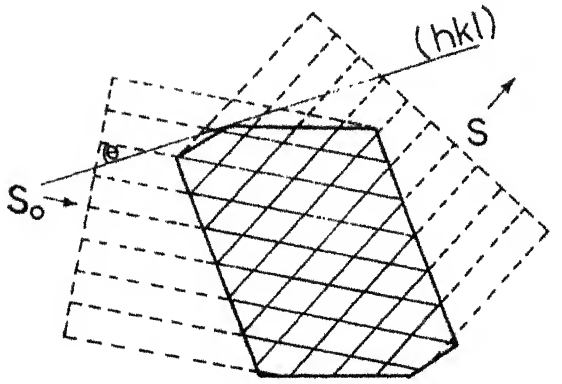

FIG. 4.8: Projection of the crystal, showing the ray inter sections (n) to be considered for a given reflections hkl, within the boundaries of the crystal.

S_o. If the projection of a volume element is represented by the intersection of the two rays, it is possible to obtain a value for the summation of the Eq. (4.9) by adding quantities of the type $e^{-\mu x_i}$ and dividing the sum by n, the number of ray intersections associated with the diagram. The number of intersections within the boundaries of the crystal is equal to the number of volume elements chosen. The path length for a given volume element can be measured with rulers and the quantity $e^{-\mu x_i}$ can be readily obtained from a table of exponentials. It is thus only necessary to draw a cross-section of actual crystal to the scale; draw in the incident and emergent rays in the direction appropriate to the plane under consideration; measure the path lengths, and count the number of intersections. If a large number of calculations are to be performed the work may be carried out on computer. In the present case calculations of absorption factors are carried out on IBM 7044 Computer.

The amount by which the intensity of the hkl reflexion is reduced by absorption is denoted by $A_{hkl} = \sum_i e^{-\mu x_i}/n$. The reciprocal of A_{hkl} is the absorption factor $A^*_{hkl} = 1/A_{hkl}$. A^* represents the factor by which the observed intensity is multiplied to obtain the corrected intensity.

4.5.6 Second order diffuse scattering correction:

Main contribution to the diffuse intensity is due to first order diffuse reflection. From equations 1.16, 1.19 and 1.23

the ratio of the intensity of first and second order diffuse reflection is given by

$$\frac{\sigma_2}{\sigma_1} = \frac{\pi^3}{2} kT \vec{X}^2\vec{q} \; K'[u,v,w]_{hkl} / K[u,v,w]_{hkl} \qquad (4.10)$$

In the photographic method used for (4 0 0) reflection the thermal wave vectors are very small and hence the correction is neglected. However in the diffractometer method correction has been applied to (6 0 0), (0 0 6), (0 4 0), (4 0 0) and (0 0 4) relps: as suggested by Ramachandran and Wooster (1951), Prasad and Wooster (1955) and Amoros (1968).

$$\therefore \quad K'[u,v,w]_{hkl} = K^2[u,v,w]_{hkl} \quad \ldots \text{ (Approximation)}$$

$$\therefore \quad \frac{\sigma_2}{\sigma_1} = \frac{\pi^3}{2} kT \vec{X}^2\vec{q} \; K[u,v,w]_{hkl}$$

or

$$\sigma_2 = \sigma_1 \frac{\pi^3}{2} kT \vec{X}^2\vec{q} \; K[u,v,w]_{hkl}$$

The diffuse intensity due to first order only is obtained by subtracting σ_2 from the observed diffuse intensity σ_1 (corrected for divergence, skew etc.). Third and higher order corrections are fairly small and hence neglected. Very recently a least square fit method for the determination of the above correction is given by Lucas (1968, 1969). This method is particularly useful when the second order correction is large and very accurate values of the same are needed. However in the present investigation appreciable difference between the two methods of correction are not found.

4.5.7 White radiation and mosaic - structure corrections:

Unlike the skew correction and the divergence corrections, which have to be made for every measurement, the corrections considered here arise only for measurements made at points along certain rekhas. Thus, if the crystal is appreciably mosaic, then the Bragg reflexion would extend over a range of angles on either side of the peak, e.g. along the arc BQB' in the section shown in Fig.4.9. Thus, enhanced values would be observed for the diffuse flux for points lying on rekhas close to the rekha AQA'. If this additional flux is not large compared with the true diffuse flux, then it can be eliminated by interpolation from measurements along neighbouring rekhas. This procedure of interpolation is called the correction for mosaic structure.

The white radiation correction is important for rekha C'QC, i.e. rekha lying along the rel-vector OQ and is similar to mosaic-structure correction, since it is intended to correct for a slightly enhanced diffuse reflexion observed for points along the rekha. The enhancement is due to small amount of white radiation diffusely reflected by the crystal under study. The enhancement is generally less than 10 percent, and it can be corrected by interpolation from measurements at points such as C_1 C_2 C_3 and C_4 lying on the same circle as C_1 but on rekhas at $\pm$ 10° and $\pm$ 20° to the rel-vector at other angles as suitable. It is however important to make this correction for every measurement lying on this rekha.

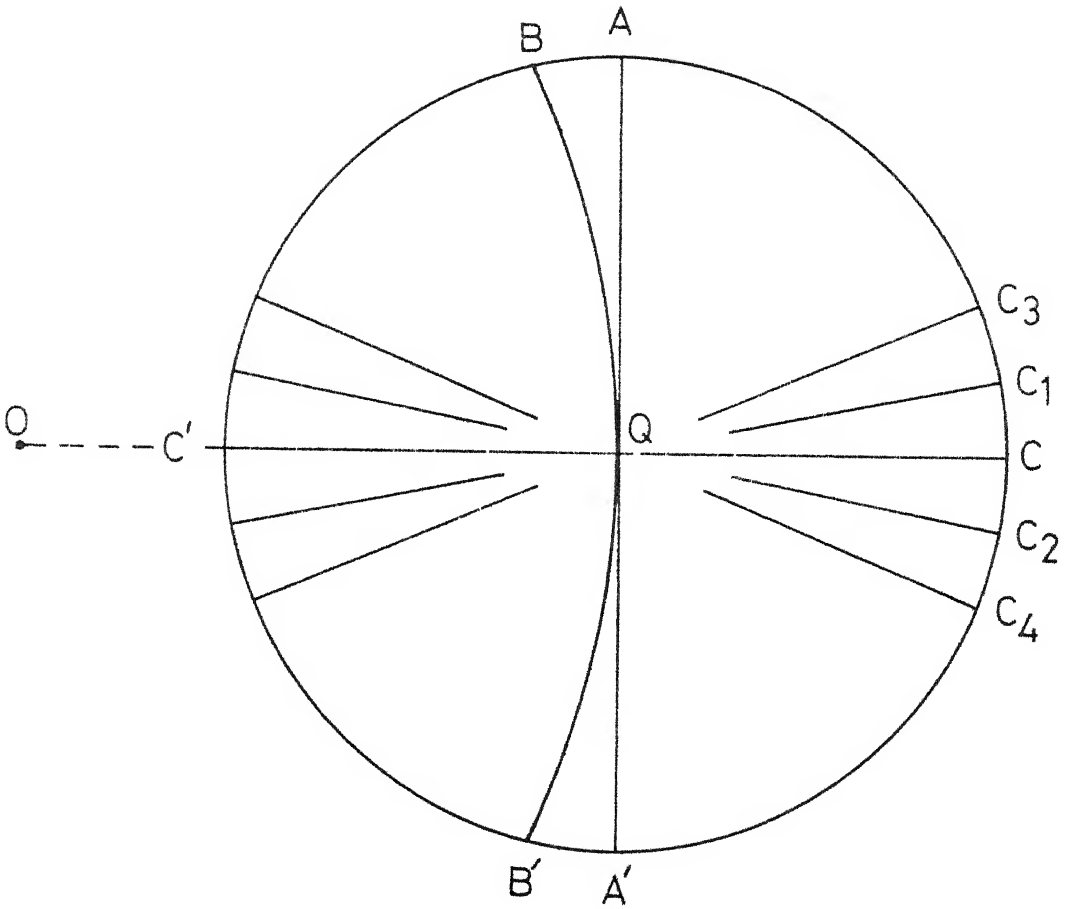

Fig. 4.9: Diagram showing the rekhas AQA' and CQC' affected respectively by mosaic structure and white radiation.

The final intensity (I_d) is obtained after applying all these corrections.

4.5.8 Trigonometric evaluation of a Thermal wave vector:

The wave vector $\vec{q}$ (QP_1 QP_2, $0Q_1$ etc. Fig. 4.10) for any particular direction of propagation of the thermal wave and the corresponding angle of scattering 2θ can be calculated by establishing trigonometrical relations by considering the geometrical position of the circle of reflection in the reciprocal lattice net for a particular setting of the crystal. The position of the circle is completely determined by the knowledge of the correct orientation of the crystal with respect to the incident beam. This can be readily determined by measuring the angle of diffraction of some known reflection in the orientation pictures. The parameters used for making these calculations are given below:

$$a^* = 0.1755 \quad \text{Å}^{-1}$$
$$b^* = 0.2518 \quad \text{Å}^{-1}$$
$$c^* = 0.1748 \quad \text{Å}^{-1}$$
$$\frac{1}{\lambda^*} = 1.40 \quad \text{Å}^{-1}$$

where a^*, b^*, c^* are unit vectors in the reciprocal lattice. It is evident from the equation (3.1, 3.2) that graph between I_d and λ_t^2, for a particular reciprocal lattice point and direction of propagation of thermal wave should be a straight line passing through the origin (after subtracting general scattering correction). The slope of this straight line would give

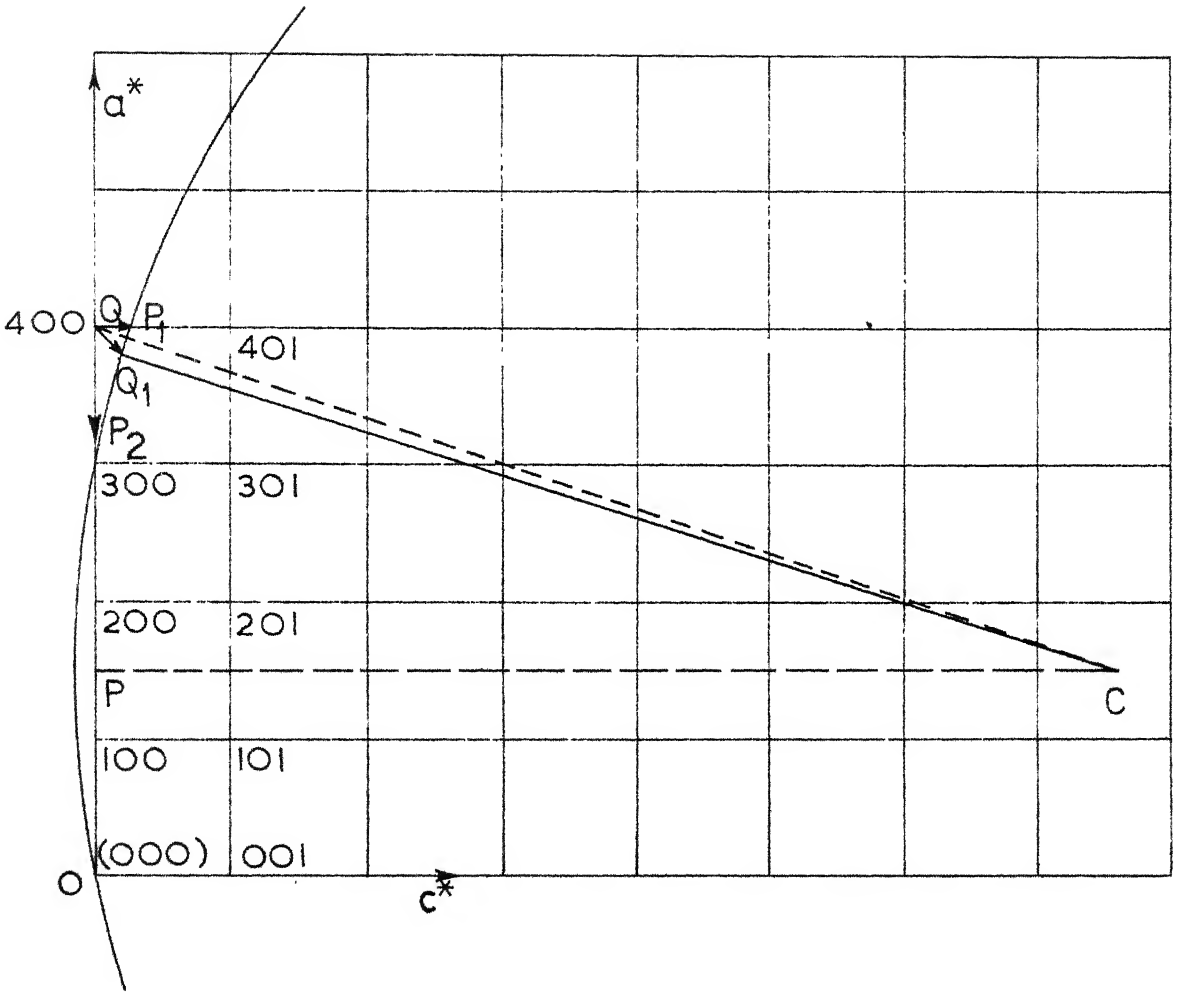

FIG. 4.10: A section of the reciprocal lattice plane a*c* of Potassium Niobate. The figure shows the formation of (4 0 0) diffuse reflection QP_1, QP_2 and QQ_1 are the wave vectors of thermal waves propogating along $[0\,0\,1]_{400}$, $[1\,0\,0]_{400}$ and $[1/\sqrt{2},\ 0,\ 1/\sqrt{2}]_{400}$ directions respectively.

$I_d \vec{q}^2$. These graphs were drawn for all the cases and were used for evaluating $I_d \vec{q}^2$ (or $(I_d/I_o)/q^2$ in the photographic method). All other factors in Eqs. 3.1 and 3.2 being known the value of $K[u,v,w]_{hkl}$ have been calculated. These graphs have been reproduced in the Appendix I.

4.5.9 Equiscattering Contours around a node and K surfaces:

A surface surrounding a reciprocal point over which I_d/I_o has a constant value is called a iso-diffusion or equi-diffusion contour.

The procedure for drawing equiscattering contours in the photographic method is discussed first.

In order to see the variation of diffused intensity with the wave length in different directions of propagation of thermal waves responsible for diffuse reflections, equiscattering contours around (h 0 0) reflection in a*c* and a*b* reciprocal lattice planes can be drawn in the following way. A curve I'_d/I_o vs. ϕ for a (h 0 0) reflection in a*c* and a*b* planes corresponding to different orientations is obtained. From this curve corresponding to a maximum misorientation from the Bragg reflection position a sufficiently high value of I_d/I_o (of the order of 10^{-6}), was chosen, because this value will be available in all the curves. From each of the I'_d/I_o versus ϕ curves the approximate angles (ϕ's since each curve will give two angles) which correspond to the above chosen value of I_d/I_o were noted down and then the skew and polarization factors for these two

ϕ's were calculated. The required corrections thus being approximately known, the values of I_d'/I_o which will give the corrected value equal to the chosen value of I_d/I_o at ϕ_1 and ϕ_2 were easily found out for each case.

An equiscattering contour is drawn on a reciprocal net as follows (Fig. 4.10). A reciprocal net on a large scale (0.1 Å^{-1} = 1 cm) was drawn. Using the direction of incidence of X-rays as the diameter, the circle of reflection was drawn with radius = $1/\lambda$ where $\lambda = 0.7107$ Å for MoKα. radiation. Then, a line corresponding to the vector of diffusion (i.e. line making the angle of diffraction ϕ with the diameter of the circle of reflection e.g. OQ_1 in Fig. 4.10) was drawn. Intersection of vector of diffusion and the circle of reflection gives the corresponding pole of diffusion. Thus poles of diffusion corresponding to a particular value of I_d (or I_d/I_o in photographic method) at different orientations for a particular diffuse reflection were plotted in a reciprocal lattice plane. These curves are known as equiscattering contours or iso-diffusion contours for a particular diffuse reflection.

Now turning to the diffractometer method, the procedure for drawing equiscattering contours is exactly identical as described above for the photographic method, except that in the diffractometer technique the graphs for a given reflection are drawn between I_d (corrected diffuse intensity) and λ_t^2, instead I_d/I_o vs. ϕ as in the photographic method. This is so because

I_d and I_o are measured separately in the diffractometer method, while they are recorded simultaneously in the camera method. ϕ corresponds to a definite value of λ_t, the wave length of the elastic wave. A graph of I_d vs. λ_t^2 is a straight line, drawn on both sides of a given relp. From these two graphs of I_d vs. λ_t^2 for a given relp, a value of I_d corresponding to maximum misorientation from Bragg reflection position such that a sufficiently high value of I_d is obtained. Dividing this by I_o it gives the value of I_d/I_o. Now substituting this value of I_d/I_o for a given relp in the intensity formula for the diffractometer (Section 3.1.1), i.e.,

$$\frac{I_d}{I_o} = \frac{\epsilon^2 kT \Omega}{2\mu_c v^2} F_T^2 \vec{X}^2/\vec{q}^2 K[u,v,w]_{hkl}$$

$$\left(\frac{I_d}{I_o}\right)_{hkl} = \text{Constant value.}$$

One gets,

$$\vec{q}^2 = \text{Const. } K[u,v,w]_{hkl} \qquad (4.11)$$

A curve can be traced which is an equiscattering contours for the given relp. Such equiscattering contours are drawn for (4 0 0) and (6 0 0) nodes (Sec. 5.1.4).

4.5.9.1 K-surface for Orthorhombic $KNbO_3$:

The variation of the diffuse scattering from points round a given reciprocal lattice point can be conveniently expressed by means of a surface, first used by Jahn (1942), Prasad and Wooster (1956) which we shall describe as K-surface. This is

defined by Eq. (1.19).

$$K\,[u,v,w]_{hkl} = L^2 A_{11}^{-1} + M^2 A_{22}^{-1} + N^2 A_{33}^{-1} + 2MNA_{23}^{-1} + 2NLA_{31}^{-1} + 2LMA_{12}^{-1} \ldots$$

Thus the value of $K[u,v,w]_{hkl}$ is determined simply by elastic constants and the directions of (a) the wave normal corresponding to the source of the diffuse scattering, and (b) the rel vector. The expression for $K\,[u,v,w]_{hkl}$ in terms of the elastic constants and the direction cosines contained in the equation (1.19) is applicable to any system of symmetry. As the symmetry decreases more and more elastic constants become involved and the labour of computation increases. By inserting the particular values of elastic constants and giving u,v,w all possible values, the whole range of K-values may be covered for a given relp. K-surfaces are drawn for (0 0 6) and (6 0 0) relps projected on [0 1 0] and [0 0 1] respectively (Sec. 5.1.4).

4.5.10 Choice of the planes for the determination of the elastic constants (see table 4.1).

The diffuse flux to be observed should be as large as possible, since the intensity of diffuse reflection in the first order depends directly on $\vec{X}^2$ and F_T^2 i.e. F_T^2/d_{hkl}^2, other conditions remaining the same. Therefore, it is best to choose for study those relps for which this quantity is largest. The convenient range of suitable Bragg angles is $20^\circ - 50^\circ$. The lower

limit arises from the fact that the skew correction is appreciably different from unity for angles of reflexion smaller than 20°, and slight missetting of the crystal is liable to produce large errors. The upper limit arises from two causes (i) The mechanical limit to the movement of the instrument which goes only upto 120° conveniently, so that θ should be less than 50°. (ii) The formula used by Laval, based on the assumption that the amplitudes of atomic vibrations are small compared with the lattice spacing. The mean amplitude of thermal vibrations at room temperature is of the order of 0.2Å for most crystals (Lonsdale 1942), we may therefore assume that $\sim$ 1 Å is a safe lower limit for the lattice spacing.

The Bragg angle corresponding to 1 Å with Cu Kα is $\simeq 50^{\circ}$, while with Mo Kα $\simeq 25^{\circ}$. Considering now the wavelength of X-rays to be used, it is preferable to use as long a wave length as possible, for several reasons as explained in detail by Ramachandran and Wooster (1951). But the absorption factor has also to be taken into account. It is very large for a long wavelength, thereby causing a large error in intensity. Hence the choice of proper wavelength for a given case should be made. For the planes with larger $\vec{X}$ (i.e. higher Bragg angle), second order diffuse scattering will be larger (as discussed earlier). Therefore correction on this account will be necessary; P, the polarization factor is smaller at higher angles and diffuse intensity will be reduced due to this factor. Hence, planes which have high Bragg angles can be used only if the values of their structure factors are very high.

TABLE 4.1

A. Planes studied with [0 1 0] axis vertical

Indices	d in Å	Diffraction angle 2 θ in degrees	F_T
4 0 0	1.424	28.88	72.73
0 0 4	1.430	28.76	71.92
0 0 6	0.952	43.78	38.77
B. Planes with [1 0 0] axis vertical			
0 4 0	0.996	41.94	62.83
C. Planes with [0 0 1] axis vertical			
6 0 0	0.946	43.96	41.44

Structure factor data are taken from Katz and Megaw (1967) and Dwivedi and Srivastava (1969).

4. REFERENCES

Albrecht, G. — Rev. Sci. Instrum, 10 221 (1939).

Amoros, J.L. and Amoros, M. — Molecular Crystals, John Wiley, (1968)

Arndt, U.W. and Willis, B.T.M. — Single Crystal Diffractometry, Cambridge University Press (1966).

Azaroff, L.V. — Acta Cryst. 8, 701, (1955).

Burbank, R.D. — Acta Cryst. 18, 88 (1965)

Ibid, 19, 957 (1965).

Chakraborty, S.C. — D. Phil. (Thesis), Allahabad Univ.(1958

Chipman D. and Warren B.E. — J. Appl. Phys. 21, 696 (1950).

Dwivedi, G.L. and Srivastava, R.C. — Unpublished work (1969).

Furnas, T.C. — Single Crystal Orienter Instruction Manual (G.E.) (1957).

Guinier, A. — Radio Cristallographie, Dunod Paris, (1945).

International tables for X-ray crystallography, Vo. II 161-163, 291-312, III 5, 68-88, 133, 157-194, 232, 247-253, Kynoch Press, (1963).

Jahn, H.A. — Proc. Roy. Soc. A179, 320 (1942).

Katz, L. and Megaw, H.D. — Acta Cryst. 22, 639 (1967).

Lonsdale, K. — Nature (London) 149, 21 (1942).

Lucas, B.W. — Acta Cryst. A24, 336 (1968).

Acta Cryst. A25, 627 (1969).

Miller, C.E. — J. Appl. Phys. 29, 233 (1958).

Prasad, S.C. and Wooster, W.A. — Acta Cryst. 8, 361, 506, 682 (1955); Ibid, 9, 38, 169, 304, (1956).

Peiser, et al	X-ray diffraction by Polycrystalline Materials, Institute of Physics, (1955
Ramachandran, G.N. and Wooster, W.A.	Acta Cryst. 4, 335, (1951).
Robinson, B.W.	J. Sci. Instrum. 10, 253 (1933).
Ross, P.A.	J. Opt. Soc. Am. 16, 375, 433, (1928).
Tanaka et al	Rev. Sci. Instrum. 30, 430 (1959).
Umanskii, M.M.	Apparatus for Crystal Structure Investigation, Moscow (1960).
Wood, E.	Acta Cryst. 4, 353, (1951).
Wooster, W.A.	Diffuse X-ray reflections from crystals, Clarendon Press, Oxford (196
	Adv. Methods of X-ray Crystallography, 121-156, edited by Ramachandran, Academic Press, (1964).

5. RESULTS AND DISCUSSION

5.1 Results

5.1.1 Elastic constants: Old theory

The diffractometer study of orthorhombic Potassium Niobate crystal at room temperature resulted in the following nine elastic constants, based on old (Voigt's) theory (Table 5.1). Various corrections, described in Sec. 4.5 have been applied to the diffractometer data before obtaining the final results. The details of calculations of these elastic constants are given in Appendix I.

Table 5.1

Elastic constant	Value
C_{11}	0.3(54) x 10^{12} dynes/cm^2 or 10^{11} Newton/Meter^2
C_{22}	0.5(16) "
C_{33}	0.6(32) "
C_{44}	3.5(58) "
C_{55}	3.6(51) "
C_{66}	2.0(69) "
C_{12}	-1.0(58) "
C_{13}	-2.0(27) "
C_{23}	-1.9(14) "

5.1.2 Elastic constants: New theory

It is seen in Sec. 3.1.2 that fifteen elastic constants are necessary for completely specifying the elastic behaviour of Potassium Niobate crystal. But six of them do not occur independently but appear only in combinations $(C'_{12} + C'_{69})$, $(C'_{23} + C'_{47})$, $(C'_{13} + C'_{58})$ in the expressions for propagation of elastic waves in the crystals for the particular case; therefore, all the dynamical methods would only give these combinations and not the individual constants (Wooster 1961). One is thus left with only twelve dynamical constants. Namely, C'_{11}, C'_{22}, C'_{33}, C'_{44}, C'_{55}, C'_{66}, C'_{77}, C'_{88}, C'_{99}, $(C'_{12} + C'_{69})$, $(C'_{23} + C'_{47})$ and $(C'_{13} + C'_{58})$. Out of these C'_{11} to C'_{66} can be identified with the constants C_{11} to C_{66} of the classical theory (Tables 3.1 to 3.3). So the values of these constants are unaffected due to the implications of the new theory as applied to the present case.

Further, it is possible to distinguish between the following pairs of elastic constants in the new theory: (C'_{55}, C'_{88}; C'_{66}, C'_{99}; C'_{44}, C'_{77}; C'_{69}, C'_{66}; C'_{58}, C'_{55}; C'_{47}, C'_{44}). For example, according to old classical theory the rekhas $K[\,1\,0\,0\,]_{001}$ and $K[\,0\,0\,1\,]_{h00}$ would give the same elastic constant, namely C_{55} but according to new theory, they give rise to two different elastic constants i.e. $K[1\,0\,0]_{001}$ gives C'_{55} while $K[0\,0\,1]_{h00}$ gives C'_{88}. Now it is known that C'_{55} is identified with C_{55}.

C'_{55} and C'_{88} have been determined independently from individual values of $K[1\,0\,0]_{006}$ and $K[0\,0\,1]_{400}$ respectively. Details of observations and calculations are given in the Appendix I in the tables for (0 0 6) and (4 0 0) planes; whence we get,

$$C'_{55} = 3.6(5) \times 10^{12} \text{ dynes/cm}^2$$
$$C'_{88} = 3.4(6) \times 10^{12} \text{ dynes/cm}^2$$

The difference between the two is about 6%. Since the two values depend on the structure factors of the two different planes and because of the limitation of the accuracy attainable by the method (Sec. 5.4) used in the present investigations, this difference is not considered very significant. Additional planes were tried to distinguish between other constants like C'_{77}, C'_{99} etc but without any success. It should be pointed out further that if the difference between two constants say $C'_{55} \sim C'_{88}$ etc. is not large compared to the inaccuracy (8% for these constants) involved in the measurements, then they would not be detected and the results can be interpreted in terms of the classical theory.

Evidently therefore, the difference between C'_{55} and C'_{88} and such differences in other constants (constants involved should be determinable from individual K-values independently) can be employed to differentiate between the two theories, the limitation being that the difference should be larger than 10%, if the X-ray method is employed. Due to limitations of the accuracy of the method employed, it is not possible, on the basis

of our experimental results to make any assertion regarding the differences between the classical and new theory of elasticity, particularly for the case which has been investigated.

5.1.3 Comparison of the experimental methods:

5.1.3.1 Photographic method:

In the present investigation only one relp (4 0 0) is studied by this technique . Five misset positions on one side of the relp have been observed to give the elastic constant C_{55}. The results are in good agreement with those obtained by the diffractometer technique where equally small crystal for the same relp (4 0 0) was employed (e.g. C_{55} = 3.49(5) x 10^{12} dynes/cm^2 by photographic method, C_{55}=3.46(3)x 10^{12} dynes/cm^2 by diffractometer). Each exposure for diffuse spot ran around 30 to 50 hrs. The accuracy is limited due to the various other causes described earlier (Sec. 4.1). The photographic method takes very long time for the complete data collection compared to the diffractometer method. Results are given in Appendix I.

5.1.3.2 Diffractometer method:

As pointed out in Sec. 4.2, small crystals of the size ($\sim 10^{-4}$ cc) are generally used for the photographic methods and larger crystals of the size $\sim$ 5 mm x 5 mm are (Ramachandran and Wooster 1951) customarily employed for the diffractometer technique. In the present investigation a very small crystal of $\sim 10^{-4}$ cc has been successfully used not only in the photographic

method but also in the counter diffractometer method. The agreement between the results obtained by two methods with small crystals is considered good. As a result, one of the limitations normally associated with the counter technique is no longer considered necessary. Further, crystals varying in size by an order of magnitude led to essentially the same values of elastic constan when studied by diffractometer method (namely C_{11} from $K[100]_{400}$ and from $K[100]_{600}$ are same within the experimental limit). The additional advantage with such a small crystal is that the divergence correction is further reduced.

5.1.4 Equiscattering contours around relps (400) and (600):

Equiscattering contours are the surfaces surrounding each reciprocal lattice point over which diffuse intensity has a constant value. These may also be called surfaces of equal diffusion. Jahn (1942) has shown how to calculate the approximate form of these surfaces.

The method of drawing equiscattering contours for diffractometer and photographic technique is the same. These equiscattering contours which are drawn for the given value of the diffuse intensity becomes a particular case of K-surface calculations (Sec. 5.1.5).

The shape of equiscattering contours around the node (400) and (600) in the reciprocal plane a^*c^* and a^*b^* respectively, is a typical form of Cassini's oval family of curves. Consider

the equiscattering contour for node (4 0 0) for $I_d/I_o = 0.77 \times 10^{-5}$ in the reciprocal plane a^*c^* (Fig. 5.1a). The curve is symmetrical about a^* and c^*. The extension of the contour along a^* shows that amplitude of vibration of the longitudinal wave is higher than transverse wave. Equiscattering contours around node (6 0 0) in reciprocal plane a^*b^* drawn for $I_d/I_o = 3.683 \times 10^{-}$ is also similar in shape to that around (4 0 0) node (Fig.5.1b). It is symmetrical about a^* an b^*. Let us now investigate the nature of these two iso-diffusion contours in relation to the mathematical expressions derived from the thermal theories of diffuse scattering of X-rays. From equation (3.1), We have

$$\vec{q}^2 = e^2 \frac{kT\,\Omega}{2\mu_c v^2} F_T^2 \vec{X}^2 \frac{K[u,v,w]_{hkl}}{I_d/I_o}$$

where I_d/I_o is corrected for all factors including polarization factor.

Or, $\vec{q}^2 = (\text{ a constant }) \times \frac{K[u,v,w]_{hkl}}{I_d/I_o}$ (For any particular node of a given crystal).

Now for an equiscattering contour around (4 0 0) in a^*c^* plane;

$v = 0$, and $I_d/I_o = \text{Const.}$ (L=1, M=0, N=0),

hence,

$$\vec{q}^2 = (\text{Const.}) \times K[u,v,w]_{400} = \text{Const.}\ (A^{-1})_{11}$$

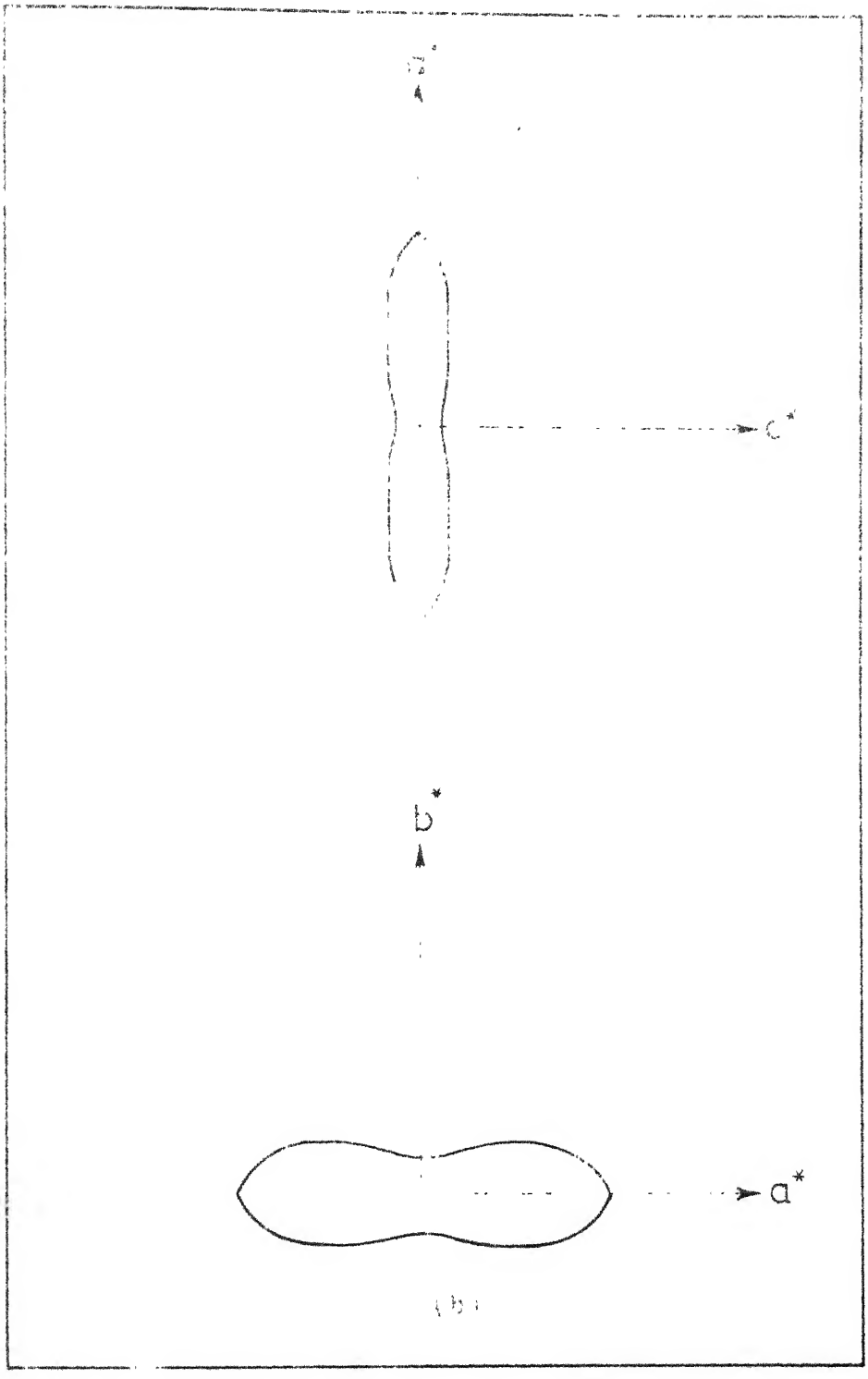

Fig. 3.1(a): Precession curve around the zone (0 k l) in c*a* plane.

(b): Precession curve around the zone (h 0 l) in a*b* plane.

where,

$$A_{11}^{-1} = \frac{(C_{55}u^2+C_{33}w^2)}{((C_{11}u^2+C_{55}w^2)(C_{55}u^2+C_{33}w^2)-(C_{13}+C_{55})^2u^2w^2)} \quad \ldots (5.1)$$

$$= f(u^2, w^2)$$

or $\vec{q}^2 = C.f(u^2, w^2)$ where C is a constant ... (5.2)

$f(u^2, w^2)$ a function of u^2 and w^2 given by Eq. (5.1). So the wave vector for a point on the contour is guided by the relation (Eq. 5.2), Since the function 'f' is dependent only on the squares of the variables u, w, (u and w being the direction cosines of the direction of propagation of the thermal wave corresponding to wave vector $\vec{q}$). The value of $\vec{q}^2$ does not depend on the signs of u and w and hence equiscattering contour would be symmetrical about a* and c* axes and in general it would be an ellipse with its axes along a* and c*. Let us now consider the values of $\vec{q}^2$ for [0 0 1] and [1 0 0] directions. From relations (Eq. 5.1) and (Eq. 5.2) and tables 3.1, 3.2, 3.3, we have,

$$\vec{q}^2_{001} = \text{Const. x } f(0, w^2) = \text{Const. x } \frac{1}{C_{55}} \quad (\because w = 1)$$

or $\vec{q}^2_{001} \times C_{55} = \text{Constant} \ldots$ (5.3)

and $\vec{q}^2_{100} = \text{Const. x } f(u^2, 0) = \text{Const.} \times \frac{1}{C_{11}} \quad (\because u = 1)$

or $\vec{q}^2_{100} \times C_{11} = \text{Constant} \ldots$ (5.4)

From Fig. 5.1a, it may be easily seen that

$$\vec{q}_{100} > \vec{q}_{001}$$

This inequality leads us to the conclusion (from Eqs.5.3 and 5.4) that the elastic constants for this particular crystal would be such as to satisfy the inequality, $C_{55} > C_{11}$. A glance at tables in Appendix I for (4 0 0) relp would indicate that the results derived from the analysis of the equiscattering surface around the node (4 0 0) in a^*c^* plane, are in complete agreement with the elastic constants and vice versa.

Now consider the nature and the shape of the equiscattering contour around the node (6 0 0) in a^*b^* plane. The closed curve is symmetrical about a^* and b^* axes.

Proceeding as before it would be seen that

$$\vec{q}^2 = \text{Const. } A_{11}^{-1} = c.f\,(u^2,\ v^2)$$

where,

$$f(u^2,\ v^2) = \frac{(C_{66}u^2+C_{22}v^2)}{\left[(C_{11}u^2+C_{66}v^2)\ (C_{66}u^2+C_{22}v^2) - (C_{12}+C_{66})^2u^2v^2\right]} \quad \ldots \quad (5.5)$$

Thus $\vec{q}^2$ depends on $f(u^2,v^2)$ whose value is independent of the sign of u and v. Consequently there would be symmetry of the isodiffusion contours in a^*b^* plane. Further from Eq. (5.5),it is seen that,

$$\vec{q}^2_{010} = \text{Const.} \times \frac{1}{C_{66}} \qquad (u = 0,\quad v = 1) \qquad (5.6)$$

Similarly,

$$\vec{q}^2_{100} = \text{Const.} \times \frac{1}{C_{11}} \qquad (5.7)$$

From relations (Eqs. 5.6 and 5.7), we see the inequality $\vec{q}_{100} > \vec{q}_{010}$, this leads us to the conclusion that elastic sonstant of this particular crystal would be such as to satisfy the inequality $C_{66} > C_{11}$. A glance at tables given in Appendix I for relp (6 0 0), once again shows that the results derived from an analysis of the equiscattering surface around the node (6 0 0) in a^*b^* plane are in complete agreement with the elastic constants and vice versa.

The sensitiveness of the form of the surface to the elastic properties of the crystal suggests that the study of the diffuse scattering may become an important method of investigating those crystals which have marked anisotropy of elastic properties such as the present crystal, whose elastic properties depend in more marked way on the directions than do those of a cubic crystal. This variation of elastic properties along the surface is described in detail in Sec. 5.1.5.

5.1.5 K-surfaces:

The thermal diffuse scattering from a crystal varies markedly with direction. Along any line (rekha) through a given reciprocal lattice point (relp) the directional factor is denoted by $K[u,v,w]_{hkl}$ (Ramachandran and Wooster 1951), the value of which is proportional to the direction cosines (u,v,w) of the rekha and hkl, the indices of the relp.

The expression for K may be written (Eq. 1.19),

$$K[u,v,w]_{hkl} = L^2(A^{-1})_{11}+M^2(A^{-1})_{22}+N^2(A^{-1})_{33}+ \ldots$$

where $L = h/(h^2+k^2+l^2)^{1/2}$ etc.

and $A_{11} = C_{11}u^2 + C_{66}v^2 + \ldots\ldots$ etc.

By inserting particular values of elastic constants and giving (u,v,w) all possible values, the whole range of K-values may be covered. In the present investigation, the number of non-zero elastic constants is 9, as the symmetry is orthorhombic and expression for K contains correspondingly more terms. Although h, k, l may have any integral values, in practice very few values suffice for the study and representation of elastic properties. For orthorhombic crystals [1 0 0], [0 1 0] and [0 0 1] cover most of the requirements.

5.1.5.1 Construction of K-surfaces:

For an orthorhombic crystal, we have studied K-surface for the relps (6 0 0) and (0 0 6) projected on the [0 0 1] and [0 1 0] respectively. These values of h,k,l and elastic constants are inserted into the formula for $K[u,v,w]_{hkl}$ and the evaluation is carried out on IBM 7044 computer for large number of directions defined by the direction cosines (u,v,w). The values of K are plotted (3 times the actual scale) on a stereogram, small circles (constant δ-values) separated by 2° intervals and great circles (constant γ -values) also having a separation of 2° from one another are used. The dimensions of K are in cm^2-$dyne^{-1}$, same as those of elastic moduli. K-contours are therefore numbered in units of 10^{-13}.

There are a number of applications of K-surfaces given in detail by Prasad and Wooster (1956). The present investigation demonstrates how K-surfaces are useful in showing which points on a given density contour are least likely to be affected by the second order correction (carried out in a similar way as the divergence correction).

The density contour (solid curve) for first order thermal diffuse scattering for (6 0 0) relp projected on [0 0 1] (Fig. 5.2a) shows a large K-value along [1 0 0] and relatively very small K-value, along [0 1 0]. The K-value in any given direction is proportional to the reciprocal of the corresponding elastic constants hence a large K-value (Fig. 5.2a) along [1 0 0] means a small value of elastic constant (C_{11}) and vice versa. The same is true for small K-value along [0 1 0] i.e. for (C_{66}), this also shows that the thermal wave vector $q_{100} > q_{010}$. Same conclusion was drawn from the equiscattering contour for the node (6 0 0) (Sec. 5.1.4 and Fig. 5.1b).

The dotted line represents the K-surface (Fig. 5.2a) corrected for second order correction (Ramachandran and Wooster 1951, Lucas 1968, 1969) for relp (6 0 0). From the contours (solid and dotted) over the whole stereogram, one can easily see the rekha $K[1\,0\,0]_{600}$ is affected most while $K[0\,1\,0]_{600}$ is affected the least and the intermediate K-values ($K[u,v,w]_{hkl}$) are affected correspondingly.

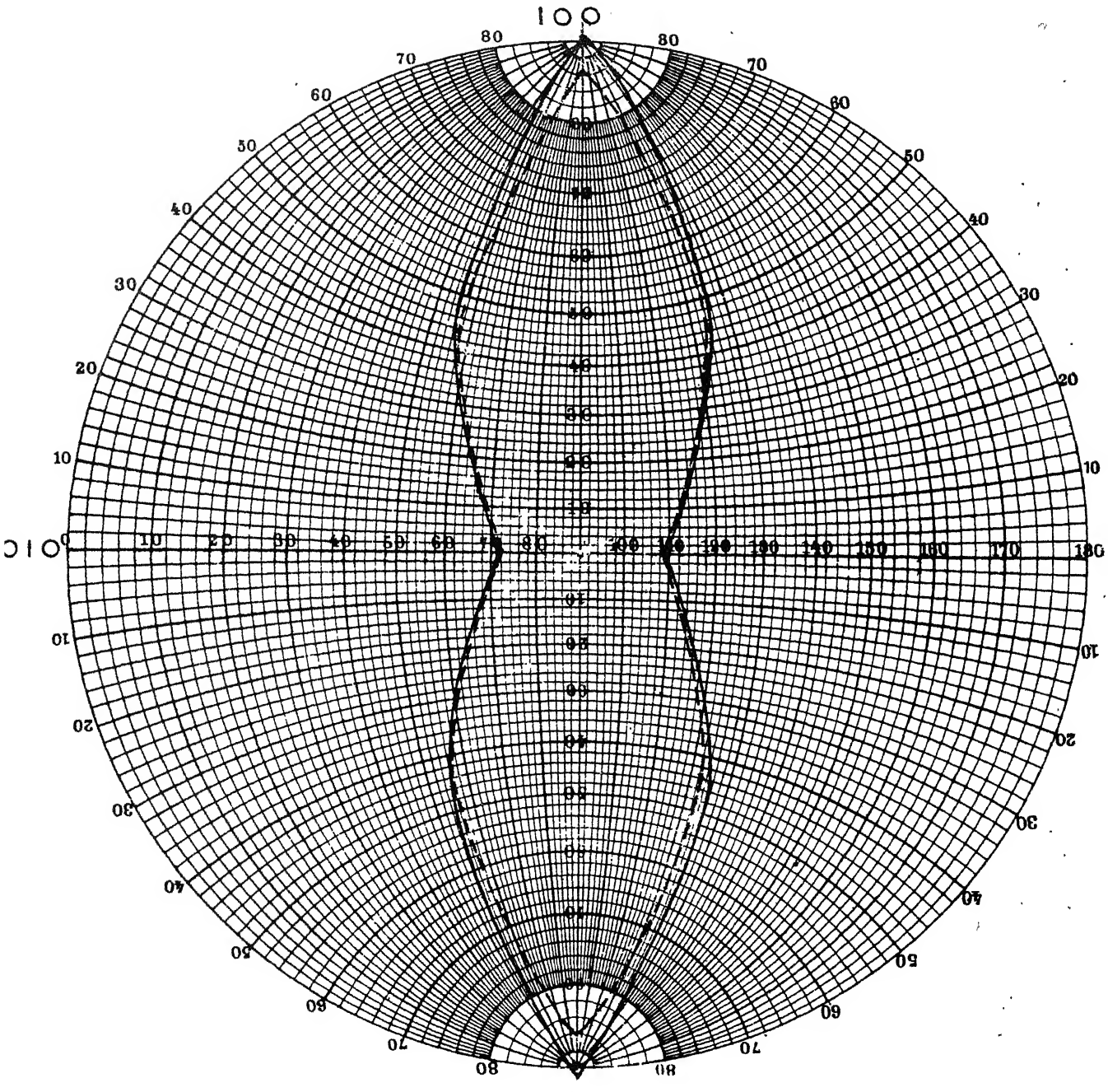

FIG.5.2(a) STEREOGRAPHIC PROJECTION OF THE K-SURFACE FOR POTASSIUM NIOBATE; RELP (6 0 0) PROJECTED ON [0 0 1]

Thus a large change is observed in a K-value along [1 0 0] after applying a second order correction (dotted curve), meaning thereby that the second order correction for C_{11} is largest and least for C_{66}. This is in excellent agreement with the corrected and uncorrected values C_{11} and C_{66}. For convenience only a single contour is drawn with and without the second order correction. Similarly the contour projected on the [0 1 0] for the relp (006) (Fig. 5.2b) shows that C_{33} is affected most by second order correction $[1/K\ [0\ 0\ 1]_{006} = C_{33}]$ and C_{55} the least ($C_{55}=1/K[1\ 0\ 0]_{006}$) Thus the nature and shape of the isodiffusion contours around (4 0 0 and (6 0 0) relps, and K-surfaces for relps (6 0 0) and (0 0 6) are in complete agreement with the theory of diffuse scattering of X-rays. The information given by the equiscattering and K-surface studies regarding the relative values of the elastic constants is consistent with the values of the elastic constants of Potassium Niobate determined by X-ray diffuse scattering.

5.2 Discussion

5.2.1 Accuracy of the results:

Accuracy of the results of the elastic constants, determined by the X-ray diffuse scattering method depends upon the following factors,

1. Choice of the reflecting plane (relp) and the rekha.
2. Various corrections 2(i) absorption (ii) divergence (iii) skew, (iv) polarization (v) second and higher order, (vi) Mosaic, (vii) white radiation and (viii) general

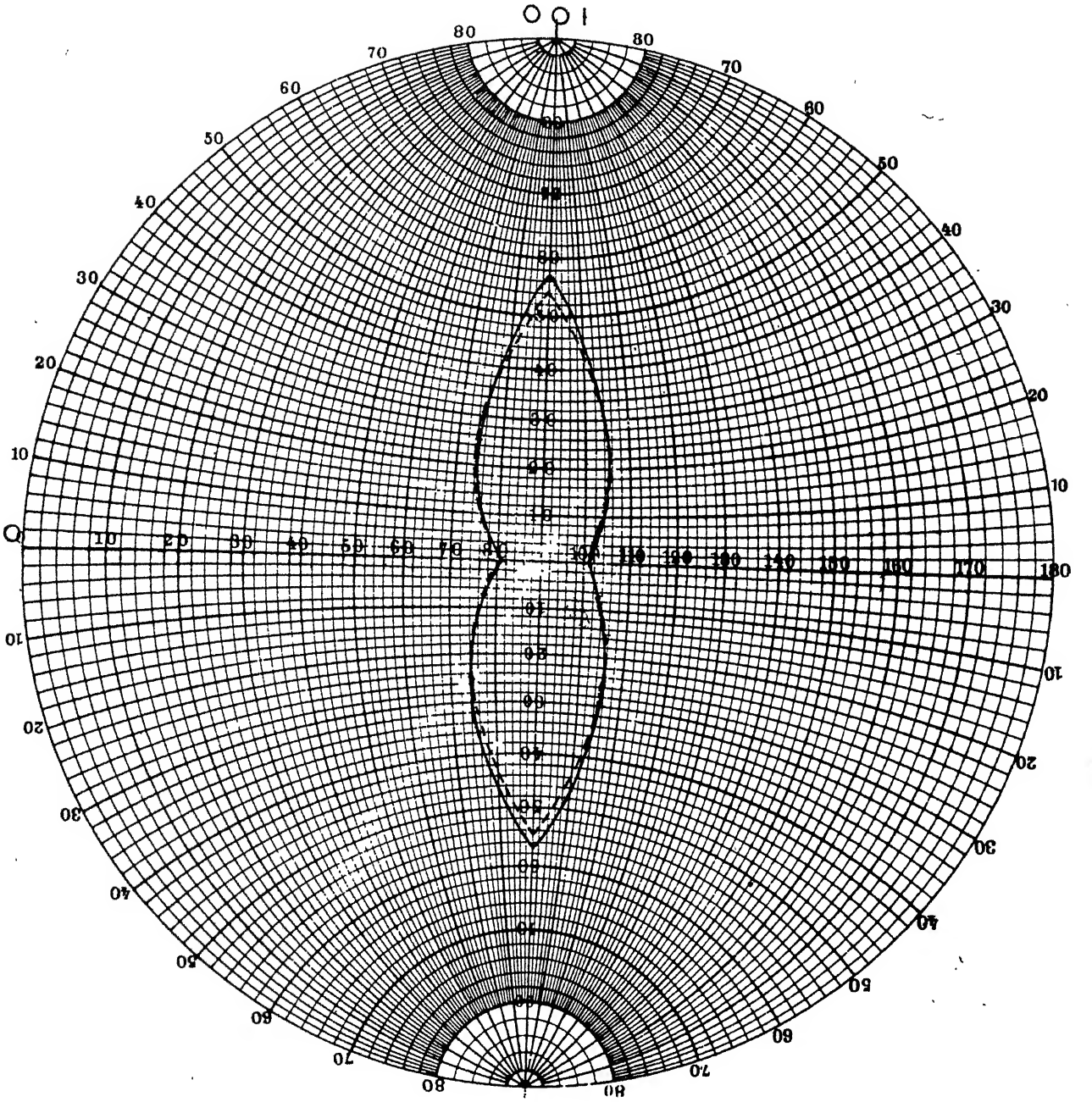

FIG·5.2(b) STEREOGRAPHIC PROJECTION OF THE K-SURFACE FOR POTASSIUM NIOBATE; RELP (0 0 6) PROJECTED ON [010]

scattering.

3. Absolute intensity (I_o) measurements.

4. Cochran's optical mode contribution.

The first two factors affect the accuracy of an individual constant in different ways, on the other hand the factors 3 and 4 affect all the elastic constants to the nearly same extent and hence will be discussed latter.

Constants C_{11}, C_{22} and C_{33} are determined from the rekhas $[1\,0\,0]_{600}$, $[0\,1\,0]_{040}$, $[0\,0\,1]_{006}$ respectively. These constants involve quite a large error $\sim$ 7%. The wave vectors for them are relatively large i.e. measurement is made away from reciprocal lattice points, thereby making second order correction larger $\sim$ 8% even if the higher orders are neglected. One could in principle make observations close to the relp but the divergence corrections (particularly i divergence) increases rapidly nearer the relp and becomes uncertain. There are limitations due to little mosaic spread also, alternative way to reduce the second order correction is to obtain the elastic constants C_{11} etc. from relps of lower indices i.e. at smaller 2θ. This obviously increases skew correction to $\sim$10% or so. In fact C_{11} obtained from (400) relp does not show any appreciable difference from the one obtained from (6 0 0) relp. Higher the plane index higher is the diffuse intensity which improves the accuracy, and the structure factor value for these planes are also quite high. Therefore diffuse intensity can be measured with better accuracy. Divergence

correction has been reduced by using a small crystal $\sim 10^{-3}$ c.c. and small slits for beam and detector collimators. The absorption factor is the most serious source of error affecting the accuracy of the results in the X-ray work. This is reduced by using a well shaped crystal of suitable size, further μ the linear absorption coefficient of this crystal is very carefully determined (Appendix III) and is accurate within 5%. Errors due to mosaic spread, white radiations and optical vibrations etc. are corrected by taking mean of the intensity readings at points equidistant from the given reciprocal lattice point. All errors are further reduced by studying the rekhas on either side of the Bragg reflection and taking the average value of elastic constants. Therefore the accuracy of the C_{11}, C_{22} and C_{33} is 7%. The constants C_{44}, C_{55}, C_{66} are obtained from the rekhas $[0\,0\,1]_{040}$, $[1\,0\,0]_{006}$, $[0\,1\,0]_{600}$ respectively. Here the thermal wave vectors involved in the calculations are very small compared to the case of C_{11}, C_{22} and C_{33}. Thus, second order correction is much reduced (2%) while other corrections are nearly the same as for C_{11}, C_{22}, C_{33}. Therefore the accuracy of the C_{44}, C_{55} and C_{66} is 5%.

Constants C_{12}, C_{13} and C_{23} are obtained from the rekhas, $\left[\pm\frac{1}{\sqrt{2}}, \pm\frac{1}{\sqrt{2}}, 0\right]_{600}$, $\left[\pm\frac{1}{\sqrt{2}}, 0 \pm\frac{1}{\sqrt{2}}\right]_{006}$ and $\left[0, \pm\frac{1}{\sqrt{2}}, \pm\frac{1}{\sqrt{2}}\right]_{040}$ respectively, for example, the constant C_{12} can be determined as follows,

$$C_{12} = -C_{66} + \sqrt{\ } C_{66}^2 + C_{22}C_{66} + (C_{22}+C_{66})(C_{11}-\ /K\left[\pm\frac{1}{\sqrt{2}} \pm\frac{1}{\sqrt{2}}, 0\right]_{60}$$

similar is the case of C_{13} and C_{23}. The accuracy of these constants is obviously low as they depend upon the values of the independent constants. Second order correction is quite appreciable in these cases ($\sim$5%). All other corrections remain practically the same as for C_{11} etc. It may be noted that the accuracy of C_{12}, C_{13}, C_{23} mainly depends upon the accuracy with which the K-values for the relps are known. Any small error in the K-value introduces a large error in these elastic constants. An idea of the accuracy of K-values can be obtained by comparing the experimentally determined K-values with those derived from the elastic constants. For example, the mean of the experimentally observed value $K\left[\pm\frac{1}{\sqrt{2}}, \pm\frac{1}{\sqrt{2}}, 0\right]_{600}$ relp is given as 0.986×10^{-12} cm^2/dyne (Appendix I) (after the second order correction).

$$K\left[\pm\frac{1}{\sqrt{2}}, \pm\frac{1}{\sqrt{2}}, 0\right] = \frac{2(C_{22}+C_{66})}{C_{11}(C_{22}+C_{66})+C_{22}C_{66}-2C_{12}C_{66}-C_{12}^2}$$

The value of the right hand side of this expression can be found by substituting the evaluated values of the elastic constants (Table 5.1).

Thus,

$$K\left[\pm\frac{1}{\sqrt{2}}, \pm\frac{1}{\sqrt{2}}, 0\right] = 0.965 \times 10^{-12} \text{ cm}^2/\text{dyne}$$

The observed and calculated K-values agree well within the estimated error ($\sim$ 3 to 4%). The remaining two factors which reduce accuracy of the elastic constants may now be

discussed. The accuracy of the determination of the elastic constants from the study of diffuse reflections mainly depends on the accuracy with which the ratio I_d/I_o can be measured (in both diffractometer and photographic methods) separately in addition to the accuracy of the structure factor values. The measurement of the direct beam intensity I_o is a very difficult task on the diffractometer owing to its very high value ($\sim 10^6$ times the diffuse intensity I_d). Therefore some intermediate standards are chosen. In the present investigation Compton intensity I_c, from a diamond, which is of the order of diffuse intensity, is measured and from that the direct beam intensity I_o is determined. The method is discussed in detail in the Appendix II. Such a standardization of the incident intensity can be made with an accuracy of a few percent ($\sim 3\%$). The accuracy of intensity measurements by photographic photometry is limited due to several factors (Sec. 4.1.). But in the present investigation I_d and I_o have been measured simultaneously on the same photograph: The blackening for the diffuse spot and direct beam impression is adjusted or rather matched with the help of suitable numbers of Zr filters placed in the path of the direct beam. For measuring the intensity from the blackening of the photographic emulsion of the film, standard wedges were developed (simultaneously) with each photograph. The piece on which the standard wedge was recorded was cut from the same sheet as was used for the corresponding diffuse intensity records (or monochromatic pictures). So it is believed

that the accuracy in the measurement of I_d/I_o is within 3% provided the linear absorption coefficient of zirconium foil is absolutely correct. Allowing for other errors like structure factor, optical vibration etc., accuracy in the photographic method for the constant C_{55} is $\pm$ 8%.

Lastly we shall describe the deviation in the values of elastic constants due to the low frequency transverse optical phonon mode or socalled Cochran's mode responsible for the ferroelectric property in the crystal. In the Sec. 1.4, a brief summary of Cochran's theory has been presented. The theory predicts the existence of a low frequency mode which goes to nearly zero as the critical temperature is approached in a given crystal. Such a low frequency optical mode would obviously contribute to the diffuse intensity besides the usual acoustic modes and hence the values of the elastic constants determined on the assumption of negligible optical contribution, would deviate from their true values. The recent study of Potassium Niobate by Perry et al (1969) by laser Raman spectroscopy does not show any such low frequency phonon mode in the room temperature orthorhombic phase. Other data such as the dielectric dispersion etc. which can throw light on the existence of the Cochran mode are not available. Further, the transition from ferroelectric to paraelectric phase in the case of $KNbO_3$ takes place near 435°C, while elastic constants have been obtained at room temperature in the present study.

The frequency is not abnormally low at this temperature (Perry et. al 1969). If one makes a very crude approximation that the crystal is cubic and follow the procedure outlined by Bell and Rupprecht (1963) for $SrTiO_3$, it is found that the deviation in the elastic constants due to low frequency (Cochran's) mode is not more than 2 to 3%. Therefore taking into account all the factors which influence the accuracy of the elastic constants, it is found that C_{11}, C_{22}, C_{33} can be measured with an accuracy of $\pm$ 10%, C_{44}, C_{55} and C_{66} with an accuracy of $\pm$ 8% while the dependent constants C_{12}, C_{23} and C_{13} with an accurary of $\pm$ 12%.

5.2.2 On the new theory of elasticity:

The new theory has been discussed in Sec. 1.1.2. In Sec. 5.1.2 attempts were made to determine the elastic constants on the basis of the new theory but it was observed that the experimental errors in the present method were larger than the difference between elastic constants based on the old and the new theories. In recent years, there have been few experiments performed to verify the new theory but it is surprising that even in the simple cubic crystals e.g. $NaBrO_3$, the difference in the elastic constants obtained by new and old theory is hardly 0.1% (Radha and Rajgopal, 1968) which is well within the limit of experimental error of the method employed (pulse technique). Unequivocal results justifying the validity of the new theory have yet to appear.

5.2.3 Relationship of diffuse scattering with other properties like thermal expansion, structure etc.

A qualitative correlation between thermal expansion and diffuse scattering has been discussed in detail in Sec. 5.2.4. A brief mention of it may be made here. The diffuse scattering is entirely due to the amplitude of vibrations of the atoms, the larger the amplitude the greater is the observed diffuse intensity. Similarly thermal expansion is normally a function of lattice vibrations. Large thermal expansion coefficient along certain directions indicates a loose binding between the atoms i.e. the existence of weak atomic forces or in other words, large amplitude of vibrations. This is what has been observed in study of diffuse scattering also. Large thermal expansion is observed along [0 1 0] Similarly diffuse intensity is also having a comparatively large spread around (0 k 0) reciprocal point. No studies on the thermal expansion of this single crystals are available to date to make any definite conclusion in the establishment of such relation and extending it to the individual values of the elastic constants. Among the elastic constants, it is worth mentioning that the direction [0 0 1], along which the constants C_{55} and C_{33} are measured, undergoes a minimum change with the temperature, as it can be seen from the thermal expansion studies (Shirane et al 1954) of the polycrystalline sample along this direction. Our studies of equiscattering contours and K-surfaces give information which is consistent with the experimental values of the

elastic constants obtained in the present study. The Debye temperature of Potassium Niobate has been estimated, from the room temperature elastic constants, to be 302°K. The details of these computations are given in Appendix IV. The ratio of $\frac{\theta_D}{T_m} = \frac{302}{(1050 + 273)} \simeq 0.23$. This value may be compared with that for isostructural $BaTiO_3$ $\frac{\theta_D}{T_m} = \frac{400}{(1618 + 273)} = 0.21$ (Volger 1952, Bhide et al 1965).

5.2.4 The relation between the structure of ferroelectric Potassium Niobate: its thermal expansion and the X-ray diffuse scattering:

In the present investigation an attempt has been made to investigate a relation between the structure of the Potassium Niobate and its thermal expansion behaviour in the orthorhombic phase, it is also shown that this relation is in full agreement with the observations of the thermal diffuse scattering.

The graph (reproduced from Shirane et al 1954) Fig. 5.3 shows the variation of lattice parameters with the rising temperatures.

On looking carefully into the graph (Fig. 5.3) of thermal expansion, a contraction is observed in the lattice parameters along a and c (a graph is plotted for Monoclinic parameters equivalent to given orthorhombic cell) $a_{ortho.} = 2a'\sin \beta/2, c_{ortho} = 2a' \cos \beta/2$, $b_{ortho} = b$ (symbols have their usual meaning) while

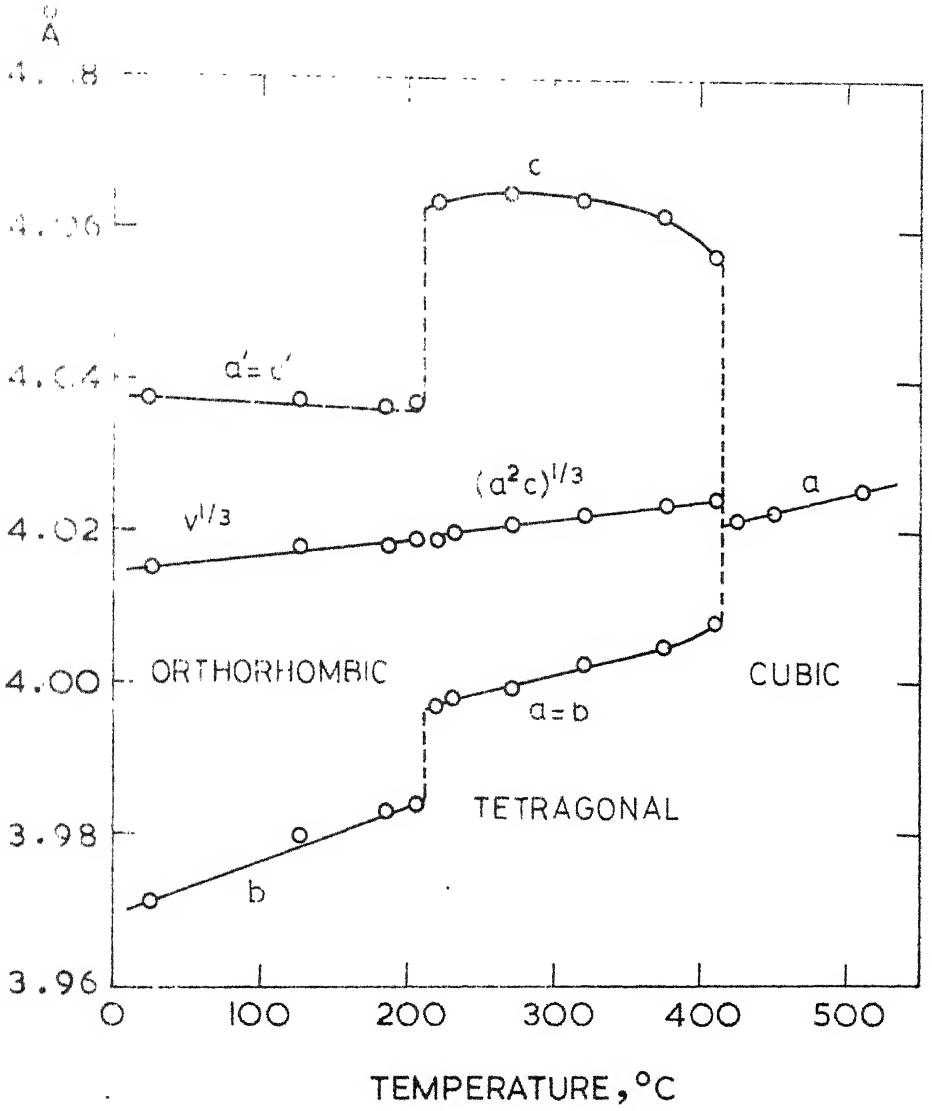

FIG. 5.3: Lattice parameters of $KNbO_3$ as a function of temperature. (Shirane et al 1954)

there is considerably large expansion of the lattice parameter along the b direction, which is smallest ($\sim 4^{\circ}A$) parameter. The rate of change of lattice parameters with temperature in the orthorhombic phase and the linear thermal expansion coefficients, calculated from the data of Shirane et al (1954) are given here.

$$\frac{da}{dt} = -0.944 \times 10^{-5}\ \text{Å}/^{\circ}C, \quad \alpha_a = -1.650 \times 10^{-6}\ /^{\circ}C$$

$$\frac{dc}{dt} = -0.222 \times 10^{-6}\ \text{Å}/^{\circ}C, \quad \alpha_c = -3.896 \times 10^{-8}\ /^{\circ}C$$

$$\frac{db}{dt} = 7.111 \times 10^{-5}\ \text{Å}/^{\circ}C, \quad \alpha_b = +1.791 \times 10^{-5}\ /^{\circ}C$$

It follows from above that the linear thermal expansion coefficients are slightly negative for a and c, while it is markedly positive for b-axis. The small thermal expansion coefficients in (h 0 0) and (0 0 l) direction means that the binding forces along these directions are very strong, while the linear thermal expansion coefficient in the (0 k 0) direction which is large, shows that the atoms in this direction are loosely bound compared to other directions. We get this qualitative information from the thermal expansion studies of a polycrystalline sample of $KNbO_3$. The thermal expansion is highly anisotropic and its direct relation to the unit cell dimensions and bond directions, seems quite difficult (Krishnan et al 1969). The directions of minimum expansion (h 0 0) and (0 0 l) seem to have a close relation with dielectric anomaly (Wood 1951), while the direction of maximum expansion suggests a large displacement of atoms from their equilibrium positions.

One can see that a very careful study on the single crystal of this compound may throw light on the direction of maximum dielectric anamoly and mechanism of spontaneous polarization (Krishan et al 1969).

Now the diffuse scattering studies on the single crystal of the same compound ($KNbO_3$) supports the above observations. Let us take the relps (4 0 0), (0 0 4), and (0 4 0). Their structure factor is not too different (F_{400} = 72.73; F_{004} = 71.92; F_{040} = 62.83). In the Fig. 5.4 we have observed variation of the diffuse flux or reflecting power for these relps vs. the misset from their respective Bragg positions on either side. It is clear from the Fig. 5.4 that the diffuse flux or power (0 4 0) relp is well spread over 5° to 6° on either side of the Bragg position for (0 4 0), while the diffuse flux for (4 0 0) and (0 0 4) relps is hardly observable after 3° on either side of their respective Bragg positions.

As we know that the thermal diffuse scattering is entirely due to atomic vibrations, more the amplitude of vibration, more is the thermal diffuse scattering, therefore for (0 4 0) relp we see that atoms in this direction have relatively large amplitude of vibrations (displacements) than atoms along (4 0 0) and (0 0 4). Even the Bragg intensity for (0 4 0) relp is large compared to (4 0 0) and (0 0 4) relps ($I_{B(040)} > I_{B(400)} > I_{B(004)}$). This shows that atoms in (0 4 0) having large amplitude of vibrations

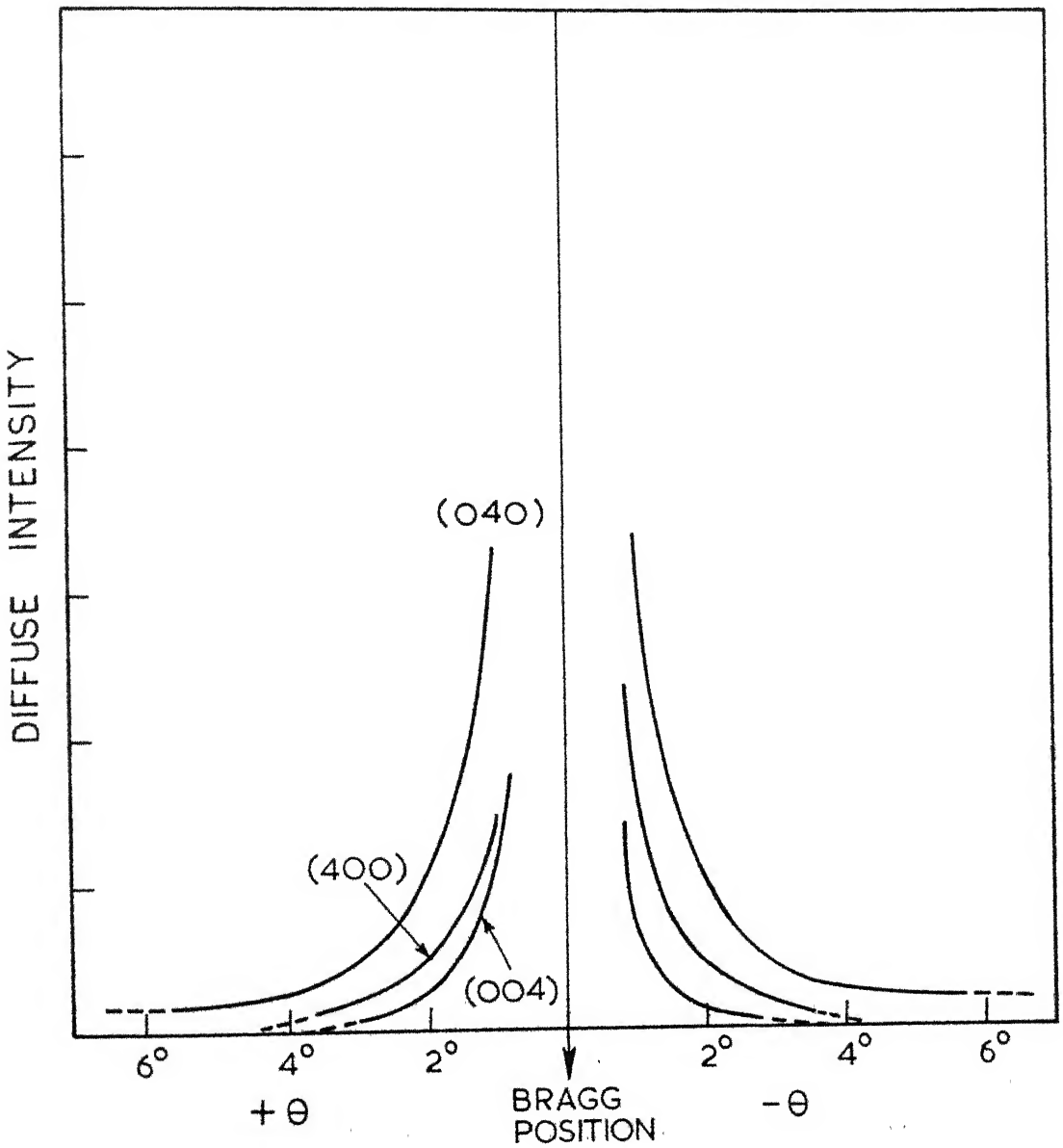

FIG. 5.4: Variation of diffuse intensity on either side of the Bragg positions for (0 4 0), (4 0. 0) and (0 0 4) relps.

or binding forces between them are weaker than the atoms in (4 0 0). Similarly atoms in the (4 0 0) have slightly larger amplitude of vibrations than atoms in (0 0 4). The thermal expansion can be defined as follows.

When a solid is heated, the atoms in the solid begin to execute vibrations about their equilibrium positions. The amplitude of these vibrations increase with the temperature. If the atoms were executing purely harmonic vibrations the mean positions of the atom would not alter with temperature; hence solid would not expand. It is the anharmonicity of these atomic vibrations which causes a displacement of the mean positions of the atoms and thus brings about an expansion of the crystal. When the mean position of rest of an atom gets displaced, the forces acting on the atom tending to restore it to equilibrium position as it vibrates, also alter and may cause a change in lattice frequencies.

So expansion in the orthorhombic phase, means that since atoms along (0 4 0) direction have large amplitude of vibrations it should show large diffuse intensity, as is shown in the Fig. 5.4. Very recently some observations of this type are reported by Lambert, Comes and Guinier (1968, 1969) and they found a disordered structure along (0 k 0) direction in the orthorhombic phase.

From the aniostropy observed in the thermal expansion studies in the orthorhombic phase of the polycrystalline sample of $KNbO_3$, it is very difficult to establish a quantitative relationship with the observed elastic constants obtained from the diffuse scattering studies of a single crystal. Constants C_{33}, (longitudinal component) and C_{55} (transverse component) both having highest value along the respective directions and corresponding thermal expansion in these directions is minimum. It shows that these constants are relatively temperature independent.

Thus our studies of thermal expansion and the diffuse scattering are in complete agreement, since they draw the same conclusion.

5. REFERENCES

Bell, R.O., and Rupprecht, G. — Phys. Rev. 129 90 (1963)

Bhide, V.G. and Multani, M.S. — Phys. Rev. 139 A1983 (1965)

Comes, R., Lambert, M. and Guinier, A. — Solid State Commun. 6 715 (1968).

Abs. Second Int. Conf. Ferroelectricity 123, Kyoto Japan (1969).

Jahn, H.A. — Proc. Roy. Soc. A179 320 (1942)

Krishnan, R.S. Narayanan, P.S. and Devanarayanan, S. — Abs. Second Int. Conf. Ferroelectricity 258 Kyoto Japan (1969)

Ibid, 259

Lambert, M., Comes, R. and Guinier, A. — Service de Physique des solides Faculte des Sciences 91-ORSAY Phy. Sol. 69/81 (1969).

Lucas, B. — Acta Cryst. A24, 336 (1968)

Ibid A25 627 (1969)

Perry, C.H. and Tornberg, N.E., — Int. Conf. Light Scattering Spectra of Solids 467-76 Springer Verlag (1969).

Prasad, S.C. and Wooster, W.A. — Acta Cryst. 9 35, 38, 169, 304, (1956)

Radha, V. and Rajagopal, E.S. — J. Ind. Inst. Sci 50 26, (1968)

Ramachandran, G.N. and Wooster, W.A. — Acta Cryst. 4 335 (1951).

Shirane, G. et al — Phys. Rev. 93, 672 (1954).

Ibid 96, 581 (1954).

Volger, J. — Philips. Res. Rep. 7 26 (1952)

Wood, E.A. — Acta Cryst. 4 353 (1951)

Wooster, W.A. — Acta Cryst. 14 571 (1961).

APPENDIX I

Calculations: Tables, Graphs and Plates.

Table A-1(a)

CRYSTAL DATA ON POTASSIUM NIOBATE

Chemical Formula $KNbO_3$

Crystal Class Orthorhombic {mm2}

AXIAL PARAMETERS OF $KNbO_3$

a(Å)	b(Å)	c(Å)	Reference
5.702±.01	3.984±.01	5.739±.01	Wood (1951)
5.6946 ±.01%	3.9714 ±.01%	5.7203 ±.01%	Vousden (1951)
5.6974	3.9711	5.7223	Shirane et al (1954)
5.697	3.971	5.721	Katz and Megaw (1967)
5.697	3.970(9)	5.721	Present study

Space group Bmm2

Number of molecules per unit cell = 2

Volume of the unit cell = 129.425 $Å^3$

Density

Measured density D_M = 4.62 gm/cc

Linear absorption coefficient μ_c for MoKα

μ_c (calculated) = 58.207 cm^{-1}

μ_c (observed by diffractometer method) = 55.934 cm^{-1}

Description of the Tables A-2 to A-15 (Diffractometer Observations)

Column No.	Description
I.	The angle of incident beam with certain given direction.
II.	Observed diffuse Intensity (units counts/sec. or C.P.S.) Corrected for Absorption Mosaic and white radiation corrections are applied. wherever necessary.
III.	Correction factor = $\frac{\text{Skew factor}}{\text{Polarization factor}}$ x Divergence factc
IV.	Corrected intensity I_d (C.P.S.) due to 1st order .
V.	Square of the wavelength (λ_t^2) of the elastic wave relevant to the specific direction.

(General Formula: Symbols and Calculations, Diffractometer Observations).

$$\frac{I_d}{I_o} = \frac{\epsilon^2}{2\mu_c V^2} kT \Omega F_T^2 \frac{\vec{X}^2}{\vec{q}^2} K[u,v,w]_{hkl} \quad .. \qquad (3.1)$$

or

$$I_d x \vec{q}^2 = \frac{I_d}{\lambda_t^2} = \frac{\epsilon^2 kT \Omega I_o}{2\mu_c V^2} F_T^2 \vec{X}^2 K[u,v,w]_{hkl}$$

The slope I_d/λ_t^2 is obtained from I_d vs. λ_t^2 graph plotted for each rekha, after subtracting the background..

Therefore,

$$K[u,v,w]_{hkl} = \frac{I_d}{\lambda_t^2} x \frac{2\mu_c V^2}{\epsilon^2 kT \Omega F_T^2 \vec{X}^2 I_o} = \frac{I_d}{\lambda_t^2} x \text{ (Const.)}$$

$$C_{ij} = \frac{1}{K[u,v,w]_{hkl}} = \frac{\lambda_t^2}{I_d} . G \qquad A-1$$

Where $G = \frac{e^2 k T \Omega \lambda I_o}{2 \mu_c V^2} F_T^2 \vec{X}^2$

G depends upon structure factor (F_T), rel vector ($\vec{X}$), solid angle (Ω) and the volume (V) of the crystal. μ_c, the linear absorption coefficient and T the room temperature at which observations are made, are both constant throughout the study.

One gets the value of an elastic constant from Eq.(A-1), knowing, λ_t, I_d and G for a given rekha of a given plane. Below some relevant data required for planes studied are given.

Table A-1(b)

Plane studied	Axis of rotation	Structure factor F_T	Rel. vector $\vec{X}$ x10^{-8} cm^{-1}	Solid angle Ω x10^3	Volume of the crystal V x 10^3cc	Constant G x 10^{-11}
0 4 0	1 0 0	62.83	1.0072	9.797	1.838	336.1
6 0 0	0 0 1	41.44	1.053	9.797	1.838	159.8
0 0 6	0 1 0	38.77	1.049	9.797	1.750	138.70
4 0 0	0 1 0	72.73	0.702	1.382	0.178	3.323
0 0 4	0 1 0	71.92	0.699	1.382	0.178	3.22

Table A-2(a,b)

Rekha $[00\bar{1}]_{040}$

(a)

Angle of incident beam with [001] direction	Obs. diffuse intensity corrected for Absorption x 10^{-4}	Correction Factor S.D/P	Corrected Intensity I_d (due to 1st order) x 10^{-4}	$\lambda_t^2 (= \frac{1}{q^2}) \text{Å}^2 \times 10^{-3}$
19.89	3.319	1.178	3.910	2.889
19.79	2.547	1.178	3.001	2.328
19.69	2.175	1.185	2.578	1.980
19.49	1.647	1.169	1.926	1.482
18.99	0.997	1.177	1.173	0.841

Rekha $[001]_{040}$

(b)

21.87	3.388	1.225	4.150	3.969
21.99	2.561	1.152	2.950	3.080
22.09	2.361	1.098	2.592	2.575
22.19	2.248	1.030	2.315	2.209
22.29	2.246	0.935	2.100	1.827
22.39	2.127	0.889	1.891	1.580
22.99	1.208	0.845	1.021	0.770

	2(a)	2(b)
Mean value of the slope I_d/λ_t^2 (less background) from the graphs	10.0	9.0
Mean value of C_{44}(1st order) x 10^{-12} dynes/cm^2	3.361	3.734
Mean value of C_{44}, corrected for second order x 10^{-12} dynes/cm^2	3.372	3.744

Average value of C_{44} = 3.5(58) x 10^{12} dynes/cm^2 from Tables 2(a) and 2(b).

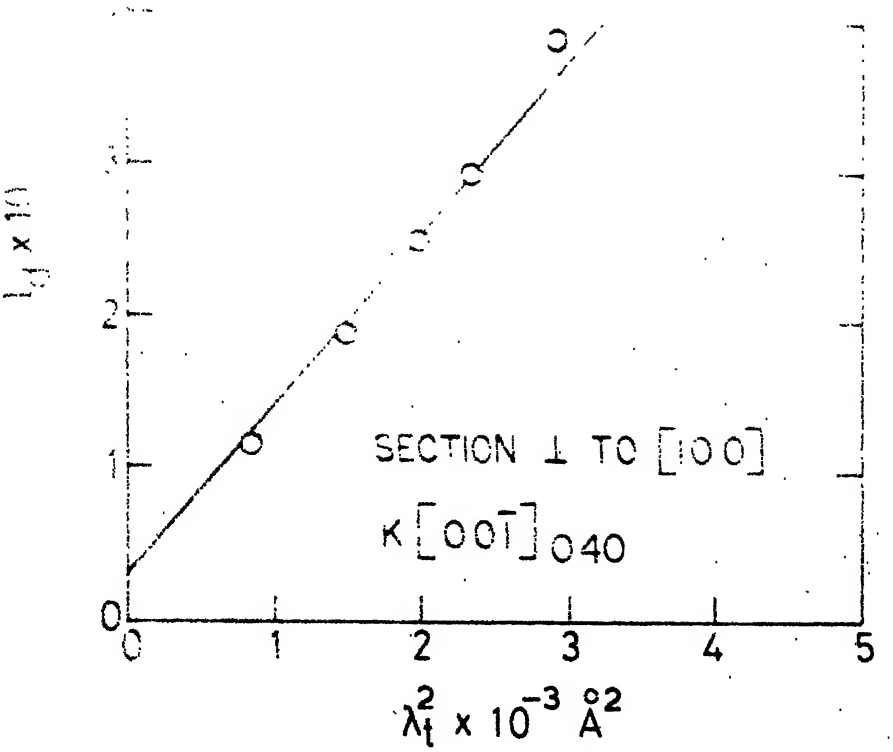
SECTION ⊥ TO [100]
K[00$\bar{1}$]040
0
1
2
3
4
5
$\lambda_t^2 \times 10^{-3}$ Å^2

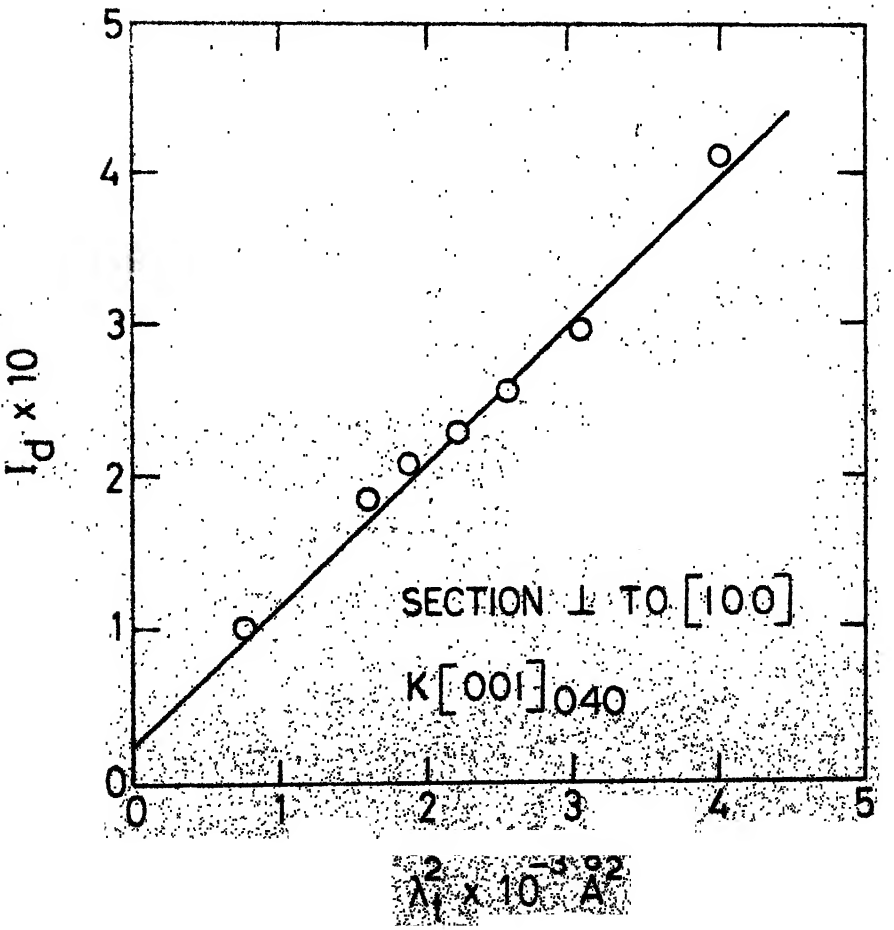
$I_d \times 10^{-4}$
SECTION ⊥ TO [100]
K[001]040
0
1
2
3
4
5
$\lambda_t^2 \times 10^{-3}$ Å^2

Table A-3(a, b)

Rekha $[0\bar{1}0]_{040}$

(a)

Angle of incident beam with [001] direction	Obs. diffuse intensity corrected for Absorption x 10^{-4}	Correction Factor S.D/P	Corrected Intensity I_d (due to 1st order) x 10^{-4}	λ_t^2 (= $\frac{1}{q^2}$)Å^2 x 10^{-3}
21.87	3.298	1.226	4.044	0.600
21.99	2.212	1.153	2.550	0.462
22.09	2.183	1.100	2.401	0.381
22.19	2.077	1.035	2.150	0.315
22.29	2.050	0.951	1.950	0.272
22.39	1.988	0.890	1.770	0.233

(b) Rekha $[010]_{040}$

19.97	3.756	1.230	4.620	0.462
19.89	3.178	1.180	3.751	0.400
19.79	2.413	1.181	2.850	0.333
19.69	2.016	1.191	2.401	0.298
19.49	1.622	1.170	1.900	0.210
18.99	0.865	1.182	1.023	0.132

	3(b)	3(a)
Mean value of the slope I_d/λ_t^2 (less background) from graphs	73.0	66.0
Mean value of C_{22} (1st order) x 10^{-12} dynes/cm^2	0.460	0.509
Mean value of C_{22} corrected for second order x 10^{-12} dynes/cm^2	0.492	0.540

Average value of C_{22} = 0.5(16) x 10^{12} dynes/cm^2 from Tables 3(a) and 3(b).

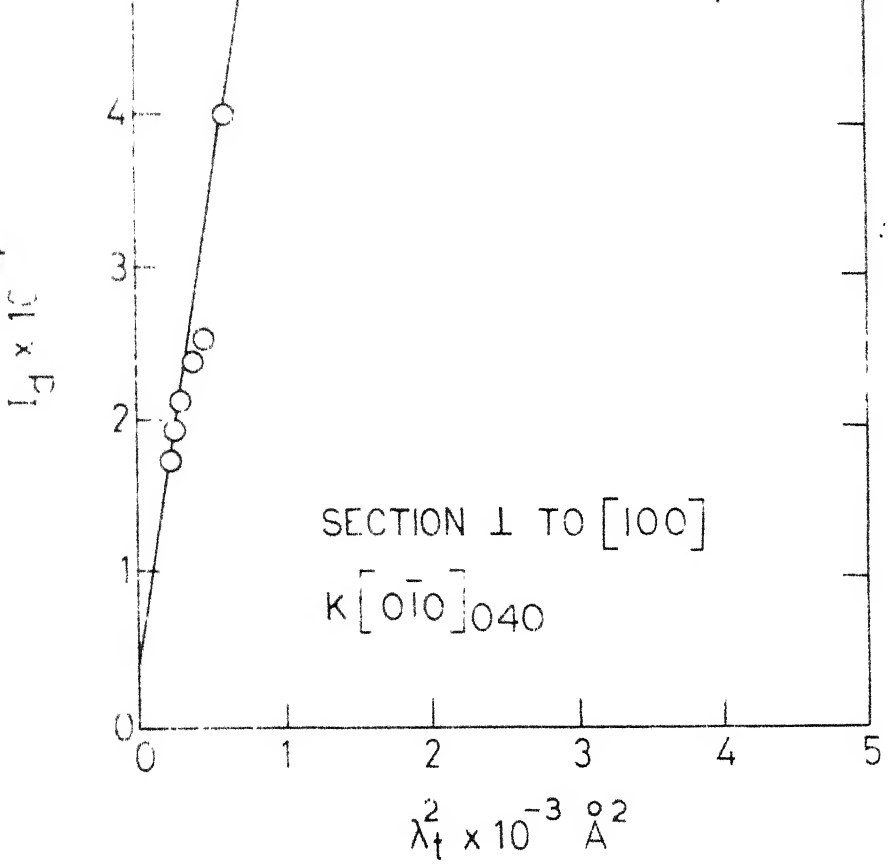
SECTION ⊥ TO [100]
K [0$\bar{1}$0]040
$I_d \times 10^{-4}$
$\lambda_t^2 \times 10^{-3}$ Å^2

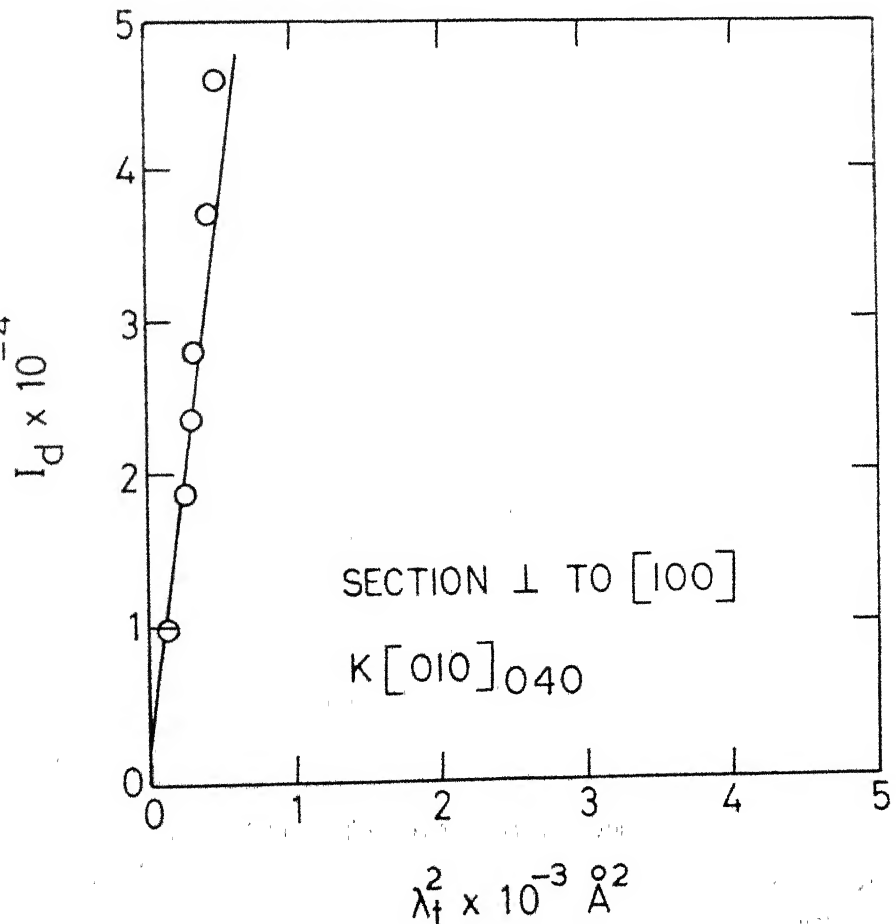
SECTION ⊥ TO [100]
K [010]040
$I_d \times 10^{-4}$
$\lambda_t^2 \times 10^{-3}$ Å^2

Table A-4(a, b)

Rekha $[0, -\frac{1}{\sqrt{2}}, \frac{1}{\sqrt{2}}]_{040}$

(a)

Angle of incident beam with [001] direction	Obs. diffuse intensity corrected for Absorption x 10^{-4}	Correction Factor S.D/P	Corrected Intensity I_d (due to 1st order) x 10^{-4}	λ_t^2 ($= \frac{1}{q^2}$) $Å^2$ x 10^{-3}
21.87	3.459	1.227	4.244	1.984
21.99	2.610	1.150	3.002	1.540
22.09	2.343	1.089	2.552	1.289
22.19	2.329	1.031	2.401	1.104
22.29	2.326	0.935	2.175	0.913
22.39	2.100	0.900	1.890	0.790
22.99	1.176	0.850	1.000	0.385

Rekha $[0, \frac{1}{\sqrt{2}}, -\frac{1}{\sqrt{2}}]_{040}$

(b)

19.89	3.241	1.176	3.812	1.444
19.79	2.472	1.179	2.915	1.164
19.69	2.161	1.180	2.550	0.991
19.49	1.625	1.172	1.905	0.741
18.99	0.979	1.180	1.155	0.421

	4(a)	4(b)
Mean value of the slope I_d/λ_t^2(less background) from the graphs	= 22.000	18.50
Mean value of $1/K[0, -\frac{1}{\sqrt{2}}, \frac{1}{\sqrt{2}}]_{040}$ and $1/K[0, \frac{1}{\sqrt{2}}, -\frac{1}{\sqrt{2}}]_{040}$ (1st order)x10^{-12}dynes/cm^2	= 1.527	1.816
Mean value of $1/K[0, \frac{1}{\sqrt{2}}, \frac{1}{\sqrt{2}}]$ and $1/K[0, \frac{1}{\sqrt{2}}, -\frac{1}{\sqrt{2}}]$ corrected for second order x 10^{-12} dynes/cm^2	= 1.669	1.759

Average value from Tabs.A-4(a) and A-4(b) = 1.714x10^{12} dynes/cm^2

contd..

Contd...

From Tables (3.1), (3.2) and (3.3),

$$\frac{1}{K\left[0, \pm\frac{1}{\sqrt{2}}, \mp\frac{1}{\sqrt{2}}\right]_{040}} = \frac{C_{22}(C_{33}+C_{44})+C_{33}C_{44}-2C_{23}C_{44}-C_{23}^2}{2(C_{33}+C_{44})}$$

or $$C_{23} = -C_{44} \pm \sqrt{C_{44}^2+C_{33}C_{44}+(C_{33}+C_{44})\left(C_{22}-\frac{2}{K\left[0, \pm\frac{1}{\sqrt{2}}, \mp\frac{1}{\sqrt{2}}\right]_{040}}\right)}$$

(Negative sign before the surd is never applicable)

by substituting the values of C_{44}, C_{33}, C_{22} and mean value of $1/K\left[0, \pm\frac{1}{\sqrt{2}}, \mp\frac{1}{\sqrt{2}}\right]$ (due to Ist order).

One gets,

Mean value of C_{23} (1st order) x 10^{-12} dynes/cm^2 = -1.854

Average value of C_{23} corrected for second order calculated from Tabs. 4(a) and 4(b) = $-1.9(14) \times 10^{12}$ dynes/cm^2

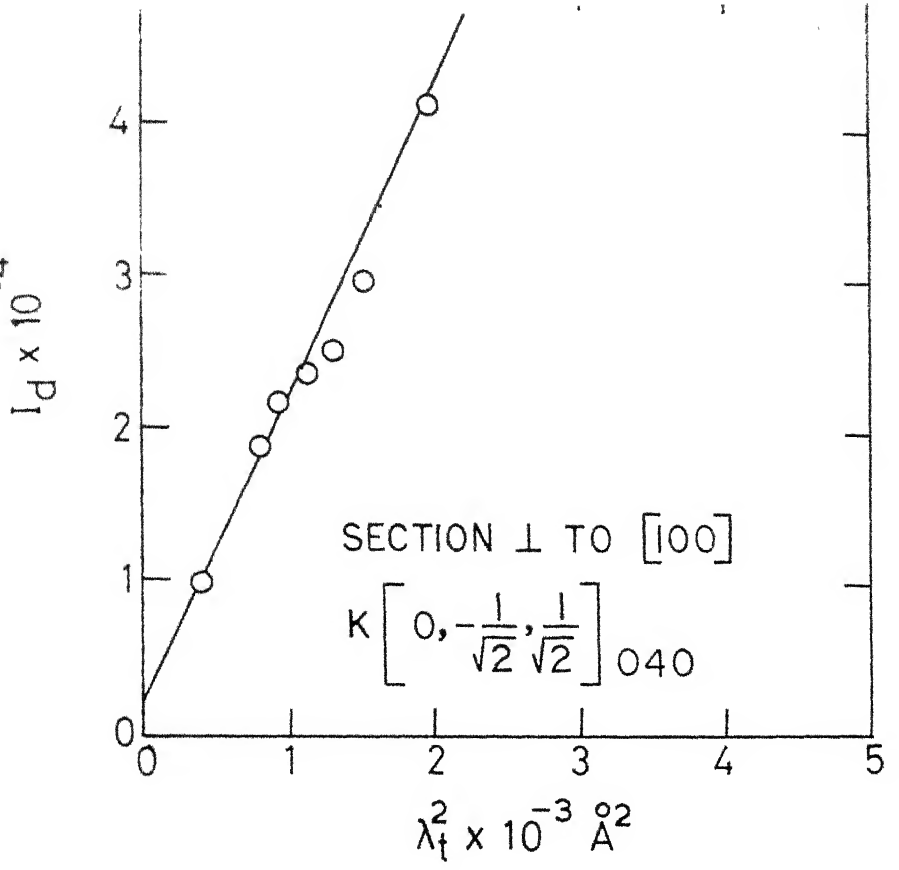
$I_d \times 10^{-4}$
0
1
2
3
4
5
$\lambda_t^2 \times 10^{-3}$ Å^2
SECTION ⊥ TO [100]
$K\left[0, -\frac{1}{\sqrt{2}}, \frac{1}{\sqrt{2}}\right]$ 040

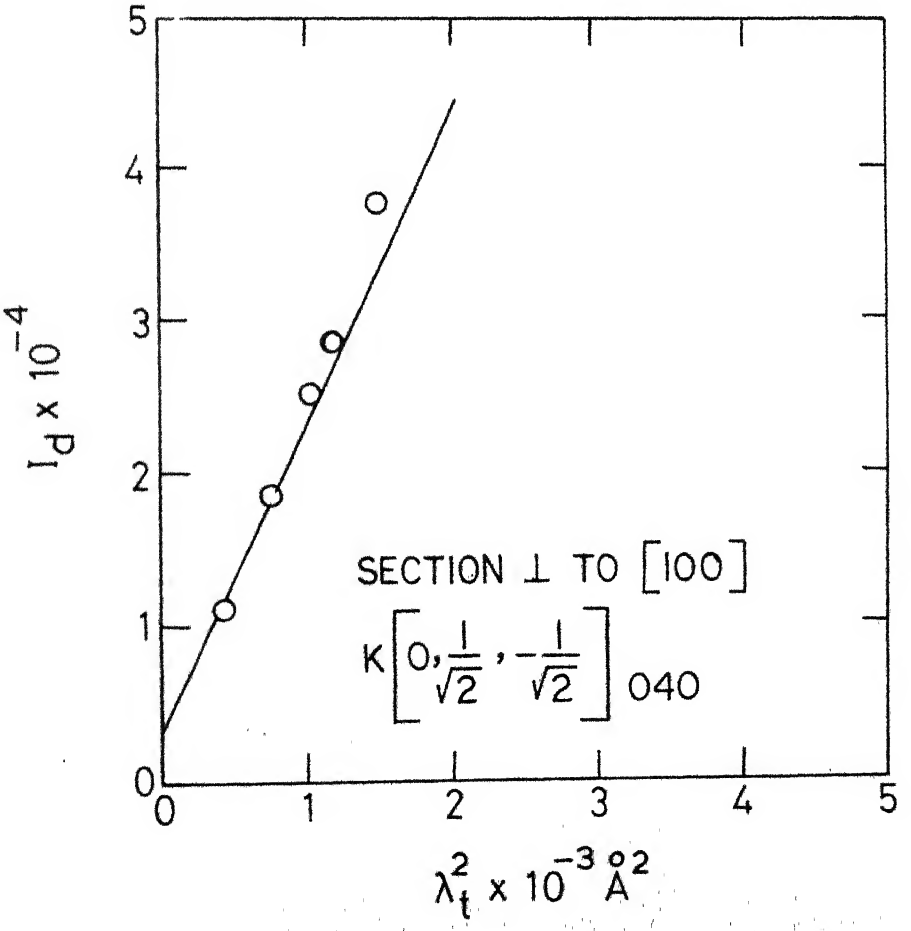
$I_d \times 10^{-4}$
0
1
2
3
4
5
$\lambda_t^2 \times 10^{-3}$ Å^2
SECTION ⊥ TO [100]
$K\left[0, \frac{1}{\sqrt{2}}, -\frac{1}{\sqrt{2}}\right]$ 040

Fig. I-3

Table A-5(a,b)

(a) Rekha $[010]_{600}$

Angle of incident beam with [010] direction	Obs. diffuse intensity corrected for Absorption. x 10^{-4}	Correction Factor S.D/P	Corrected intensity I_d (due to 1st order x 10^{-4}	λ_t^2 (= $\frac{1}{q^2}$) $Å^2$ x 10^{-3}
21.10	3.105	1.063	3.301	3.906
21.03	2.492	1.118	2.786	3.249
20.96	2.147	1.125	2.416	2.809
20.90	1.915	1.163	2.227	2.525
20.80	1.573	1.177	1.852	2.116
20.50	0.834	1.200	1.001	1.332

(b) Rekha $[0\bar{1}0]_{600}$

22.95	2.383	1.100	2.621	3.164
23.00	2.071	1.038	2.150	2.862
23.10	1.759	0.997	1.754	2.352
23.20	1.428	1.012	1.445	1.936
23.50	0.909	1.110	1.000	1.296

	5(a)	5(b)
Mean value of the slope I_d/λ_t^2 (less background) from graphs	= 8.0	7.62
Mean value of C_{66} (1st order) x10^{-12}dynes/cm^2	= 1.997	2.096
Mean value of C_{66} corrected for second order x 10^{-12} dynes/cm^2	= 2.02	2.118

Average value of C_{66} = 2.0(69) x 10^{12} dynes/cm^2 from Tables 5(a) and 5(b).

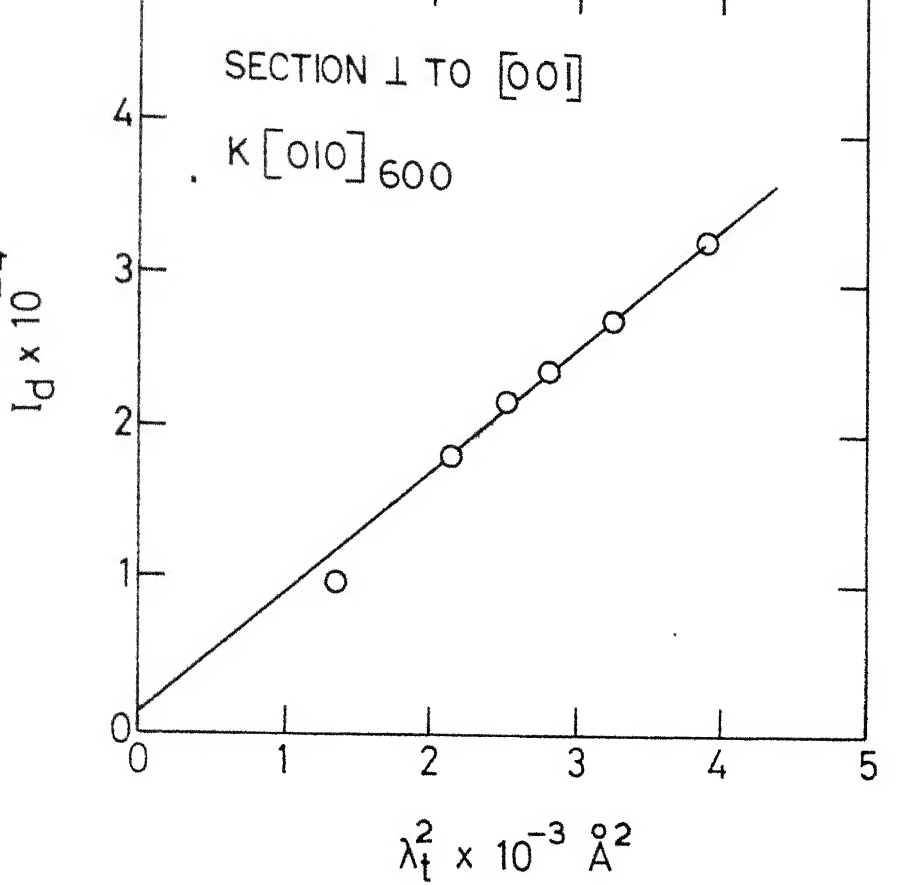
SECTION ⊥ TO [001]
K [010]600
$I_d \times 10^{-4}$
$\lambda_t^2 \times 10^{-3}$ Å^2
0
1
2
3
4
5

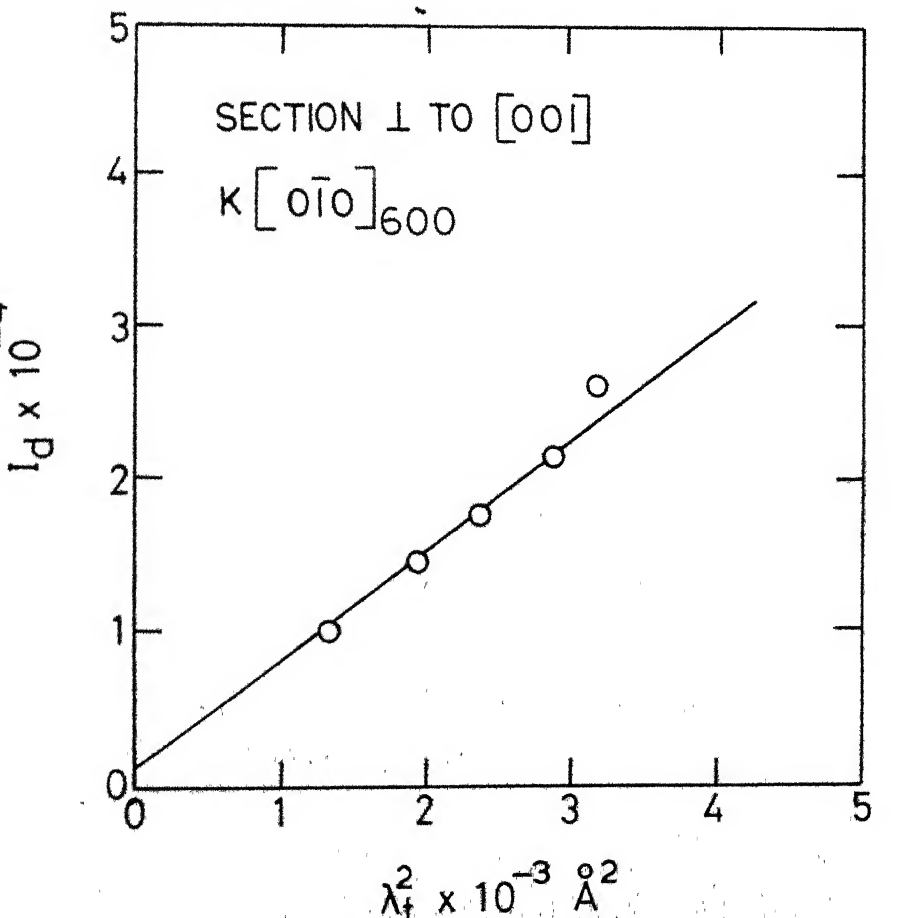
SECTION ⊥ TO [001]
K [0$\bar{1}$0]600
$I_d \times 10^{-4}$
$\lambda_t^2 \times 10^{-3}$ Å^2
0
1
2
3
4
5

Fig. I-4

Table A-6(a,b)

Rekha $[\bar{1}00]_{600}$

(a)

Angle of incident beam with [010] direction	Obs. diffuse intensity corrected for Absorption x 10^{-4}	Correction Factor S.D/P	Corrected Intensity I_d (due) to 1st order) x 10^{-4}	$\lambda_t^2 \left(= \frac{1}{q^2}\right)$ Å^2 x 10^{-3}
21.10	2.328	1.065	3.012	0.600
21.05	2.139	1.192	2.550	0.529
20.95	1.908	1.127	2.150	0.462
20.90	1.693	1.165	1.973	0.400
20.80	1.276	1.185	1.512	0.342
20.70	0.974	1.213	1.182	0.289

Rekha $[100]_{600}$

(b)

22.85	3.092	1.300	4.020	0.638
22.90	2.671	1.125	3.005	0.576
22.95	2.380	1.099	2.616	0.506
23.00	2.167	1.039	2.252	0.473
23.10	1.738	0.998	1.735	0.390
23.20	1.478	1.015	1.500	0.324

	6(a)	6(b)
Mean value of the slope I_d/λ_t^2 (less background) from graphs	49.5	47.5
Mean value of C_{11} (1st order) x 10^{-12} dynes/cm^2	0.323	0.336
Mean value of C_{11} corrected for second order x 10^{-12} dynes / cm^2	0.347	0.361

Average value of C_{11} = 0.3(54)x10^{12} dynes/cm^2 from Tables 6(a) and 6(b).

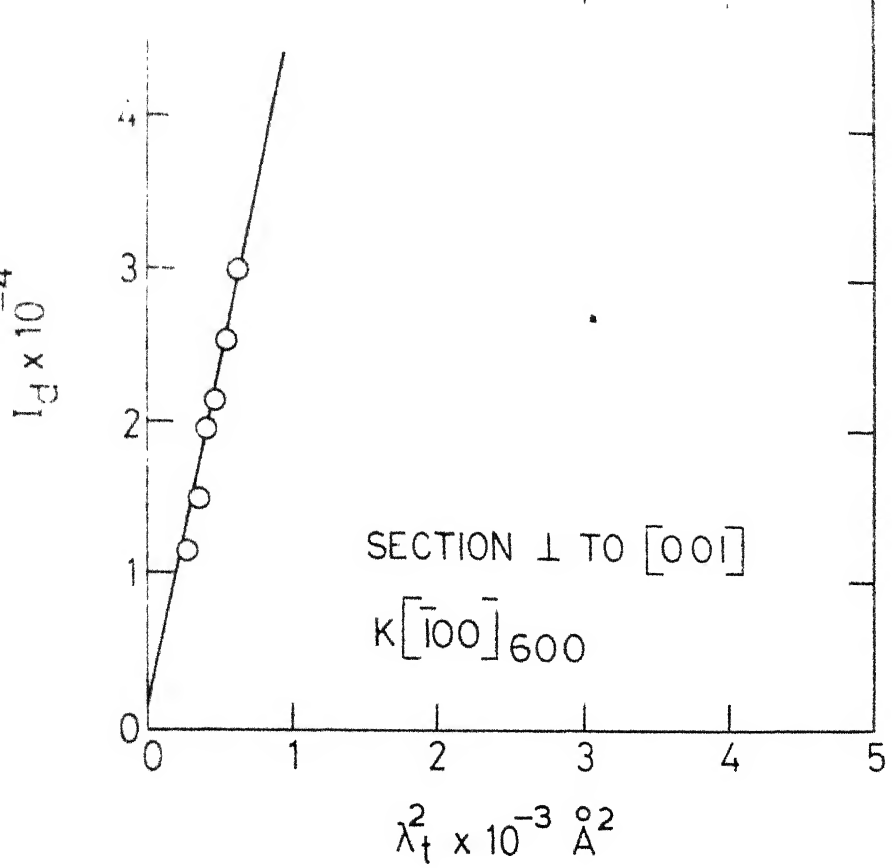
$I_d \times 10^{-4}$
0
1
2
3
4
5
SECTION ⊥ TO [001]
K[$\bar{1}$00]600
$\lambda_t^2 \times 10^{-3}$ Å^2

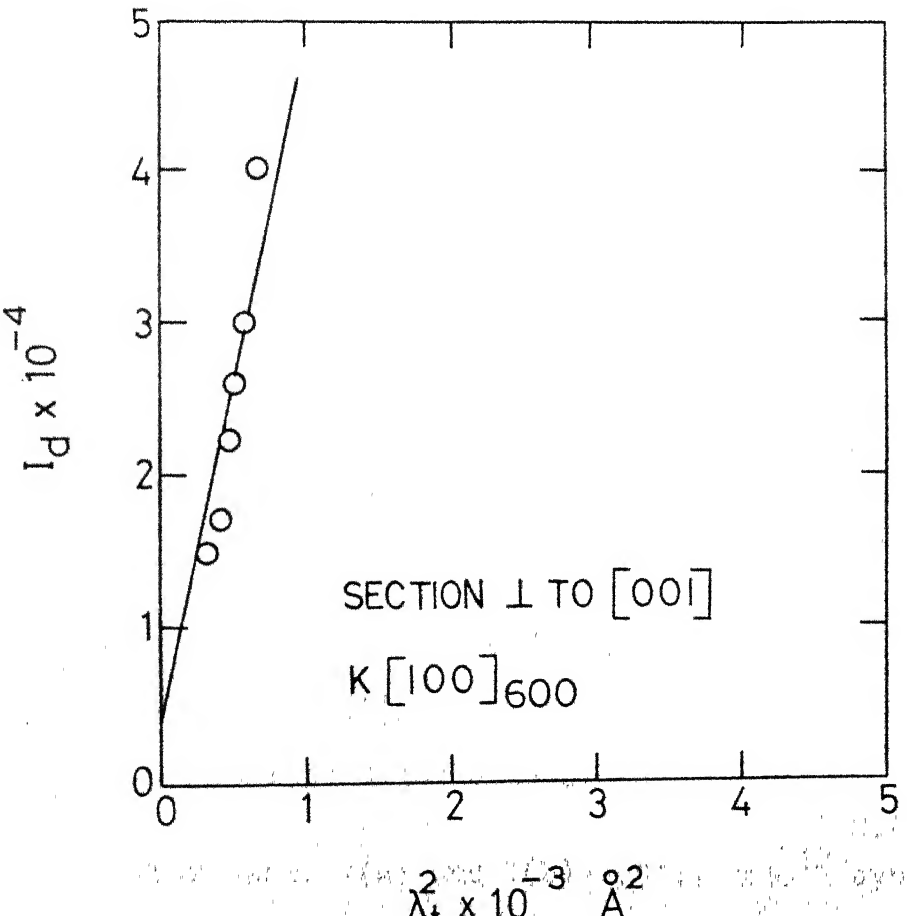
$I_d \times 10^{-4}$
0
1
2
3
4
5
SECTION ⊥ TO [001]
K [100]600
$\lambda_t^2 \times 10^{-3}$ Å^2

Table A-7(a,b)

Rekha $\left[\frac{1}{\sqrt{2}}, -\frac{1}{\sqrt{2}}, 0\right]_{600}$

(a)

Angle of incident beam with [010] direction	Obs. diffuse intensity corrected for Absorption x 10-4	Correction Factor S.D/P	Corrected Intensity I_d (due to 1st order) x 10^{-4}	λ_t^2 $(=\frac{1}{q^2})$ Å^2 x 10^{-3}
22.90	2.573	1.128	2.902	1.755
22.95	2.362	1.101	2.601	1.582
23.00	2.212	1.040	2.301	1.437
23.10	1.747	1.030	1.800	1.176
23.20	1.485	1.010	1.500	0.968
23.50	0.913	1.150	1.050	0.648

Rekha $\left[-\frac{1}{\sqrt{2}}, \frac{1}{\sqrt{2}}, 0\right]_{600}$

(b)

21.10	2.934	1.065	3.125	1.953
21.03	2.377	1.115	2.651	1.625
20.96	2.066	1.125	2.324	1.404
20.90	1.853	1.160	2.150	1.263
20.80	1.441	1.180	1.700	1.058
20.70	1.101	1.226	1.350	0.903
20.50	0.843	1.210	1.020	0.666

	7(a)	7(b)
Mean value of the slope I_d/λ_t^2 (less background) from graphs	= 16.4	15.6
Mean value of $1/K\left[\frac{1}{\sqrt{2}}, -\frac{1}{\sqrt{2}}, 0\right]_{600}$ and $1/K\left[-\frac{1}{\sqrt{2}}, \frac{1}{\sqrt{2}}, 0\right]_{600}$ (1st order)x10^{-12} dynes/cm^2	= 0.974	1.024
Mean value of $1/K\left[\frac{1}{\sqrt{2}}, -\frac{1}{\sqrt{2}}, 0\right]_{600}$ and $1/K\left[-\frac{1}{\sqrt{2}}, \frac{1}{\sqrt{2}}, 0\right]_{600}$ corrected for second order x 10^{-12} dynes / cm^2	= 0.983	1.045

Average value from tabs. 7(a) and 7(b)=1.0(14) x 10^{12} dynes/cm^2

contd..

Contd...

From Tables (3.1), (3.2) and (3.3)

$$1/K\left[\pm\frac{1}{\sqrt{2}}, \mp\frac{1}{\sqrt{2}}, 0\right]_{600} = \frac{C_{11}(C_{22}+C_{66})-2C_{12}C_{66}-C_{12}^2+C_{22}C_{66}}{2(C_{22}+C_{66})}$$

or

$$C_{12} = -C_{66} \pm \sqrt{C_{66}^2+C_{22}C_{66}+(C_{22}+C_{66})\left(C_{11} - \frac{2}{K\left[\pm\frac{1}{\sqrt{2}}, \mp\frac{1}{\sqrt{2}}, 0\right]_{600}}\right)}$$

(Negative sign before the surd is never applicable)

Substituting the values of C_{11}, C_{22}, C_{66} and mean value of $1/K\left[\pm\frac{1}{\sqrt{2}}, \mp\frac{1}{\sqrt{2}}, 0\right]_{600}$ (due to 1st order).

One gets,

The mean value of C_{12}(1st order)$\times 10^{-12}$ dynes/cm^2 = -1.069

Average value of C_{12} corrected for second order calculated from Tabs. 7(a) and 7(b) = $-1.0(58)\times 10^{12}$dynes/cm^2

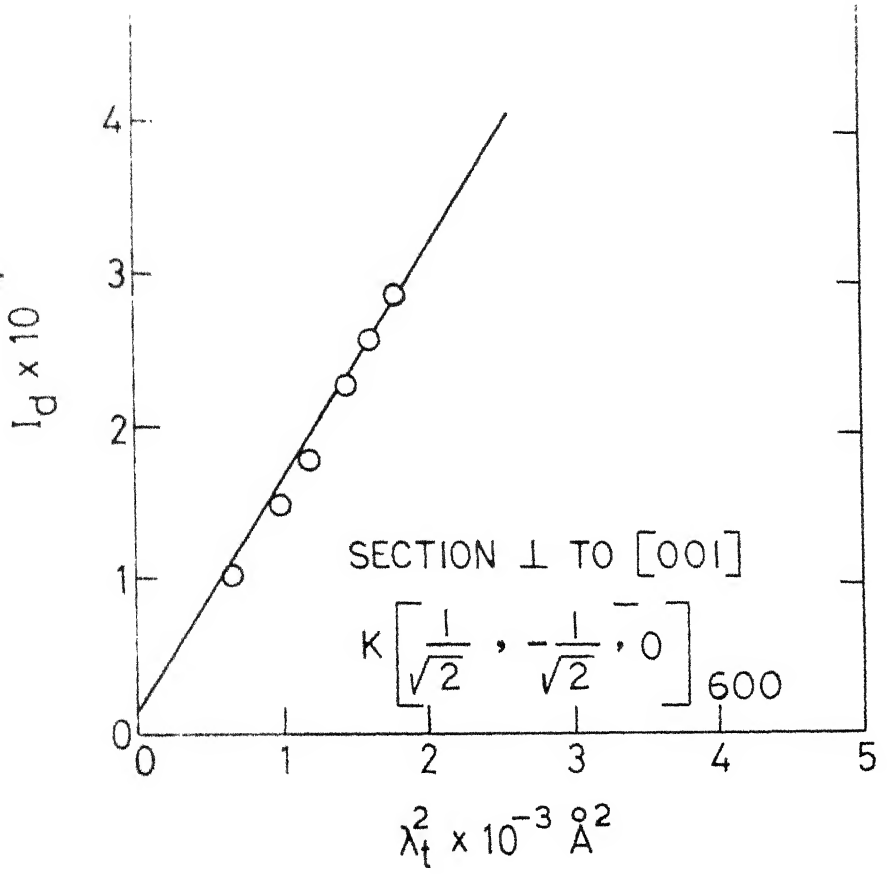
$I_d \times 10^{-4}$
SECTION ⊥ TO [001]
$K\left[\frac{1}{\sqrt{2}}, -\frac{1}{\sqrt{2}}, 0\right]$ 600
$\lambda_t^2 \times 10^{-3}$ Å^2

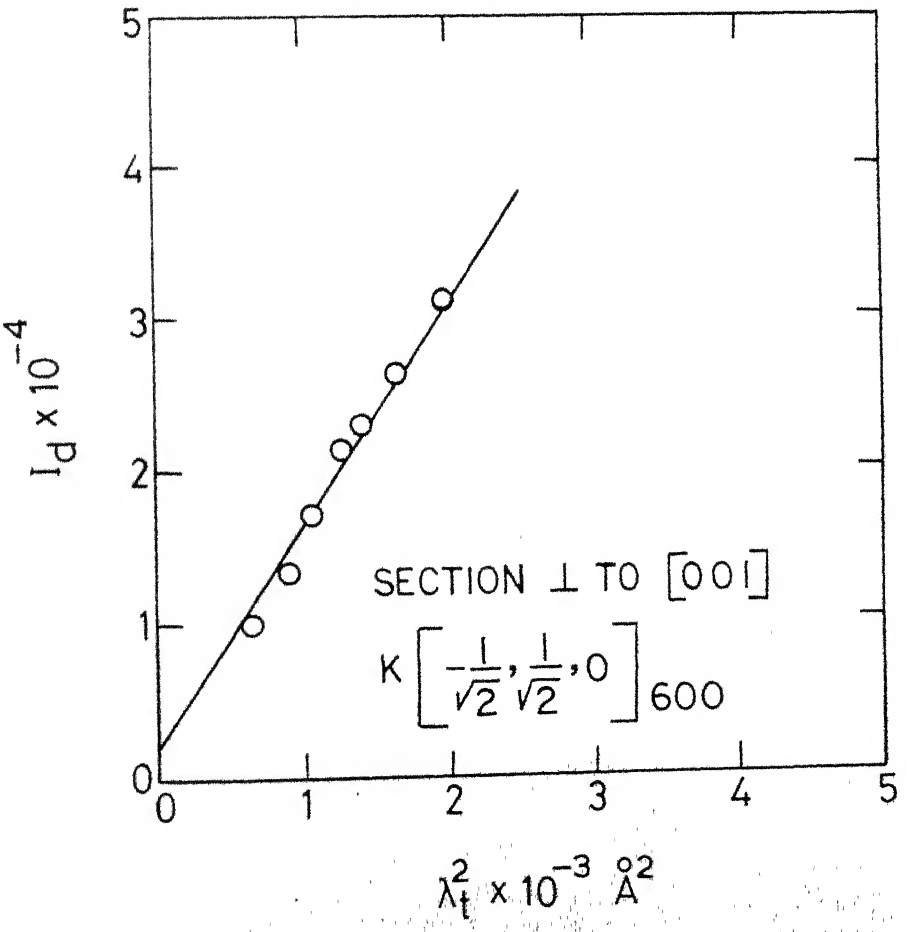
$I_d \times 10^{-4}$
SECTION ⊥ TO [001]
$K\left[-\frac{1}{\sqrt{2}}, \frac{1}{\sqrt{2}}, 0\right]$ 600
$\lambda_t^2 \times 10^{-3}$ Å^2

Fig. I-6

Table A-8(a,b)

Rekha $[\bar{1}00]_{006}$

(a)

Angle of incident beam with [100] direction.	Obs. diffuse intensity corrected for Absorption x 10^{-4}	Correction Factor S.D/P	Corrected Intensity I_d (due to 1st order) x 10^{-4}	λ_t^2 ($= \frac{1}{q^2}$) $Å^2$ x 10^{-3}
22.69	1.564	1.279	2.000	4.692
22.73	1.387	1.255	1.741	4.225
22.83	1.092	1.193	1.303	3.364
22.93	0.840	1.244	1.045	2.782
23.13	0.669	1.204	0.805	2.093

Rekha $[100]_{006}$

(b)

21.09	1.449	1.314	1.905	4.624
20.98	1.053	1.329	1.400	3.540
20.93	0.954	1.366	1.303	3.192
20.83	0.816	1.244	1.015	2.652
20.43	0.579	1.079	0.625	1.369

	8(a)	8(b)
Mean value of the slope I_d/λ_t^2 (less background) from graphs	3.89	3.80
Mean value of C_{55}(1st order)x10^{-12} dynes/cm^2	3.566	3.651
Mean value of C_{55} corrected for second order x 10^{-12} dynes / cm^2	3.610	3.691

Average value of C_{55} = 3.6(51) x 10^{12} dynes/cm^2 from Tables 8(a) and 8(b).

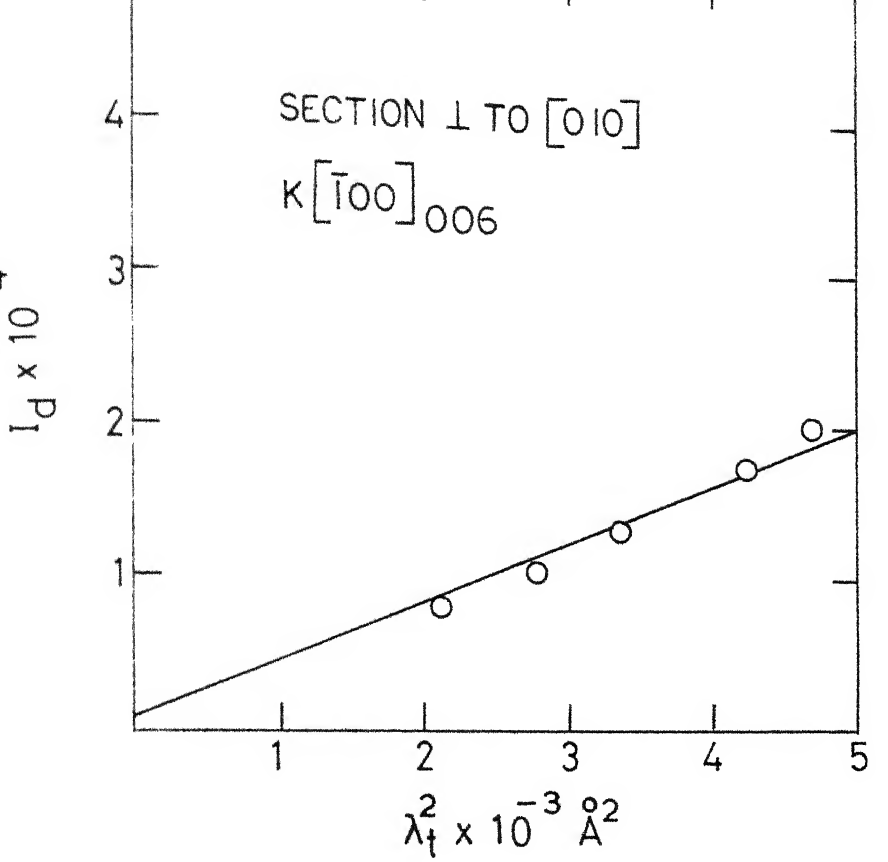
SECTION ⊥ TO [010]
K[T00]006
$I_d \times 10^{-4}$
$\lambda_t^2 \times 10^{-3}$ Å^2
1
2
3
4
5

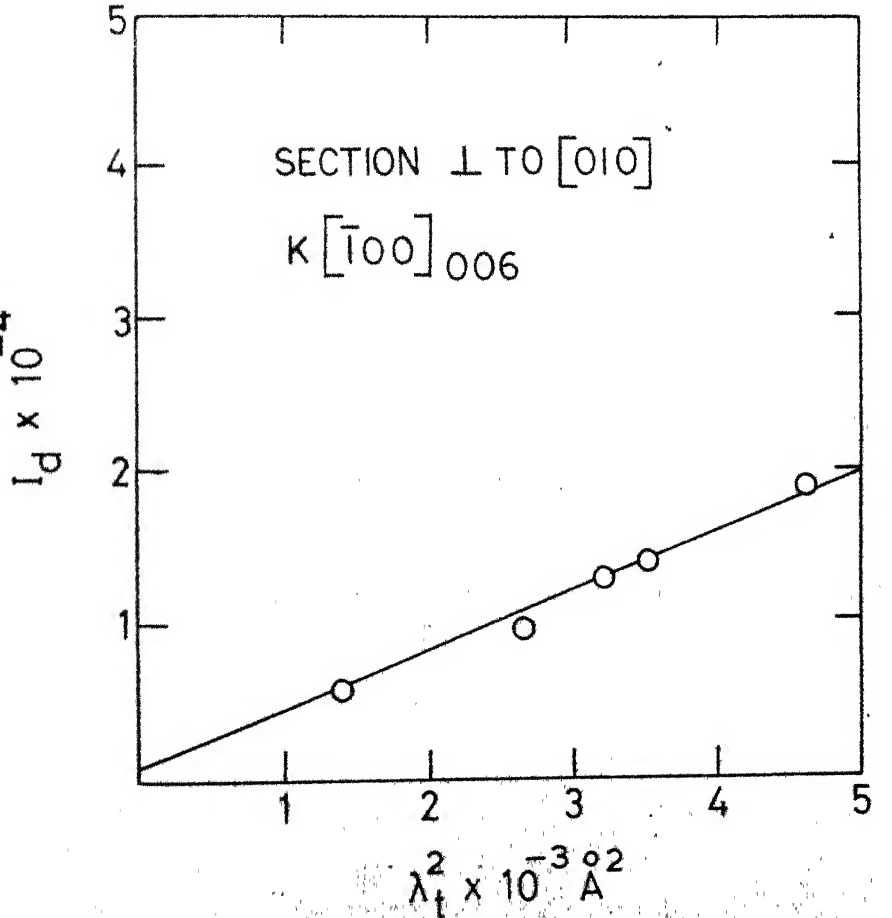
SECTION ⊥ TO [010]
K[T00]006
$I_d \times 10^{-4}$
$\lambda_t^2 \times 10^{-3}$ Å^2
1
2
3
4
5

Table A-9(a,b)

Rekha $[\ 001\ ]_{006}$

(a)

Angle of incident beam with [100] direction.	Obs. diff. fuse intensity corrected for Absorption x 10^{-4}	Correction Factor S.D/P	Corrected Intensity I_d (due to 1st order) x 10^{-4}	λ_t^2 (= $\frac{1}{q^2}$) $Å^2$ x 10^{-3}
22.69	1.446	1.279	1.850	0.756
22.73	1.269	1.265	1.605	0.576
22.83	1.040	1.202	1.250	0.506
22.93	0.693	1.226	0.850	0.421
23.13	0.537	1.210	0.650	0.225

Rekha $[\ 00\bar{1}\ ]_{006}$

(b)

21.09	1.381	1.304	1.801	0.756
20.98	1.032	1.309	1.351	0.689
20.93	0.901	1.360	1.225	0.552
20.83	0.598	1.250	0.748	0.441
20.43	0.536	1.085	0.582	0.324

	9(a)	9(b)
Mean value of the slope I_d/λ_t^2 (less background) from graphs	= 23.5	22.15
Mean value of C_{33} (1st order) x 10^{-12} dyes/cm^2	= 0.590	0.626
Mean value of C_{33} corrected for second order x 10^{-12} dynes/cm^2	= 0.614	0.650
Average value of C_{33} from Tabs. 9(a) and 9(b)	=0.6(32) x 10^{12} dynes/cm^2	

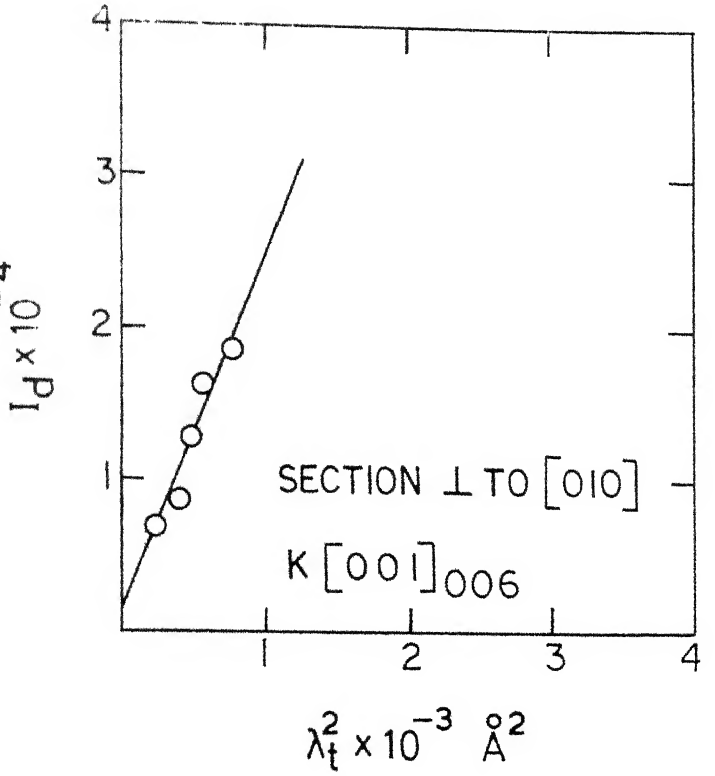
4
3
2
1
$I_d \times 10^{-4}$
SECTION ⊥ TO [010]
K [001]006
1
2
3
4
$\lambda_t^2 \times 10^{-3}$ Å^2

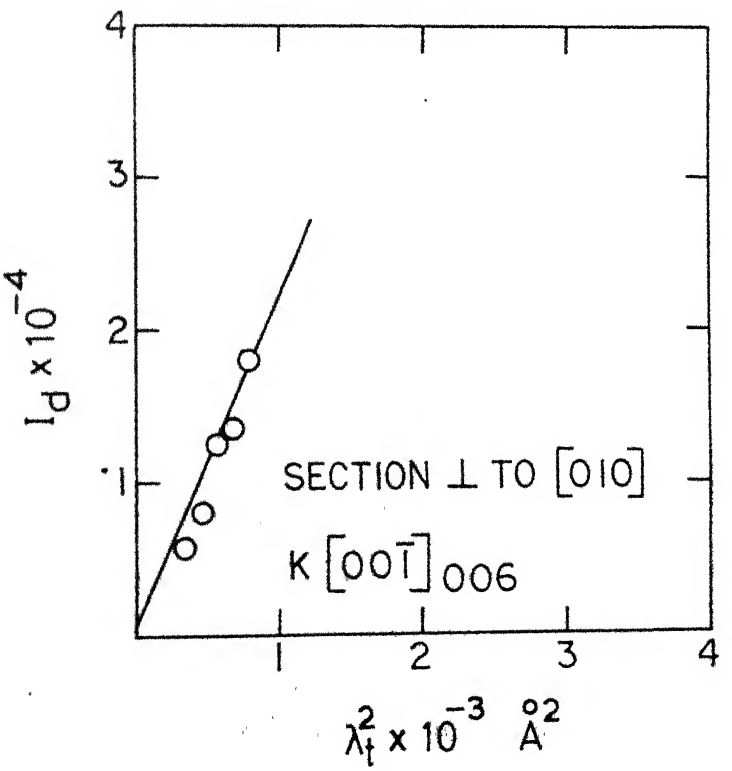
4
3
2
1
$I_d \times 10^{-4}$
SECTION ⊥ TO [010]
K [00$\bar{1}$]006
1
2
3
4
$\lambda_t^2 \times 10^{-3}$ Å^2

Fig. I-8

Table A-10(a,b)

Rekha $\left[-\frac{1}{\sqrt{2}}, 0, \frac{1}{\sqrt{2}}\right]_{006}$

(a)

Angle of incident beam with [100] direction.	Obs. diffuse intensity corrected for Absorption x 10^{-4}	Correction Factor S.D/P	Corrected Intensity I_d (due to 1st order) x 10^{-4}	$\lambda_t^2 \left(=\frac{1}{q^2}\right)$ Å^2 x 10^{-3}
22.69	1.526	1.279	1.952	2.345
22.73	1.381	1.260	1.740	2.112
22.83	1.088	1.195	1.300	1.682
22.93	0.762	1.254	0.955	1.391
23.13	0.618	1.214	0.750	1.046

(b) Rekha $\left[\frac{1}{\sqrt{2}}, 0, -\frac{1}{\sqrt{2}}\right]_{006}$

21.09	1.434	1.310	1.879	2.311
20.98	1.034	1.329	1.374	1.770
20.93	0.916	1.367	1.252	1.596
20.83	0.683	1.245	0.850	1.326
20.43	0.540	1.082	0.584	0.684

	10(a)	10(b)
Mean value of the slope I_d/λ_t^2(less background) from graphs	= 8.0	8.0
Mean value of $1/K\left[-\frac{1}{\sqrt{2}},0,\frac{1}{\sqrt{2}}\right]_{006}$ and $1/K\left[\frac{1}{\sqrt{2}},0,-\frac{1}{\sqrt{2}}\right]$ (1st order) x 10^{-12} dynes/cm^2	= 1.734	1.734
Mean value of $1/K\left[-\frac{1}{\sqrt{2}},0,\frac{1}{\sqrt{2}}\right]_{006}$ and $1/K\left[\frac{1}{\sqrt{2}},0,-\frac{1}{\sqrt{2}}\right]_{006}$ corrected for second order x 10^{-12} dynes/cm^2	= 1.786	1.786

Average value from Tabs. 10(a) and 10(b) = 1.7(86)x10^{12} dynes/cm^2

Contd...

From tables (3.1), (3.2) and (3.3),

$$1/K\left[\pm\frac{1}{\sqrt{2}},0,\mp\frac{1}{\sqrt{2}}\right]_{006}=\frac{C_{11}(C_{33}+C_{55})+C_{33}C_{55}-2C_{13}C_{55}-C_{13}^2}{2(C_{11}+C_{55})}$$

or

$$C_{13}=-C_{55}\pm\left(C_{55}^2+C_{33}C_{55}+(C_{33}+C_{55})\left(C_{11}-\frac{2}{K\left[\pm\frac{1}{\sqrt{2}},0,\mp\frac{1}{\sqrt{2}}\right]_{006}}\right)\right)$$

(Negative sign before surd is never applicable)

Substituting the values of C_{11}, C_{33}, C_{55} and the mean value of $1/K\left[\pm\frac{1}{\sqrt{2}},0,\mp\frac{1}{\sqrt{2}}\right]_{006}$ (due to 1st order).

One gets,

The mean value of C_{13}(1st order)$\times10^{-12}$ dynes/cm^2 = -2.20

Average value of C_{13} corrected for 2nd order calculated from Tabs. 10(a) and 10(b) = $-2.0(27)\times10^{12}$ dynes/cm^2.

Contd...

From tables (3.1), (3.2) and (3.3),

$$1/K\left[\pm\frac{1}{\sqrt{2}},0,\mp\frac{1}{\sqrt{2}}\right]_{006}=\frac{C_{11}(C_{33}+C_{55})+C_{33}C_{55}-2C_{13}C_{55}-C_{13}^2}{2(C_{11}+C_{55})}$$

or

$$C_{13}=-C_{55}\pm\sqrt{C_{55}^2+C_{33}C_{55}+(C_{33}+C_{55})\left(C_{11}-\frac{2}{K\left[\pm\frac{1}{\sqrt{2}},0,\mp\frac{1}{\sqrt{2}}\right]_{006}}\right)}$$

(Negative sign before surd is never applicable)

Substituting the values of C_{11}, C_{33}, C_{55} and the mean value of $1/K\left[\pm\frac{1}{\sqrt{2}},0,\mp\frac{1}{\sqrt{2}}\right]_{006}$ (due to 1st order).

One gets,

The mean value of C_{13}(1st order)$\times10^{-12}$ dynes/cm^2 = -2.20

Average value of C_{13} corrected for 2nd order calculated from Tabs. 10(a) and 10(b) = $-2.0(27)\times10^{12}$ dynes/cm^2.

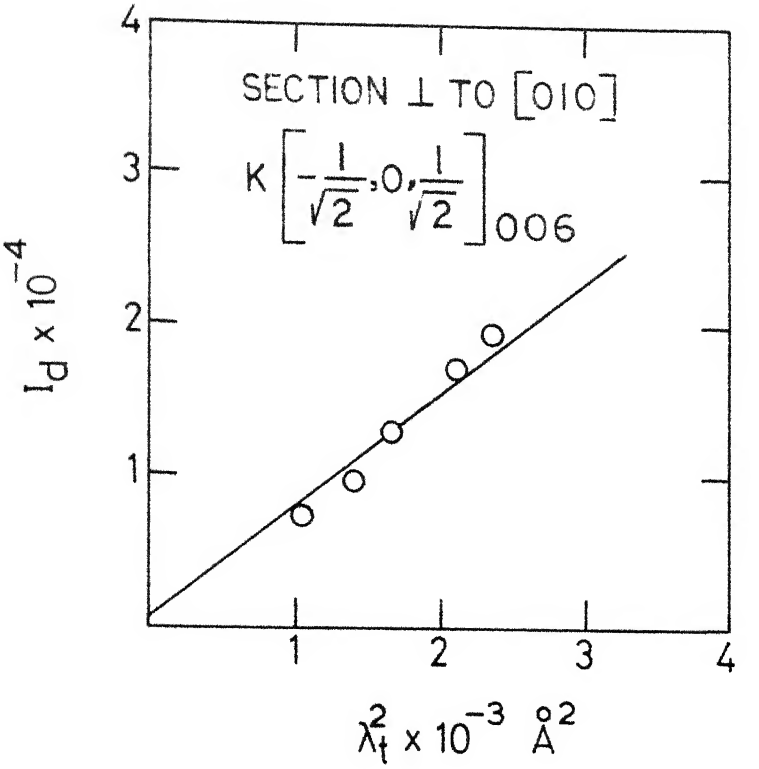
SECTION ⊥ TO [010]
K [-1/√2, 0, 1/√2] 006
I_d x 10^-4
λ_t^2 x 10^-3 Å^2
1
2
3
4

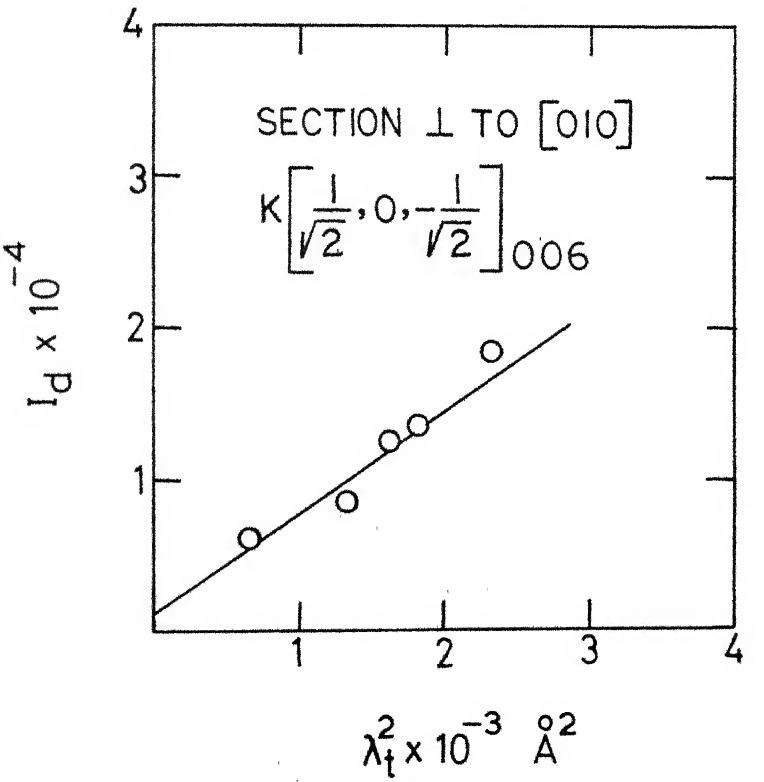
SECTION ⊥ TO [010]
K [1/√2, 0, -1/√2] 006
I_d x 10^-4
λ_t^2 x 10^-3 Å^2
1
2
3
4

Fig. I-9

Table A-11(a,b)

Rekha $[\bar{1}00]_{400}$

(a)

Angle of incident beam with [001] direction	Obs. diffuse intensity corrected for Absorption x 10^{-3}	Correction Factor S.D/P	Corrected Intensity I_d (due to 1st order) x 10^{-3}	λ_t^2 $(= \frac{1}{q^2})$ Å^2 x 10^{-3}
13.54	0.635	0.895	0.568	0.564
13.44	0.389	0.990	0.385	0.441
13.34	0.303	0.992	0.301	0.361
13.24	0.224	1.006	0.225	0.298

Rekha $[100]_{400}$

(b)

15.34	0.548	1.103	0.604	0.529
15.44	0.392	1.149	0.450	0.441
15.54	0.297	1.185	0.352	0.324
15.64	0.225	1.220	0.275	0.306

	11(a)	(b)
Mean value of the slope I_d/λ_t^2 (less background) from graphs	1.0	1.06
Mean value of C_{11} (1st order) x 10^{-12} dynes/cm^2	0.332	0.314
Second order correction is very small hence neglected.	0.332	0.314

Average value of C_{11} = 0.3(23) x 10^{12} dynes/cm^2 from Tab. 11(a) and 11(b).

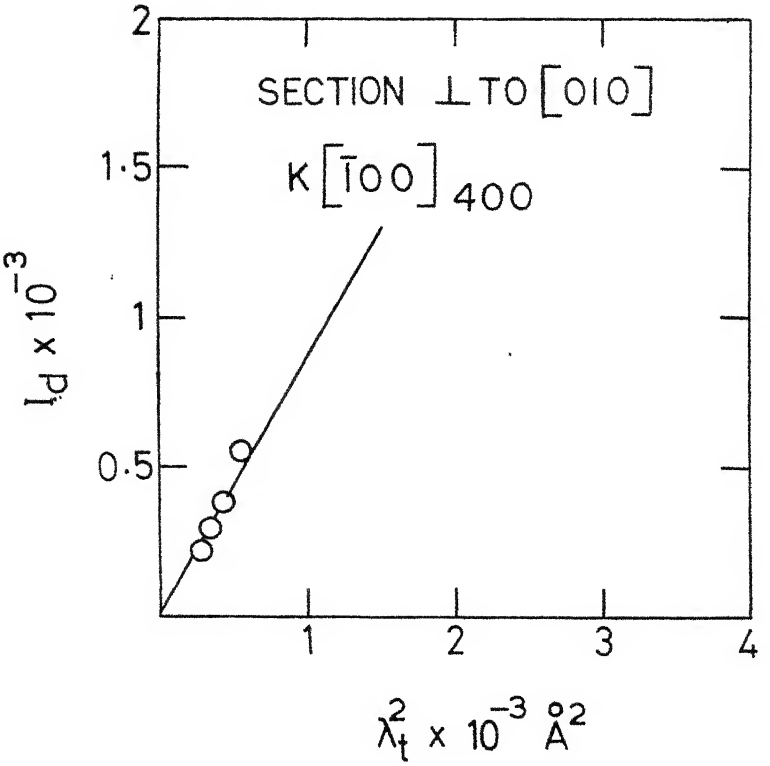
SECTION ⊥ TO [010]
K [$\bar{1}$00]400
$I_d \times 10^{-3}$
$\lambda_t^2 \times 10^{-3}$ Å^2

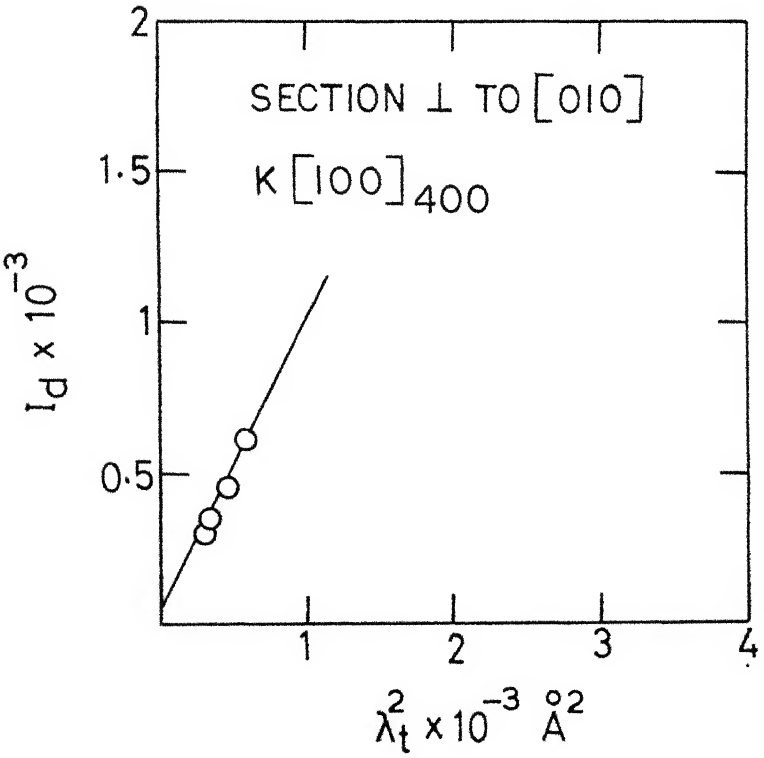
SECTION ⊥ TO [010]
K [100]400
$I_d \times 10^{-3}$
$\lambda_t^2 \times 10^{-3}$ Å^2

Fig. I-10

Table A-12(a,b)

Rekha $[001]_{400}$

(a)

Angle of incident beam with [001] direction	Obs. diffuse intensity corrected for Absorption x 10^{-3}	Correction Factor S.D/P	Corrected Intensity I_d (due to 1st order) x 10^{-3}	λ_t^2 ($= \frac{1}{q^2}$) Å^2 x 10^{-3}
13.54	0.917	0.892	0.818	8.190
13.44	0.612	0.989	0.605	6.520
13.34	0.536	0.990	0.531	5.220
13.24	0.445	1.005	0.447	4.761
12.44	0.154	1.012	0.156	1.661

Rekha $[00\bar{1}]_{400}$

(b)

15.34	0.755	1.101	0.831	8.10
15.44	0.565	1.148	0.649	6.52
15.54	0.452	1.184	0.535	5.18
15.64	0.391	1.219	0.477	4.49
16.22	0.149	1.304	0.195	2.07

	12(a)	12(b)
Mean value of the slope I_d/λ_t^2 (less background) from graphs	0.094	0.098
Mean value of C_{55} (1st order) x 10^{-12} dynes/cm^2	3.535	3.391

Second order correction is negligibly small

Average value of C_{55} = 3.4(63) x 10^{12} dynes/cm^2 from Tabs. 12(a) and 12(b).

This value of C_{55} may be compared with those obtained from rekhas $[100]_{006}$ and $[\bar{1}00]_{006}$ (tables A-8(a, b)), where a comparatively large crystal is used (Vol. 1.750 x 10^{-3} cc.).

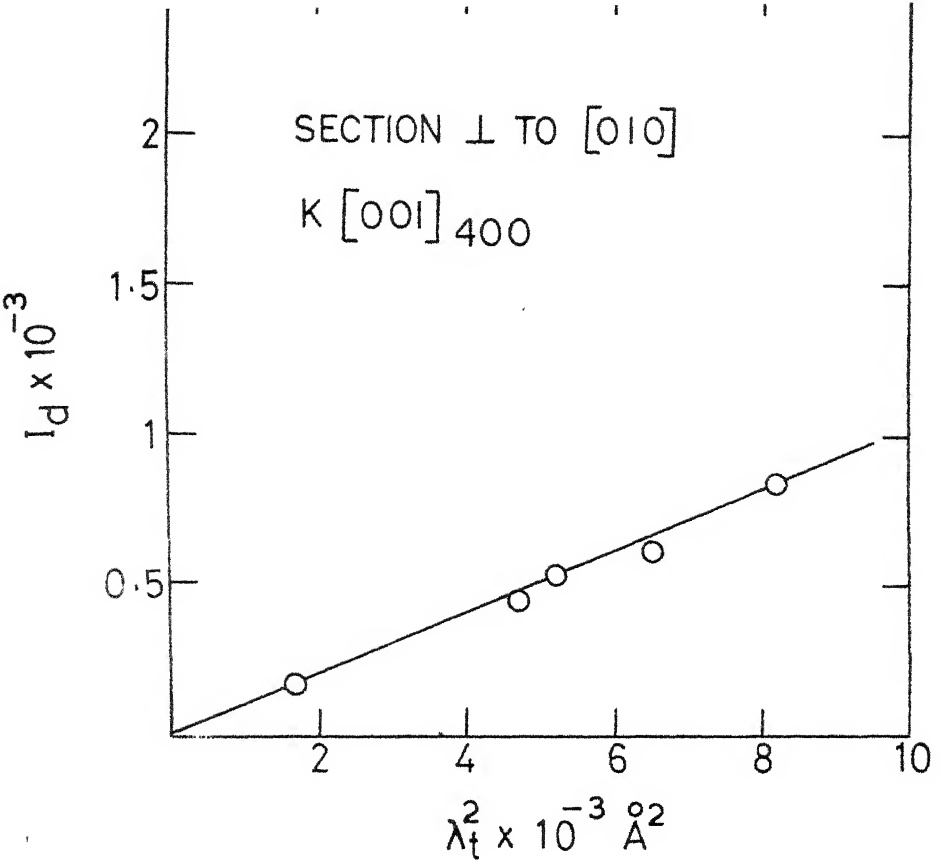
SECTION ⊥ TO [010]
K [001] 400
$I_d \times 10^{-3}$
2
1·5
1
0·5
2
4
6
8
10
$\lambda_t^2 \times 10^{-3}$ Å^2

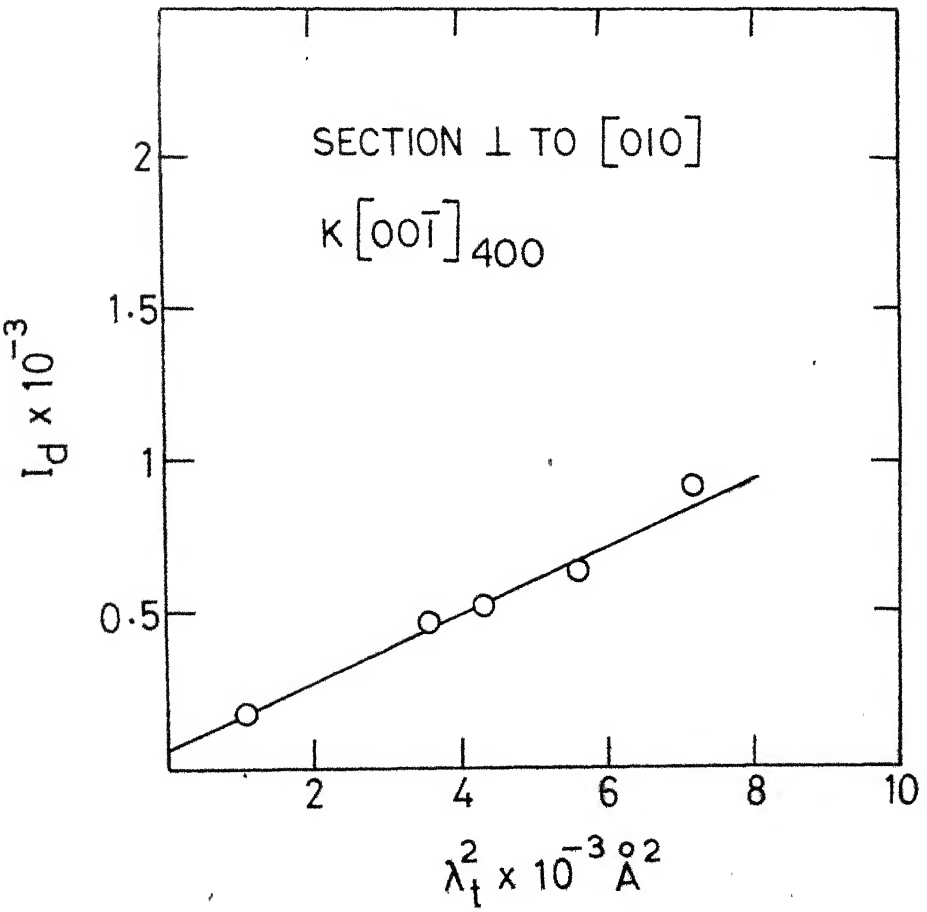
SECTION ⊥ TO [010]
K [00$\bar{1}$] 400
$I_d \times 10^{-3}$
2
1·5
1
0·5
2
4
6
8
10
$\lambda_t^2 \times 10^{-3}$ Å^2

Fig. I-11

Table A-13(a,b)

Rekha $\left[-\frac{1}{\sqrt{2}},0,\frac{1}{\sqrt{2}}\right]_{400}$

(a)

Angle of incident beam with [001] direction	Obs. diffuse intensity corrected for Absorption x 10^{-3}	Correction Factor S.D/P	Corrected Intensity I_d (due to 1st order) x 10^{-3}	λ_t^2 $(=\frac{1}{q^2})$ Å^2 x 10^{-3}
13.54	0.860	0.893	0.768	4.074
13.44	0.594	0.987	0.586	3.261
13.34	0.505	0.991	0.501	2.610
13.24	0.425	1.004	0.427	2.381
12.44	0.139	1.013	0.141	0.830
		Rekha $\left[\frac{1}{\sqrt{2}},0,-\frac{1}{\sqrt{2}}\right]_{400}$		
15.34	0.728	1.102	0.802	4.051
15.44	0.531	1.147	0.609	3.262
15.54	0.426	1.184	0.505	2.593
15.64	0.358	1.219	0.437	2.244
16.22	0.127	1.307	0.166	1.047

	13(a)	13(b)
Mean value of the slope I_d/λ_t^2 (less background) from Graphs	= 0.18	0.19
Mean value of $1/K\left[-\frac{1}{\sqrt{2}},0,\frac{1}{\sqrt{2}}\right]_{400}$ and $1/K\left[\frac{1}{\sqrt{2}},0,-\frac{1}{\sqrt{2}}\right]_{400}$ (1st order) x 10^{-12} dynes/cm^2	= 1.846	1.748

Second order correction is negligibly small.

Average value from Tabs. 13(a) and 13(b) = 1.7(97) x 10^{12} dynes/cm^2

This value may be compared with the value obtained your rekhas $1/K\left[\pm\frac{1}{\sqrt{2}},0,\mp\frac{1}{\sqrt{2}}\right]_{006}$ (tables A-10 (a,b) since they give the same constant C_{33}.

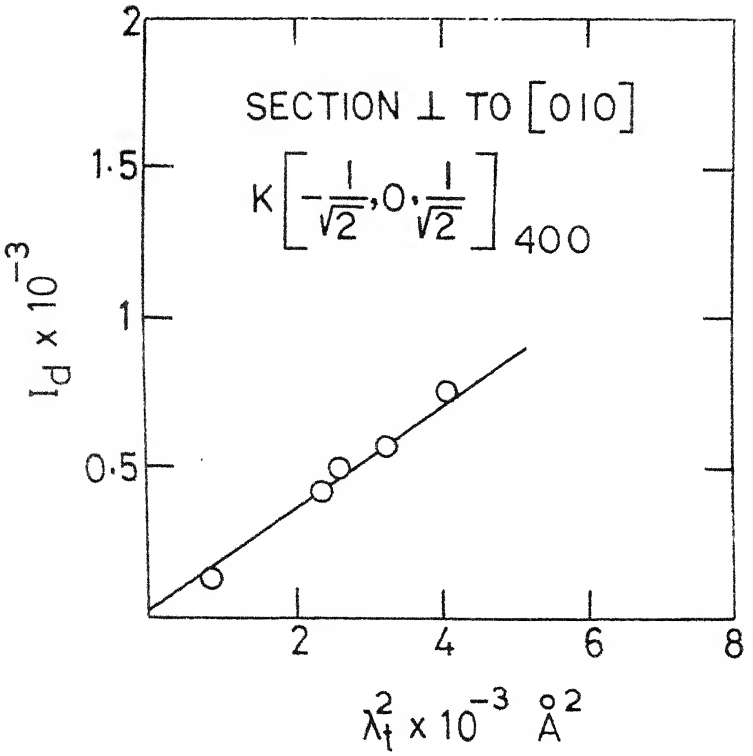
SECTION ⊥ TO [010]
K [-1/√2, 0, 1/√2] 400
I_d x 10^-3
λ_t^2 x 10^-3 Å^2
2
1.5
1
0.5
2
4
6
8

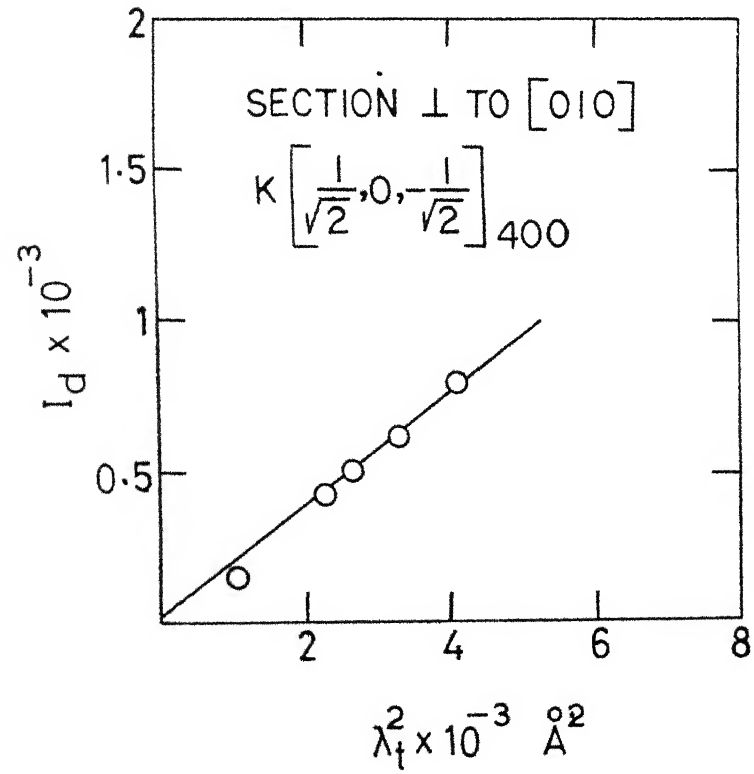
SECTION ⊥ TO [010]
K [1/√2, 0, -1/√2] 400
I_d x 10^-3
λ_t^2 x 10^-3 Å^2
2
1.5
1
0.5
2
4
6
8

Fig. I-12

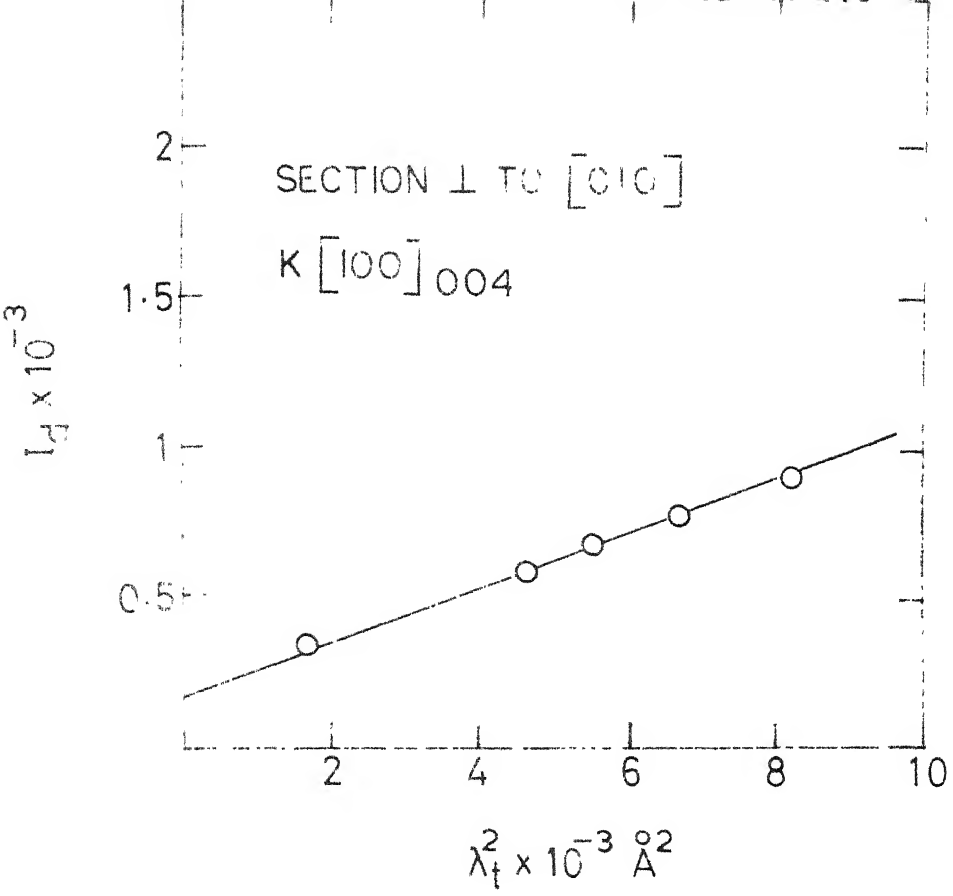
SECTION ⊥ TO [010]
K [100] 004
$I_d \times 10^{-3}$
2
1·5
1
0·5
2
4
6
8
10
$\lambda_t^2 \times 10^{-3}$ Å^2

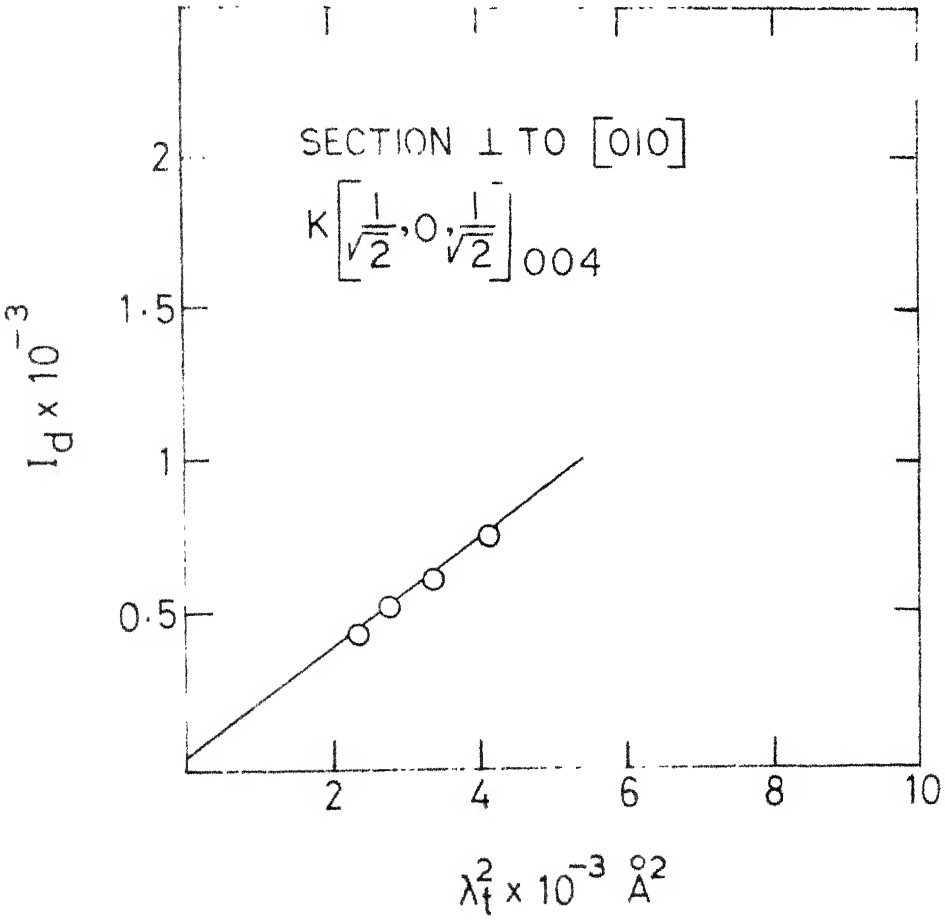
SECTION ⊥ TO [010]
K $\left[\frac{1}{\sqrt{2}}, 0, \frac{1}{\sqrt{2}}\right]$ 004
$I_d \times 10^{-3}$
2
1·5
1
0·5
2
4
6
8
10
$\lambda_t^2 \times 10^{-3}$ Å^2

Table A-15

Rekha $\left[\frac{1}{\sqrt{2}}, 0, -\frac{1}{\sqrt{2}}\right]_{004}$

Angle of incident beam with [100] direction	Obs. diffuse intensity corrected for Absorption x 10^{-3}	Correction Factor S.D/P	Corrected Intensity I_d (due to 1st order) x 10^{-3}	$\lambda_t^2 \left(= \frac{1}{q^2}\right) \text{Å}^2$ x 10^{-3}
13.48	0.848	0.892	0.756	4.096
13.38	0.666	0.922	0.614	3.342
13.28	0.553	0.936	0.518	2.775
13.18	0.439	0.974	0.428	2.313
12.38	0.150	0.982	0.147	1.601

Mean value of the slope I_d/λ_t^2 (less background) = 0.18 from the graph

Mean value of $1/K\left[\frac{1}{\sqrt{2}}, 0, -\frac{1}{\sqrt{2}}\right]_{004}$ (1st order) x 10^{-12} dynes/cm^2 = 1.7(91)

Second order correction is small hence neglected.

This value may be compared with the value of $1/K\left[\pm\frac{1}{\sqrt{2}}, 0, \mp\frac{1}{\sqrt{2}}\right]_{006}$ which is 1.7(86) x 10^{12} dynes/cm^2, corrected for second order (table A-10 (a,b)).

Appendix I Contd..

Photographic Method

Few curves (Fig. I-14 (a, b)) showing the variation of the intensity of diffuse reflection expressed as a fraction of incident intensity and uncorrected for polarization and skew corrections i.e. I'_d/I_o with the angle of diffraction ϕ observed in the Laue photographs taken with monochromatic MoKα (Plate III) radiation.

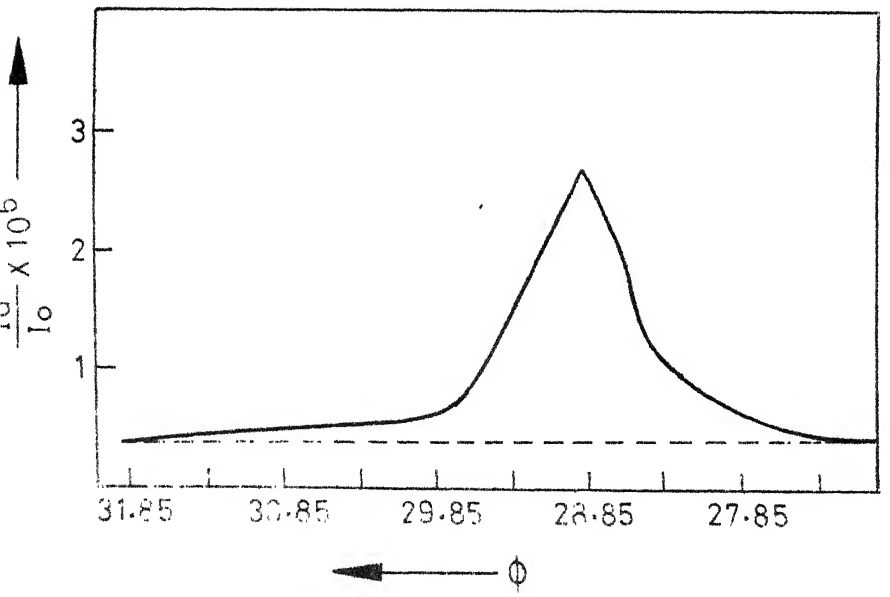

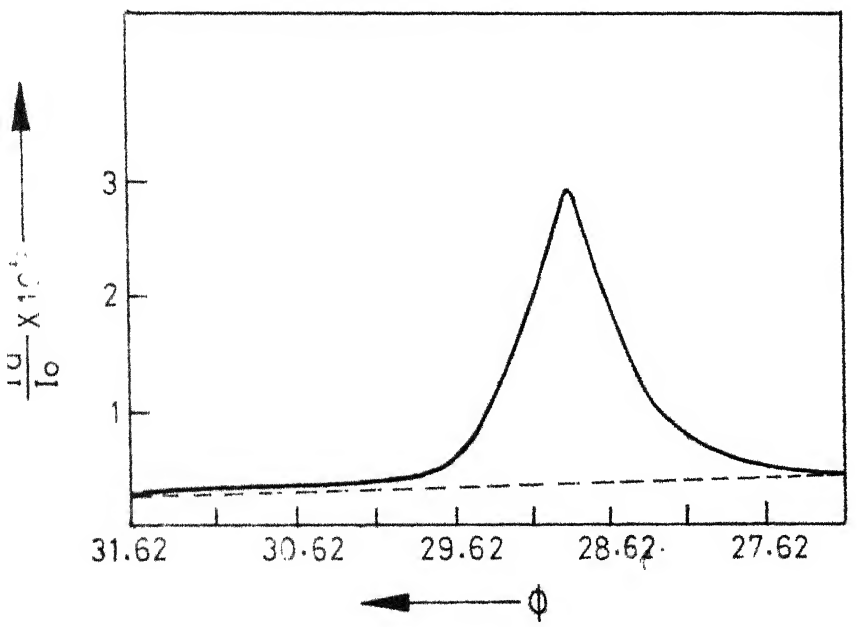

(b)

Fig. A-I-14: (4 0 0) diffuse reflection with [0 1 0] axis vertical and incident beam making with c* axis an angle of

Table A-16

(Photographic Method)

[0 1 0] axis vertical and coincident with the axis of the camera. (Radius = 5.70 cm).

Index of the plane under study	(4 0 0)
Structure factor of the plane	72.73
Thermal wave vector relevant to the table	$[0\,0\,1]_{400}$
Temperature at which study is made (Room temperature)	300°K
Wavelength of the monochromatic MoKα radiation	0.7107 Å

Volume of the crystal 0.996×10^{-4} c.c.

Rekha $[0\,0\,1]_{400}$

Angle of incident beam with [0 0 1] direction	$\frac{2}{t} \times 10^{-3}$ Å^2	Angle of diffraction Ø in degrees	$\frac{I'_d}{I_o} \times 10^6$	Corr. factor	$\frac{I_d}{I_o} \times 10^6$	$C_{55} \times 10^{-12}$ dynes/cm^2 = $1/K[001]_{400}$
13.425	6.006	28.89	2.579	1.051	2.711	3.472
13.337	5.476	28.88	2.315	1.045	2.418	3.549
13.275	4.900	28.86	2.107	1.041	2.194	3.500
13.235	4.692	28.88	2.039	1.040	2.120	3.469

The intensity I'_d/I_o is corrected for general scattering.

Average value of C_{55} from the table A-16 is 3.497×10^{12} dynes/cm^2

This value is in fair agreement with the value of $C_{55} = 3.463 \times 10^{12}$ dynes/cm^2 obtained by diffractometer method from the rekha $[0\,0\,1]_{400}$ (table A-12 (a,b)), on equally small crystal (Vol. 1.782×10^{-4} cc.).

(a)

(b)

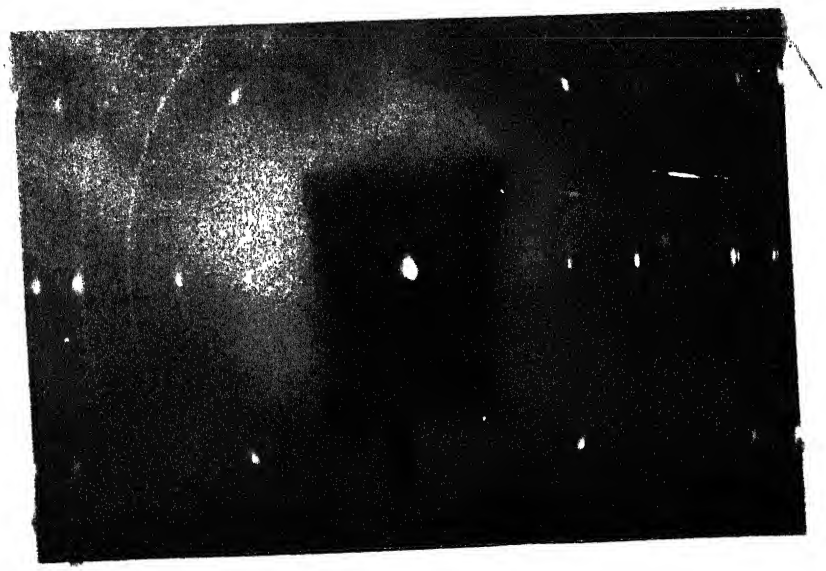

PLATE I

Rotation photographs of Potassium Niobate about b-axis

a) Monochromatic (crystal reflected) MoKα radiation, volume of the crystal 1.782×10^{-4}cc.

b) Monochromatic (crystal reflected) CuKα radiation, volume of the crystal 0.996×10^{-4}cc.

(a)

(b)

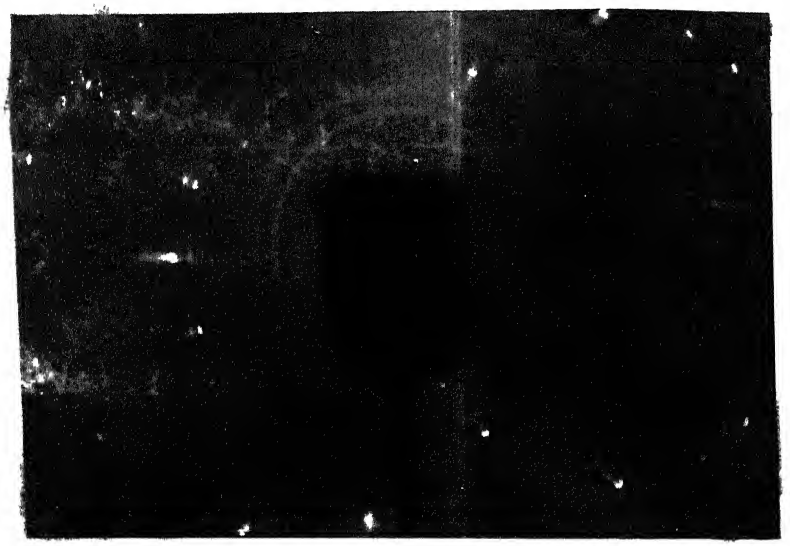

PLATE II

Orientation pictures (i.e. Laue photographs using polychromatic X-ray beam from Mo anticathode) with [0 1 0] axis vertical and incident beam making,

a) 13.275°; (4 0 0) diffuse reflection on the equatorial line,
b) 13.337°; (4 0 0) diffuse reflection on the equatorial line, with c* axis.

(a)

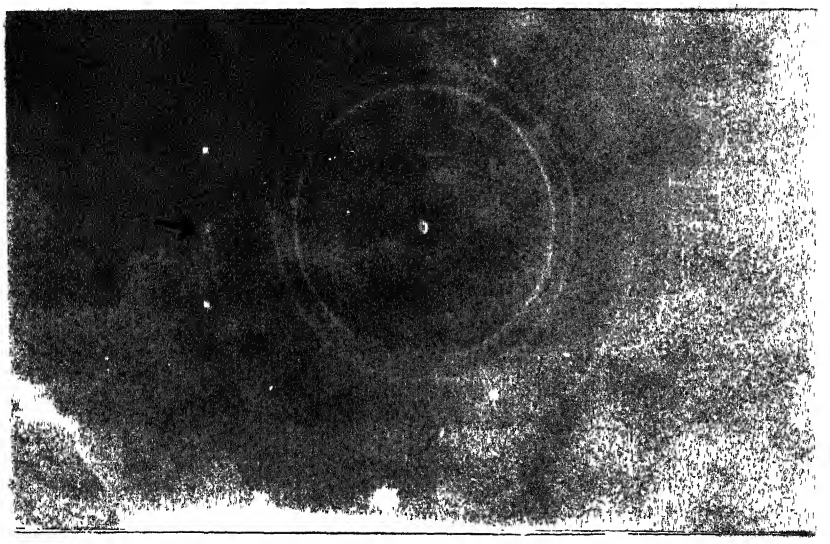

(b)

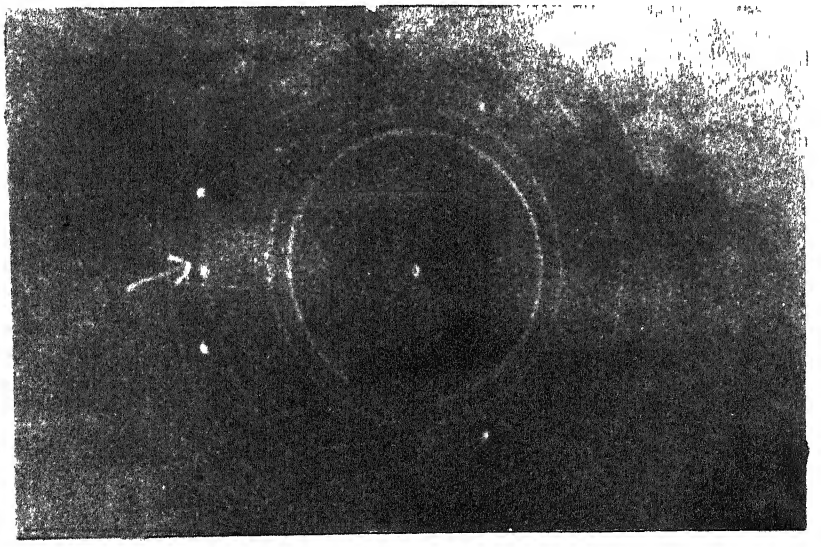

PLATE III

Laue photographs using monochromatic MoKα radiation with [0 1 0] axis vertical and incident beam making

a) 13.275°; (4 0 0) diffuse reflection (shown by arrowhead) on the equatorial line,

b) 13.337°; (4 0 0) diffuse reflection (shown by arrowhead) on the equatorial line,

with c* axis.

APPENDIX-I REFERENCES

Katz, L. and Megaw, H.D.	Acta Cryst. 22, 639, (1967).
Shirane, G. et al	Phys. Rev. 93, 672 (1954).
	Ibid. 96 581 (1954).
Vousden, P.	Acta Cryst. 4, 373, (1951).
Wood, E.A.	Acta Cryst. 4, 353, (1951).

APPENDIX II

MEASUREMENT OF DIRECT BEAM INTENSITY (I_o)

To determine the elastic constants, it is necessary to measure the absolute value of the incident flux. The direct X-ray beam is too strong to be measured directly with a proportional or scintillation counter, as it may not possess a linear response at these high counting rates; it must be attenuated first so that the dead time of the counter is appreciably less than the mean time interval between the arrival of the X-ray quanta. To evaluate the intensity I_o, the attenuation factor must be accurately known. Multiple foils can be used for attenuation, but difficulties are caused by the progressive hardening of the beam, due to preferential absorption of the softer components in the passage through successive foils. The multiple-foil technique is,therefore, most suitable for measurements with monochromatized radiation or with balanced filters. This technique is capable of establishing the intensity scale factor to within 3 % of its true value (Burbank,1964-65). Since the reduction factor is of the order 10^6, small error in measurement of thicknesses of the foils or μ, the linear absorption coefficient, may lead to large errors in the determination of I_o, the direct beam intensity (Wooster, 1962).

Another method of determining I_o (Buyers, 1964) consists of measuring the intensity scattered by a small block of paraffin

placed in the main beam, and using theoretical values for the absolute magnitude of this scattering (International tables for X-ray Crystallography). In an amorphous solid such as paraffin the scattering from each atom bears a random phase relation to that from other atoms; thus the total scattering is contributed by independent unmodified scattering and by modified (Compton) scattering, and both of these can be calculated from the unmodified and modified scattering intensities of the separate atoms. The method was abandoned since the purity of the chemical composition of the wax was not known correctly.

Another intermediate standard can be provided by the intensity of the Compton scattering from diamond (Prince and Wooster 1953) or other materials containing elements of low atomic number (Paraffin, etc., described above). The whole of the incident X-ray beam is allowed to fall on the diamond crystal set at any convenient angle (θ_{111} or θ_{220}) to the incident beam. The radiation of modified wavelength scattered in directions well away from Bragg reflections (about 8 to 10° on either side) has an intensity which may be calculated from the fundamental constants and may be compared directly with the thermal diffuse scattering under investigation. We may define a Compton diffuse scattering power, D_c, in an analogus manner to the first order thermal diffuse scattering power, i.e. as the ratio of the intensity scattered by the Compton effect per unit cell of

the crystal per unit solid angle to that scattered by a single Thomson electron under the same conditions (Wooster, 1962). For diamond this Compton diffuse intensity, D_c, may be written (James, 1948),

$$D_c = 8(6 - \Sigma f_{ec}^2)/ B^2 \qquad \text{(II-1)}$$

where Σf_{ec}^2 is a function, which describes the effect of the individual carbon atoms scattering incoherently. Compton and Allison (1935) give a table, listing the values of Σf_{ec}^2 as a function of the angle of deviation, 2θ, of the X-rays. It is also given in International tables for X-ray Crystallography Vol. III. B is Breit-Dirac correction factor, the value of which is,

$$B = 1 + \frac{2h\lambda}{mc} \frac{\sin^2\theta}{\lambda} ,$$

where the symbols have their usual meaning.

From this calculated Compton diffuse intensity, D_c, we may determine the absolute intensity of the incident beam I_o, using the measured intensity of the diffuse beam, I_c, and a formula analogous to that of the diffuse flux, namely,

$$\frac{I_c}{I_o} = \frac{\epsilon^2 D_c \Omega}{2\mu_d V} \qquad \text{(II-2)}$$

here μ_d is linear absorption coefficient of diamond for MoKα wavelength, and V is the volume of the unit cell, other symbols

are explained earlier. The experiment is performed with balanced (Zr-Y) filters as described earlier (Sec.4.4.1.1.)

Description of Table AII-1

Column	Description
1.	The angle which incident X-ray beam makes with diamond crystal.
2.	The value of $4\pi \sin\theta/\lambda_{MoK\alpha}$.
3.	The value of $1/B^3$ (Breit-Dirac factor).
4.	Polarization factor.
5.	Observed Compton diffuse intensity, I_c.
6.	Compton diffuse scattering flux, D_c.
7.	Direct beam intensity, I_o.

Thus for a brass collimator pair the average value of the direct beam intensity is 4.886×10^8 c.p.s. Similar experiment was done for G.E.Collimator pair, the average value being 5.26×10^7 c.p.s.

For diamond,

$$\mu_d = 1.9375 \text{ cm}^{-1}$$

$$V = 4.50 \times 10^{-23} \text{cc}$$

$$\Omega_{\text{brass}} = 9.797 \times 10^{-3}$$

$$\Omega_{\text{G.E.}} = 1.382 \times 10^{-3}$$

$$\epsilon^2 = 7.935 \times 10^{-26} \left(\frac{1+\cos^2 2\theta}{2} \right)$$

Table AII-1

θ^{o}	$\frac{4\pi \sin\theta}{\lambda_{MoK\alpha}}$	$\frac{1}{B^3}$	$\frac{1+\cos^2 2\theta}{2}$	I_c	D_c	$I_o \times 10^{-8}$ c.p.s.
24.375	7.300	0.966	0.717	67.185	38.640	4.676
25.375	7.580	0.963	0.700	65.615	38.520	4.870
26.375	7.858	0.960	0.683	68.625	38.784	4.995
27.375	8.134	0.958	0.667	67.610	39.086	4.999

Average value of the direct beam intensity, I_o from this table (for Brass Collimator pair) = 4.886×10^8 c.p.s.

APPENDIX II REFERENCES

Burbank, R.D. — Acta Cryst. 17, 434, 1(1964)

Ibid, 18 88, (1965)

Ibid, 19 957, (1965).

Buyers, W.J.L. — Ph.D. Thesis, University of Aberdeen, (1964).

Compton A.H. and Allison, S.K. — X-rays in Theory and Experiments, 782, Van Nostrand, (1935).

International Tables for X-ray Crystallography, Vol. III, 134, 135, 232, 247-253, Kynoch Press, (1963).

James, R.W. — Optical Principles of the Diffraction of X-rays, G. Bell and Sons, London (1948).

Prince, E. and Wooster W.A. — Acta Cryst. 6 450 (1953).

Wooster, W.A. — Diffuse X-ray Reflections From Crystals Clarendon Press Oxford (1962).

APPENDIX III

DETERMINATION OF LINEAR ABSORPTION COEFFICIENT OF $KNbO_3$

(i) Photographic Method (Chakrabbrty 1958 and Srivastava 1960):

A small crystal was mounted on a goniometer head. After adjusting one of its set of parallel and opposite faces perpendicular to the incident beam (Monochromatic and without harmonics), the direct beam impression was recorded on a piece of film . Fig. AIII (b). This impression has at its centre the shadow of the crystal and unabsorbed direct beam on either side of this shadow. This piece of film was developed simultaneously with a standard wedge and both were microphotometered under the same conditions Fig. AIII(c). The scanning spot of light was kept quite small such that it was much smaller than the shadow of the crystal and also the unabsorbed direct beam on either side of the shadow. The microphotometer record has a dip in the centre with shoulders on either side Fig. AIII(a). The intensity corresponding to the shoulders will give I_o and that corresponding to the dip will give I_a. Thickness of the crystal t traversed by undeviated beam can be accurately determined by measuring the distance between the pair of the parallel faces which were made perpendicular to the incident beam.

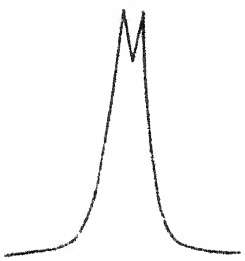

(a)

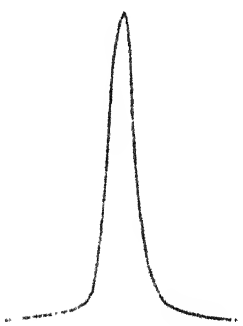

(b)

(c)

FIG. A.III (a) Direct beam impression with the crystal in the path.

(b) Direct beam impression without the crystal.

Hence μ can be evaluated from the following relation,

$$\mu = \frac{1}{t} \log_e \frac{I_o}{I_a} \qquad \text{(III-1)}$$

The linear absorption coefficient of Potassium Niobate was thus determined as 50.2 cm^{-1}. μ can also be calculated from the relation,

$$= \rho \sum_i p_i \frac{\mu_i}{\rho_i} \qquad \text{(III-2)}$$

where μ_i / ρ_i is mass absorption coefficient of individual atoms consituting the crystal (International tables) p_i their proportion and ρ the density of the crystal. The value thus calculated for the present case came to be 58.207 cm^{-1}. Incidently it may be mentioned that the agreement between the observed and calculated value of linear absorption coefficient (of $KNbO_3$) in the present investigation is fairly good compared to the data reported by other workers (Brill et al 1939 and Srivastava 1960 etc.) on other crystals.

(ii) Diffractometer method:

A thin crystal plate of $KNbO_3$ with opposite faces parallel to each other is mounted on the goniometer head which is in turn mounted on the single crystal orienter. A reflection from the plate at very low angle, close to $0^o(\emptyset)$ is balanced with Zr-Y pair of filters. The crystal plate with its opposite faces parallel is brought in the path of the direct beam such that these parallel faces are perpendicular to the direction of the

incident beam from Mo target, operated at 35 KVP and 25 mA. The detector is also in line with beam collimator i.e. the position $2\theta = 0^{\circ}$ on the 2θ circle. The intensity of the direct beam (I_o) is reduced to I_a after traversing the thickness of the plate, t cm. This is recorded with the balanced pair of filters (Zr-Y). Several observations of the time for 10,000 counts are taken for both the filters.

The crystal plate is then removed from the path of the direct beam (I_o). Keeping the detector in the fixed position ($2\theta = 0^{\circ}$), the direct beam intensity is measured with the same balanced pair.

From the formula (Eq. A III-1)

$$I_a = I_o e^{-\mu t}$$

or

$$e^{\mu t} I_a = I_o$$

$$\mu t = \log_e \frac{I_o}{I_a}$$

$$\mu = \frac{1}{t} \log_e \frac{I_o}{I_a}$$

In this way μ, the linear absorption coefficient for $KNbO_3$ crystal, is found. Observations are carried out on a number of crystals with varying thicknesses.

The value of μ of $KNbO_3$ determined on the diffractometer is 55.934 cm^{-1}, in fair agreement with the theoretically calculated value of 58.207 cm^{-1}. The value of μ observed from

the diffractometer is used in the calculations, since (i) diffractometer gives a better agreement with the calculated value than the photographic one, and (ii) the accuracy of intensity measurement is 1% in the diffractometer method compared to about 3% in the camera technique.

APPENDIX III REFERENCES

Brill, R., et al — Ann. Phys., Lpz. 34 393 (1939).

Chakraborty, S.C. — D. Phil. Thesis, Allahabad University (1958).

International Tables for X-ray Crystallography, Vol. III, 157, 162-165, 175-192, Kynoch Press (1963).

Srivastava, R.C. — Ph.D. Thesis, Allahabad University, (1960).

APPENDIX IV

Debye temperature of Potassium Niobate single crystal

Debye temperature is one of the most important physical quantities of a solid, for example, it gives a measure where quantum corrections begin to become important for each substance and provides useful information regarding vibrational spectrum in a qualitative way. Very recently Sastry et al (1969) described how one can find out the energy of formation of defects (vacancy) in a solid if the Debye temperature of the substance is known; besides this, Debye temperature is also a very useful parameter used in some thermodynamic relations. Potassium Niobate belongs to an orthorhombic crystal class {mm2} , and explicit formulae are obtained for the Debye characteristic temperature, by an extension of Houston's method (1948) described in detail by Joshi (1961).

The Debye theory of specific heat is based on a continuum model i.e. where the wavelength of the elastic waves is equal to or larger than the interatomic distances. This condition is satisfied strictly only at the low frequency region of the vibrational frequency spectrum. The low frequency waves are most important at temperatures approaching $0^{\circ}K$. One would therefore, expect that the Debye temperature (θ_D) derived from specific heat measurements should agree with the θ_D obtained

from elastic constants, since the wavelengths used for the determination of the elastic constants are large compared to the interatomic distance.

Many methods of evaluating θ(elastic) for cubic (Blackman 1955, Alers and Neighbours, 1959), hexagonal (Wolcott 1959), tetragonal and trigonal (Betts, Bhatia and Horton 1956) are described. An analogous method for orthorhombic crystals is given by Joshi (1961).

In Debye continuum model θ(elastic) is given by

$$\theta_{elastic} = \left(\frac{h}{k}\right)\left(\frac{9N}{4\pi VI}\right)^{1/2} \qquad \text{(IV-1)}$$

where N is the number of vibrating units in the volume V, h is the Planck's constant, k = Boltzmann constant and I is defined by

$$I = \sum_{i=1}^{3} \int_{o}^{4\pi} \frac{d\Omega}{v_i^3} \qquad \text{(IV-2)}$$

where, v_i are the velocities of propagation of elastic waves in the continuum at $0^{o}K$ and $d\Omega$ is the solid angle for the whole sphere. These velocities are given by three roots of the third order Christoffel equation (Love 1944) and hence, in general, involve the solution of a cubic equation. These roots will be functions of elastic constants and direction of propagation of the wave. The problem of evaluation of θ(elastic) thus reduces

to the evaluation of the above integral I.

Eq. IV-2 becomes,

$$I = \varrho^{3/2} \int_0^{4\pi} f(\theta, \phi)\, d\Omega \qquad \text{(IV-3)}$$

since $f(\theta, \phi) = \Sigma_i |\, v_i \,|^{-3}\ \varrho^{-3/2}$, where ϱ is the density of the crystal. $f(\theta, \phi)$ may be expanded in terms of harmonics, $F_{l,m}(\theta,\phi)$ having the same symmetry as the corresponding Christoffel equation (Betts, Bhatia and Horton 1956),

$$f(\theta,\phi) = \sum_{l=0}^{\infty} \sum_{m=-l}^{l} a_{lm}\, F_{lm}\,(\theta, \phi) \qquad \text{(IV-4)}$$

From the properties of spherical harmonics we have the exact relation,

$$\frac{1}{4\pi} \int_0^{4\pi} f(\theta, \phi)\, d\Omega = a_{00} = a_0 \qquad \text{(IV-5)}$$

Our approximation consists in stopping the summation in Eq. IV-4 at a particular l and m. The coefficient a_0 is found by solving the linear equations IV-4 obtained by giving various values to (θ, ϕ).

For orthorhombic crystals we take a two fold rotation axis as the polar axis, $\theta = 0$. The Christoffel equation is invariant under the transformations,

$$\theta = \pi-\theta, \quad \phi = -\phi \text{ or } \phi = \phi+\pi\ .$$

The appropriate 'orthorhombic harmonics' are

$$O_{2l,2m}(\theta, \phi) = \text{Cos } 2m\phi\ P_{2l}^{2m}\ (\text{Cos } \theta) \qquad \text{(IV-6)}$$

With $l+m \leq 2l$, l, $m = 0, 1, 2$, solving the corresponding equation (IV-4), we get,

$$a_0 = [\,7f_B - 36f_C + 16f_D + 48f_E + 25f_F\,] \;/\; 15 \qquad \text{(IV-7 i)}$$

$$a_0 = [\,20f_A + 21f_B - 48f_C + 48f_D + 64f_E + 75f_F\,] \;/\; 180 \qquad \text{(IV-7ii)}$$

$$a_0 = [\,519f_A + 45f_B - 1008f_C + 480f_D + 1344f_E + 1575f_F + 825f_G\,]/3780 \qquad \text{(IV-7iii)}$$

in which the subscripts on f signify its value in the corresponding directions. The directions chosen are A(100), B(001), C(010), D(101), E(1$\sqrt{30}$), F(021) and G(102). In deriving (IV-7i), (IV-7ii) and (IV-7iii) all orthorhombic harmonics (IV-6) upto O_{42}, O_{44} and O_{60} respectively, are utilized, since at O_{60} equations (IV-7i), (IV-7ii) and (IV-7iii) are found to be sufficiently convergent. The Chistoffel equation for the sound velocities for general direction (l, m, n) in the case of orthorhombic crystals, takes the form,

$$\begin{vmatrix} C_{11}l^2+C_{66}m^2+C_{55}n^2-\rho v^2 & (C_{12}+C_{66})lm & (C_{13}+C_{55})ln \\ (C_{12}+C_{66})lm & C_{66}l^2+C_{22}m^2+C_{44}n^2-\rho v^2 & (C_{23}+C_{44})mn \\ (C_{13}+C_{55})ln & (C_{23}+C_{44})mn & C_{55}l^2+C_{44}m^2+C_{33}n^2-\rho v^2 \end{vmatrix} = 0$$

On solving this equation along the directions A, B, ...G, defined above, one gets the following expressions for f_A, f_B etc,

$$f_A = [\,C_{11}\,]^{-3/2} + [\,C_{55}\,]^{-3/2} + [\,C_{66}\,]^{-3/2}$$

$$f_B = [\,C_{33}\,]^{-3/2} + [\,C_{44}\,]^{-3/2} + [\,C_{55}\,]^{-3/2}$$

$$f_C = [\,C_{22}\,]^{-3/2} + [\,C_{44}\,]^{-3/2} + [\,C_{66}\,]^{-3/2}$$

contd..

$$f_D=\left[\frac{1}{2}(C_{44}+C_{66})\right]^{-3/2}+\left[\frac{1}{4}(C_{11}+C_{33}+2C_{55})+\frac{1}{4}\left\{(C_{11}-C_{33})^2+4(C_{13}+C_{55})^2\right\}^{1/2}\right]^{-3/}$$
$$+\left[\frac{1}{4}(C_{11}+C_{33}+2C_{55})-\frac{1}{4}\left\{(C_{11}-C_{33})^2+4(C_{13}+C_{55})^2\right\}^{1/2}\right]^{-3/2}$$

$$f_E=\left[\frac{1}{4}(3C_{44}+C_{55})\right]^{-3/2}+\left[\frac{1}{8}(C_{11}+3C_{22}+4C_{66})+\frac{1}{8}\left\{(C_{11}-3C_{22}+2C_{66})^2\right.\right.$$
$$\left.\left.+12(C_{12}+C_{66})^2\right\}^{1/2}\right]^{-3/2}+\left[\frac{1}{8}(C_{11}+3C_{22}+4C_{66})\right.$$
$$\left.-\frac{1}{8}\left\{(C_{11}-3C_{22}+2C_{66})^2+12(C_{12}+C_{66})^2\right\}^{1/2}\right]^{-3/2}$$

$$f_F=\left[\frac{1}{5}(C_{55}+4C_{66})\right]^{-3/2}+\left[\frac{1}{10}(4C_{22}+C_{33}+5C_{44})+\frac{1}{10}\left\{(C_{33}+3C_{44}-4C_{22})^2\right.\right.$$
$$\left.\left.+16(C_{23}+C_{44})^2\right\}^{1/2}\right]^{-3/2}+\left[\frac{1}{10}(4C_{22}+C_{33}+5C_{44})\right.$$
$$\left.-\frac{1}{10}\left\{(C_{33}+3C_{44}-4C_{22})^2+16(C_{23}+C_{44})^2\right\}^{1/2}\right]^{-3/2}$$

$$f_G=\left[\frac{1}{5}(4C_{44}+C_{66})\right]^{-3/2}+\left[\frac{1}{10}(C_{11}+4C_{33}+5C_{55})+\frac{1}{10}\left\{(C_{11}+3C_{55}-4C_{33})^2\right.\right.$$
$$\left.\left.+16(C_{13}+C_{55})^2\right\}^{1/2}\right]^{-3/2}+\left[\frac{1}{10}(C_{11}+4C_{33}+5C_{55})\right.$$
$$\left.-\frac{1}{10}\left\{(C_{11}+3C_{55}-4C_{33})^2+16(C_{13}+C_{55})^2\right\}^{1/2}\right]^{-3/2} \qquad \text{(IV-9)}$$

The characteristic temperature for orthorhombic Potassium Niobate can be calculated from the formula (IV-7iii). Eqs.(IV-7ii) and (IV-7iii) differ only little from each other (< 2%),(Joshi, 1961). One has to use higher term approximations than those used here to improve the accuracy.

For an accurate evaluation of θ(elastic), the values of elastic constants measured near $0^{\circ}K$ should have been used. In the absence of such measurements, elastic constants measured at other temperatures may be used, but, then, the absolute values

of the characteristic temperature becomes unreliable to some extent. However, Blackman (1955) has pointed out that the variation in θ(elastic) values is not very large relative to the variation of elastic constants with temperature. No specific heat data are available for Potassium Niobate in the true T^3 region to estimate θ_D.

θ (elastic) for Potassium Niobate = $302^{\circ}K$

This value is obtained from (IV-7iii) which is expanded upto 60 terms i.e. until it is fairly convergent.

Inversion Temperature:

The Bragg intensity (corresponding to reflection from ideal planes) decreases with increasing T because thermal vibrations make the plane less and less perfect. Diffuse scattering increases with temperature since thermal disorder increases, but it increases only up to the point where the plane retains its physical meaning relative to the effect being studied (i.e., first, second and third order diffuse scattering). Thermal diffuse scattering (TDS) begins to decrease when, as a result of thermal agitation, the plane begins to lose its reality, that is, the crystal starts to 'melt'. The temperature where this takes place is called the inversion temperature. Later the whole structure melts, and the crystal ceases to exist. One can find out the inversion temperature $(T_{max})_1$ for Ist order

diffuse scattering (TDS_1) for a given plane, if the Debye temperature of the crystal is known, from the following relation (Amoros 1968)

$$(T_{max})_1 = \frac{1}{3} \frac{k}{h^2} m\theta_D^2 d_{hkl}^2 \qquad \text{(IV-10)}$$

Symbols have their usual meaning.

The inversion phenomenon is quite general and the expression for this is independent of the type of structure, and is a function only of the mean square amplitude of atomic vibration, $\bar{u}^2$ which is in turn related to the interplanar spacings, (d_{hkl}), therefore only certain sets of crystal planes will be potentially able to show the inversion phenomenon.

Relation between atomic-vibrational amplitude and T_{max}(inversion temperature):

The atoms in the crystal vibrate with characteristic amplitude for a given structure and temperature. Since the phenomenon of diffuse scattering is a direct consequence of this atomic vibration, there must exist a relation between the atomic-vibrational amplitude and T_{max}.

Letting $T = (T_{max})_1$, one can obtain from the well known Debye-Waller relation (James 1954, Amoros 1968),

$$\frac{(T_{max})_1}{T} = 1 = \frac{1}{4^2} \frac{d_{hkl}^2}{\bar{u}^2} \qquad \text{(IV-11)}$$

and

$$\frac{(\bar{u}^2)^{1/2}}{d_{hkl}} = 0.16 \qquad \text{(IV-12)}$$

Therefore, TDS_1 (Ist order thermal diffuse scattering) reaches its maximum value for a given crystallographic plane when $(\bar{u}^2)$ is a definite fraction 0.16 of its spacing. Gruneisen (1925) showed that melting takes place when $(\bar{u}^2)^{1/2}$ is of the order of 0.10 of the shortest interatomic distance. These relations are simple to derive for a cubic monoatomic crystal. But for the non cubic polyatomic crystals, these relations can be obtained by considering the mean square amplitude of vibration of each kind of atom separately, as well as the anisotropy of its vibration.

APPENDIX IV REFERENCES

Alers, G.A. and Neighbours, J.R.	Revs. Modern Phys. 31 675 (1959)
Amoros, J.L. and Amoros, M.	Molecular Crystals, John Wiley and Sons (1968).
Betts, D.D., Bhatia, A.B. and Horton, G.K.	Phys. Rev. 104, 43 (1956).
Blackman, M.,	Handbuch Der Physik 7 325-382 (1955).
Gruneisen, E.	Zustand des festen kor pers, " In Handbuch der Phys" 10 1-25 (1925).
Houston, W.H.	Rev. Mod. Phys. 20, 161 (1948).
James, R.W.	Optical Principles of the Diffraction of X-rays, Bell and Sons London (1954).
Joshi, S.K.	Phys. Rev. 121, 40 (1961).
Love, A.E.H.	Mathematical Theory of Elasticity, Dover (1944).
Sastry, P.V. and Mulimani, B.G.	Phil. Mag. 20 859 (1969).
Wolcott, N. W.	J. Chem. Phys. 31 536 (1959).

ERRATA

Page	Line	Correction
ix	lines 16 and 18	" Curve corresponding to" instead of " Curve corresponds to"
30	5th line from bottom (Reference)	" J. Phys. Rad." instead of " J. Rad. Phys."
69	14	" Chakraborty" instead of " Sen and Chakraborty"
70	lines 1 and 2	" adjusted at 0.02 cm in height" instead of " adjusted at 0.02 cm to 0.02 cm in height"
81	Fig. 4.6(a,b) (Caption)	" The curve corresponding to" instead of " The curve corresponds to"
81	Fig. 4.6(a) (Caption)	insert "(as shown in Fig. 4.6b)" before " is "
106	21	" of cross section $\sim$ 5 x 5 mm^2 " instead of " of the size $\sim$ 5 mm x 5 mm"